NTNU – Trondheim
Norwegian University of
Science and Technology

Prototype of a tilt rotor helicopter

A helicopter comprising a multi-rotor system
with individual collective and cyclic pitch
control.

Svein Rivli Napsholm

Summary

The use of drones and remote operated aircrafts has become a useful tool for the oil and mining industry, when searching for new production areas. The remote controlled aircrafts can perform some of the tasks during these operations such as deploy sensors, gather geographical data and perform area inspections. The smaller and cheaper aircrafts are a cost and time effective solution compared to using bigger helicopters and air planes.

In this master thesis, it is proposed a new type of remote controlled helicopter that is capable of performing the tasks mentioned above. The helicopter was designed with four rotors, where each rotor has cyclic and collective pitch control. This makes the helicopter capable of controlling the rotor thrust in the longitudinal and transversal direction, which is a necessary property to have when it is performing inspection tasks and performing 3d maneuvers (e.g upside down).

In this thesis, it has been derived equations based upon the two aerodynamic theories, the "Momentum theory" and the "Blade element theory", to compute the required power necessary for the helicopter to fly. It has been developed software for testing the rotor system and a buffer card that is used to transform the signals to and from the micro-controller. In addition it has been developed and built a test bench, which can measure the rotor system's maximum lifting capacity and rotational velocity.

It have been developed three different designs of the helicopter's rotor system and all of them have been built and tested. Among the three rotor systems, one of them was established as a working prototype, and additional tested to detect its lifting properties.

A mathematical model of the helicopter has been derived which has been used in simulations to detect the helicopter's stability properties and behavior when subjected to winds and downdrafts. To create a realistic sim-

ulation, the test results for the rotor system was used as parameters for the helicopter model.

Three different architectural designs have been proposed; a system architecture, a hardware architecture and a software architecture. The architectures give an overview on how the hardware and software are connected and how they interact. In addition, it is proposed how the software can be constructed so the helicopter can operate in autonomous and manual mode.

Based on the good results from the simulation, a complete helicopter with the desired tilt system was designed and constructed.

In the end of this report a model predictive controller was proposed as a control strategy, which could be used to optimize the helicopter's fuel/battery consumption.

The test results from the simulation showed that this helicopter can be tilted 58° without losing altitude, and can reach speeds up to 15 m/s (14 m/s levelled). It can also withstand downdrafts up to 8 m/s when leveled (4 m/s tilted) and crosswinds up to 16 m/s. The conclusion is that this helicopter's performance is about the same as for bigger quadcopters, but it has many additional advantages. The helicopter can be equipped with petrol driven motors instead of the electric ones, which makes it capable of operating over vast distances and in cold environments. It can be positioned with high accuracy during inspections tasks, due to its cyclic and collective pitch control. It can be equipped with fixed wings to the tilt rotor system which will serve two purposes; it will compensate for the reduced lift capacity caused by the tilted rotors and help minimize the fuel/battery consumption. The many unique features of this helicopter make it a very versatile flying machine, which is optimum for use in the industry.

Sammendrag

Bruk av droner og fjernstyrte luftfartøy har blitt et nyttig verktøy for olje og gruve industrien, når de søker etter nye produksjonsområder. De fjernstyrte luftfartøyene kan brukes til å utføre oppgaver som for eksempel plassere ut sensorer, samle inn geografiske data og inspisere områder. De mindre og billigere luftfartøyene er en kostnads og tids effektiv løsning samenlignet med bruk av større helikoptre og fly.

I denne master oppgaven er det blitt foreslått en ny type fjernstyrte helikopter som er i stand til å utføre oppgavene nevnt ovenfor. Helikopteret er designet med fire rotorer hvor hver av rotorene har syklisk og kollektiv vinkel regulering. Dette gjør helikopteret i stand til å kontrollere rotor kraften i langsgående og tverrgående retning, som er en nødvendig egenskap å ha når den utfører inspeksjons jobber og når den flyr 3d (for eksempel opp ned).

I denne oppgaven, har det blitt utledet ligninger basert på de to aerodynamiske teoriene "Moment teorien" og "Blad element teorien", for å beregne hvilken effekt som er nødvendig for at helikopteret skal fly. Det har blitt utviklet en programvare for å teste rotor systemet og et buffer kort som er brukt til å omforme signalene til og fra mikrokontrolleren. I tillegg så har det blitt utviklet og bygget en test benk, som kan måle rotor systems maksimale løfte kapasitet og rotasjons hastighet. Det har blitt utviklet tre ulike design av helikopterets rotor system og alle har blitt bygget og testet. Blant de tre rotor systemene ble en av dem stadfestet som en fungerende prototype og videre testet for å finne dens løfte egenskaper. Det har blitt utledet en matematisk modell av helikopteret som har blitt brukt i simuleringer for å finne helikopterets generelle stabilitets egenskaper og oppførsel

når den er utsatt for sidevind og ned vind. For å lage en realistisk simulering så ble test resultatene fra rotor systemet brukt som parametere for helikopter modellen.

Tre ulike arkitekturiske design har blitt presentert; en system arkitektur, en hardware arkitektur og en software arkitektur. Arkitekturene gir en oversikt over hvordan hardware og software er koblet sammen og hvordan de samhandler. I tillegg er det foreslått hvordan softwaren kan lages slik at helikopteret kan operere i autonom og manuell modus.

Basert på de gode resultatene fra simuleringen, så har det blitt designet og konstruert et komplett helikopter med det ønskede vippe systemet.

Til slutt i rapporten er det foreslått en modell prediktiv regulator som en regulerings strategi, som kan brukes til å optimalisere helikopterets drivstoff/batteri forbruk.

Resultatene fra simuleringen viste at helikopteret kan vippes 58° uten å miste høyde og nå hastigheter opp til 15 m/s (vippet eller vannrett). Når den er vannrett kan den motstå ned vind opp til 8 m/s (4 m/s vippet) og sidevinds hastigheter opp til 16 m/s. Konklusjonen er at ytelsen til dette helikopteret er omtrent det samme som for store quadcoptere, men har mange tilleggs fordeler. Helikopteret kan utstyres med drivstoff drevene motorer i stedet for elektriske, hvilket gjør den i stand til å operere over store avstander og i kalde miljøer. Den kan posisjoneres med høy nøyaktighet når den utfører inspeksjons jobber på grunn av dens sykliske og kollektive vinkel kontroll. Den kan utstyres med faste vinger på vippe rotor systemet, hvilket har to hensikter; det vil kompensere for den reduserte løfte kapasiteten forårsaket av de vippede rotorene og hjelpe med å minimalisere drivstoff/batteri forbruket. Dette helikopterets mange unike egenskaper gjør det til en veldig allsidig fly maskin, som er optimal for bruk i industrien.

Preface

This master thesis is a product of the work done in my final semester at the Norwegian University of Science and Technology (NTNU), when studying for the degree of Master of Science in Engineering Cybernetics. During this thesis, many people has inspired me and contributed with important knowledge, wisdom and counseling, which has been accepted with gratitude.

I would like to thank my supervisor Amund Skavhaug for his support both as a supervisor and as a friend. In the more difficult parts of this project, he has always been positive and encouraging, which has helped me to keep going and find solutions to problems that seemed impossible to solve. I hope we will keep in contact, and want you to know that your support has been very much appreciated.

Another person who has meant a great deal to me is my dear and most treasured Silje Hemre Sæthre. She has always inspired me to follow my dreams and to keep fighting for the things that I want out of life. While I was away in Trondheim, she was the rock in our relationship, and never stopped believing in us. We are now living together with her son Adrian (6), who has been a great asset for tracking pencils, papers and other important stuff needed in this project.

I also want to give my acknowledge and gratitude to my friends that have helped me with this thesis. My good and dear friend Joakim Tønnesen has given me valuable support in programming and electronics. He has a tremendous know how and is easy to discuss with and always tries to help you achieve the goals that you have set. A better friend and colleague is in my opinion very difficult to find. I would also like to give my gratitude and thanks to my two other friends Thomas Ferstad Øvervåg and Dzordzoenyenye Kwame Kufoalor (Giorgio). I want to thank Girgio for all the

discussions we have had regarding simulation and mathematical modeling, your advice and knowledge has been appreciated. I also want to thank Thomas for all the meaningful conversation that we have had, for encouraging me and for always being such a positive person.

Another person that deserves gratitude and acknowledge is my former colleague and life long friend Ulv Kjetil Hjellestad. I want to give him my thanks for his contribution to this project when building the helicopter. His knowledge and wisdom has been a great asset to this project.

Svein Napsholm
January, 2013

Contents

CONTENTS

Abbreviations

AH   Assignment Handler

AoA   Angle Of Attack

BET   Blade Element Theory

BLDC   BrushLess Direct Current

BPS   Bits Per Second

CAS   Collision Avoidance System

DAoA   Disc Angle Of Attack

DB   Development Board

DIY   Do It Your self

DMA   Direct Memory Access

DOF   Degrees Of Freedom

ECEF   Earth Center Earth Fixed

ECI   Earth Center Inertial

EPWM   Enhanced Puls Width Modulation

ESC   Electronic Speed Controller

FASST   Futaba Advanced Spread Spectrum Technology

FPU   Floating Point Unit

GPS   Global Positioning System

GS   Guidance System

I-frame Instrument frame

INS   Inertial Navigation System

IPC   InterProcess Communication

CONTENTS

LOS Line Of Sight

MCU Micro-Controller Unit

MPC Model Predictive Controller

MT Momentum Theory

NED North-East-Down

NEMA National Maritime Electronics Association

NPN Negative-Positive-Negative

OIS Identification System

P-frame Platform frame

PID Proportional–Integral–Derivative

PP Path Planner

PPM Puls Position Modulation

PWM Puls Width Modulation

RC Radio Control

RHA Rotor Head Assembly

RPM Round Per Minute

SMA SubMiniature version A

SNP Shaft Normal Plane

SPI Serial Peripheral Interface

TPP Tip Path Plane

UART Universal Asynchronous Receiver/Transmitter

UAV Unmanned Aerial Vehicle

Figures

FIGURES

Notations

FIGURES

Chapter 1

Introduction

1.1 Motivation

The modern society has evolved a great deal in just a few decades, which has led the world into a continuous search for energy. The high demands for energy force the industry to make use of new technology to keep the cost, at a minimum. The power industry have already begun searching for a cheaper way to inspect their power lines and are experimenting on the use of remote operated helicopters [8].

In the northern parts the race for oil has forced the oil sector to consider the use of drones and remote operated helicopters to perform some of the tasks when searching for new production areas. The use of big helicopters and air planes to deploy sensors, gather geographical data and inspect new production areas has become too expensive and time consuming. By deploying several small remote operated helicopters, the tasks could be performed faster and at a significantly lower cost.

Other industries that would benefit such technology are the mining industry. The mining industry searches for new minerals and precious metals in a continuously rapid pace. Since this kind of helicopter is cheap to build compared to a full-size helicopter, a dozen of these helicopters could be built and equipped with sensors for detecting minerals and metals. These helicopters could cover a much bigger area in the same time frame as a conventional helicopter.

The use of drones and small remote operated helicopters can also be used by researchers which often are dependent on rapid sensor deployment, gathering of geographical data

and area inspection. The researchers would then have a cheap and easy way to gain access to valuable sensor data which never before has been available to them.

The same technology can also be used to search for missing persons, where several remote controlled helicopters could be equipped with high resolution cameras. The helicopters could cover a vast search area a lot faster than the conventional methods used today, which again could help save lives.

Most of the ongoing experiments, which involves the use of remote controlled helicopters are mainly based on the use of standard battery driven big size quadcopters. A standard quacopter is a good helicopter that are mainly used on short missions in warm weather, to perform area photography and small inspection tasks. A quadcopter is depicted in figure 1.1.

Figure 1.1: Quadcopter - The quadcopter has four propellers with fixed pitch.

The quadcopter is equipped with fixed pitch propeller, which means that the rotor systems thrust is controlled by the motors rotational velocity. A quadcopter can never be equipped with petrol driven motors, since the rotational velocity of a petrol driven motor is very hard to control. The quadcopter is thereby limited to using battery as a main power source, which is not a very power efficient solution. This limits the quadcopter from performing long range missions, and missions in cold environments. When the quadcopter needs to move forward, it needs to raise the back of the quadcopter, and the movement is similar to a pendulum. This makes a precise positioning of the

quadcopter difficult, and in many cases useless. The tilting of the quadcopter also makes it impossible to attach wings to it, to increase the lift. The disadvantages of the quadcopter makes it unsuitable for the industry, which needs an fuel efficient helicopter that can perform long range missions in cold environments, and be positioned with high accuracy during inspection tasks. To accommodate the fuel efficiency the helicopter needs to be equipped with petrol driven motor, and it must be able to move in the horizontal direction without tilting. The helicopter can then be equipped with wings, which will increase its lifting capacity during flight and save fuel. Such a helicopter would be capable of operating in cold environments were it could deploying sensors, gather geographical data over vast areas, perform inspection task with high precision and operate over a large time frame.

1.2 Problem Statement and Thesis Objectives

The primary objective of this master thesis is to design and construct a remote operated helicopter that can perform the tasks mentioned above. Since the helicopter is supposed to carry extra weight, the helicopter must have a multi-rotor system. To accommodate the requirements of performing long range missions in cold environments and be fuel efficient, the helicopter must be equipped with petrol driven motors. This means that the thrust from the rotor systems cannot be dependent on the motors rotational velocity, and thereby it needs to be equipped with a rotor systems that have independent cyclic and collective pitch control. This allows the helicopter to control the thrust by pitching the rotor blades, which also gives it precise control features.

The cyclic pitch controls the horizontal movement by varying the pitch of the rotor blades throughout the 360 degree cycle, which is depicted in figure 1.2.
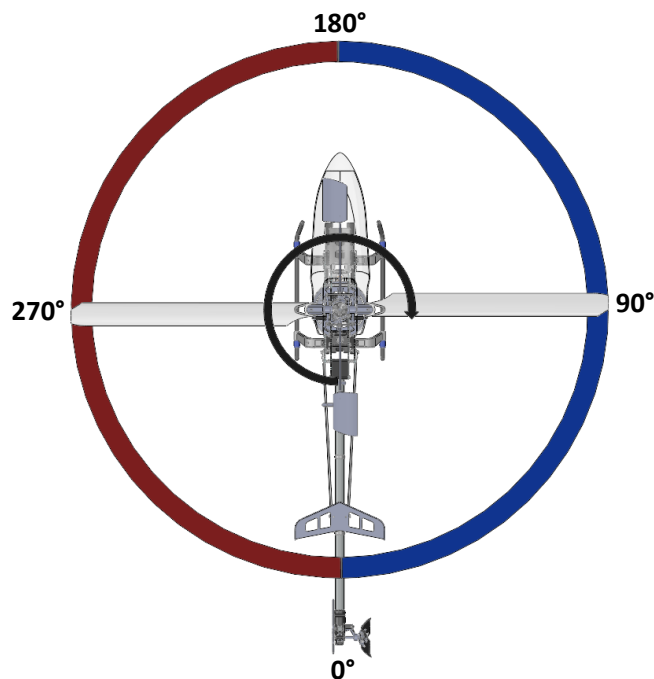
Figure 1.2: Helicopter - Cyclic pitch - The cyclic pitch controls the helicopter's horizontal movements by controlling the rotor blades pitch throughout the 360 degree cycle.

The collective pitch controls the helicopters vertical movement, by adjusting the pitch of the rotor blades, which is depicted in figure 1.3.

Figure 1.3: Helicopter - Collective pitch - The collective pitch controls the helicopter in the vertical direction. Both blades have equal pitch angle throughout the 360 degree cycle.

The last requirement, is that the helicopter can move horizontally. This is possible by using the helicopter's cyclic pitch, but the horizontal velocity would not be fast enough for the wings to create lift. The solution to this problem is to equip the helicopter with a tilt rotor system. This would ensure that the helicopter is moving fast enough in horizontal direction to create lift. The extra lift will compensate for the lower thrust when the rotors are tilted, and help save energy during long range missions. When the rotors are tilted the helicopter will be a combination between a tilt rotor air plane and a "Chinook" helicopter. A tilt rotor air plane is depicted in figure 1.4, while a "Chinook" is depicted in figure 1.5.

Figure 1.4: Tilt rotor airplane - The tilt rotor airplane has the possibility of rotating its propeller 90 degrees [9].

Figure 1.5: Chinook helicopter - The Chinook helicopter has two rotor blades, which rotates the opposite way of each other to counteract yaw movements [18].

Since it is difficult to test the helicopter with petrol driven motors, the prototype can be built with electric ones, without corrupting the concept.

The helicopter can be created by solving the subtasks given below.

1. The helicopter's lifting capacity is dependent on the lifting capacity of each of the rotor systems. A set of equations needs to be derived such that the required power for the rotor systems can be computed. The selection of the electric motor shall then be based on the results of these calculations, and used in the first prototype.

2. The helicopter's rotor system must be designed, and a working prototype built. The working prototype must be tested to verify the rotor systems lift capacity and properties. To test the rotor system, a test bench must be design and built. The test bench must be able to measure the rotor systems maximum lifting capacity and rotational velocity. It must also be built a buffer card which can transform the signals to and from the micro-controller, along with a suitable test software.

3. Before designing and building the helicopter, it must be simulated to verify its behavior and stability properties. A mathematical model of the helicopter must therefore be derived, such that it is possible to create a simulation model of the helicopter.

4. The mathematical model of the helicopter and the test results from the rotor system must then be used to simulate the helicopter stability properties and behaviour when subjected to crosswinds and downdrafts.

5. The next step before designing and building the helicopter is to design a system architecture, a hardware architecture and a software architecture. These architectures are necessary to have when building the helicopter. The architectures should propose a solution for how the helicopter can operate in autonomous and manual mode. The system architecture must give an overview of how the software and hardware operate together. The hardware architecture must give an overview on how all the hardware in the helicopter is connected together and how they communicate through the different communication interfaces. The software architecture must give an overview of the software's modular structure and describe the purpose of the different modules and how they interact.

6. If all the previous sub tasks has been completed with positive results, and if there is time, a prototype of the helicopter can be designed and built.

7. The last sub task in this project is to propose a control strategy that can be used to optimize the helicopters fuel/battery consumption.

1.3   Thesis Outline

The work done in this thesis after the introduction chapter is organized as follows:

In Chapter 2, the most common reference frames that are used in navigation systems are introduced.

Chapter 3, describes how some of helicopter functions are working. Further in this chapter two aerodynamic theories are presented and power formulas for the rotor system are derived.

In chapter 4, the required rotor power is computed. The equations used in this chapter are based on the aerodynamic equations derived in the previous chapter.

Chapter 5, introduce complete drawings of the rotor system in three different designs. The process of designing and building a prototype with all its difficulties are explained, and test results for the working prototype are presented.

In chapter 6, a dynamic model of the helicopter is derived.

In chapter 7, the dynamic model and the test results of the rotor system are used to create a realistic simulation of the helicopter. The simulations are used to detect the helicopter's stability properties and its behavior when subjected to winds and downdraft. This chapter also presents the results of the simulations.

Chapter 8, introduce a proposal of the helicopter's architectural designs; a system architecture, a hardware architecture and a software architecture. The system architecture shows how all the hardware and the software operate together. The hardware architecture describes how all the hardware components are linked together, and how they communicate through different interfaces. The software architecture give an overview of the software's modular structure and describes the purpose of the different modules and how they interact.

Chapter 9, introduce a design of the complete helicopter, along with the final product.

In chapter 10, a control strategy is proposed, which can be used to optimize the helicopter's fuel/battery consumption.

In chapter 11, the main results are presented and discussed.

In chapter 12, the main conclusion on this master thesis is presented.

Chapter 13, describes what needs to be done in the future, to finish this project.

Chapter 2

Kinematics

2.1 Reference Frames

In this chapter, the most common reference frames that are used in navigation systems will be introduced.

2.1.1 Earth Centered Frames

The Earth Center Earth Fixed (ECEF) frame has its origin located at the center of the earth and rotates with the earth, as depicted in figure 2.1. The x-axis is pointing towards the intersection of $0\,^{\circ}$ longitude *"Greenwich meridian"* and $0\,^{\circ}$ latitude *"Equator"*, the z-axis is pointing towards north and the y-axis completes the right hand orthogonal.

In contrast to the ECEF frame, the Earth Center Inertial (ECI) does not rotate with the earth, and thereby creates a time dependent angle ω_e between the two frames. The ECI frame is depicted in figure 2.1. The x-axis is pointing towards *"vernal equinox"*, while the z-axis is pointing towards north and the y-axis completes the right hand orthogonal. It is in the ECI frame that the Newton's laws of motion apply, and is used for terrestrial navigation.
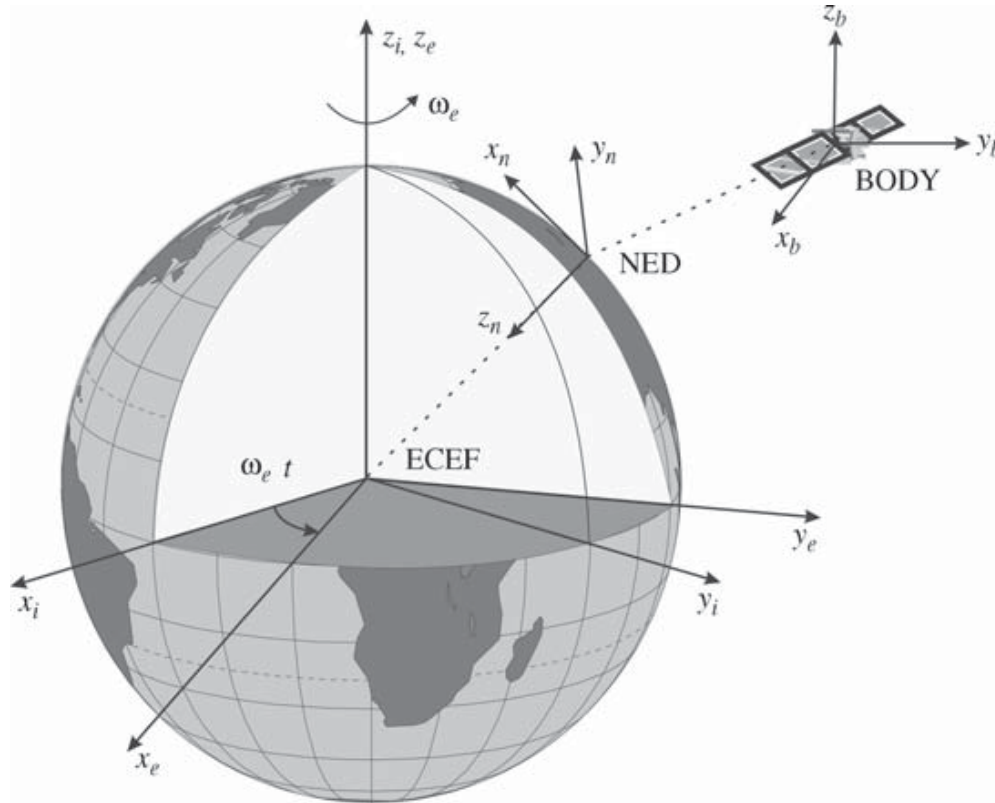
Figure 2.1: ECEF relationship to ECI - The figure shows how the ECEF frame relates to the ECI frame by an angle ω_e. The two frames coincide at $t = 0$ [4].

2.1.2 Geographical Coordinate Frame

The North-East-Down (NED) frame is sometimes referred to as the "local tangent plane", and is the coordinate system we refer to in our everyday lift. The NED frame has the; z-axis pointing downwards, perpendicular to the tangent of the ellipsoid, the x-axis pointing towards north and the y-axis pointing towards east. The NED frame is depicted in figure 2.1.

2.1.3 Helicopter Coordinate Frames

The Body frame is a moving coordinate frame that is fixed to the helicopter.
The origin coincides with the NED frame, where the x-axis pointing in the forward

direction, the y-axis pointing to the left and the z-axis downwards. The angular difference between the body frame and the NED frame is given by the Euler angles. The body frame on the helicopter is depicted in figure 2.2.
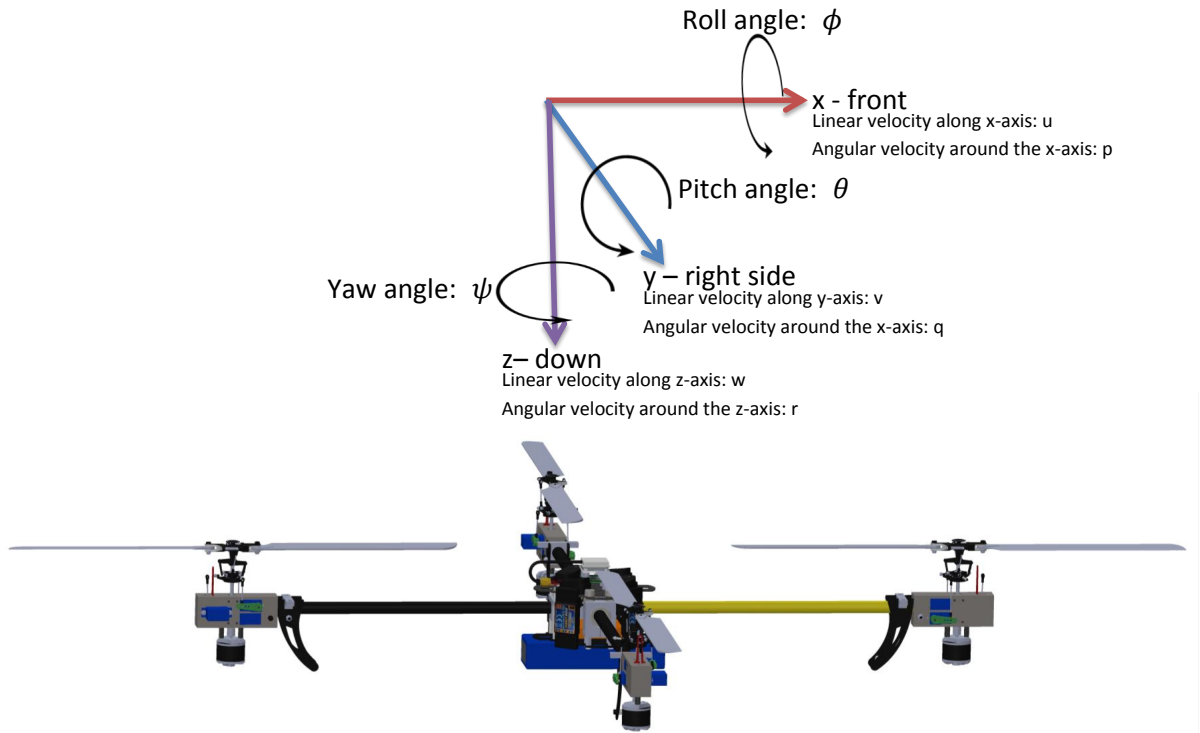
Figure 2.2: The helicopter's body frame - The helicopter's body frame has the; x-axis pointing towards the front (yellow boom), the y-axis pointing towards the right hand side and the z-axis pointing downwards.

The Platform frame (P-frame) for a strap-down system is attached to the helicopter and moves with it. The P-frames origin is usually located in the center of the accelerometer. In many situations, the platform frame is aligned with the body frame, and they are assumed to be identical.

The Instrument frame (I-frame) is where the accelerometer and the gyroscope measurements are valid. Ideally this frame should coincide with the platform frame, but because of misalignments it is not orthogonal or coincident with the platform frame. The small misalignment error can be eliminated by using an integrated GPS and INS system.

2.2 Degrees of freedom (DOF)

The degrees of freedom for a rigid body refer to the motion of the body frame in three dimensional spaces as depicted in figure 2.3.
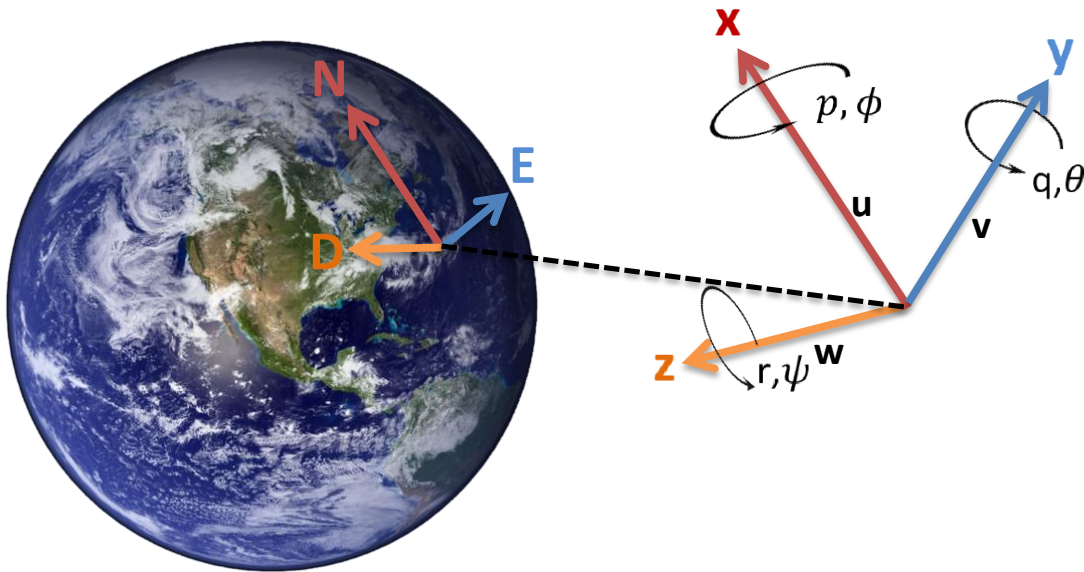
Figure 2.3: 6 Degrees Of Freedom (DOF) - The angles between the body frame and the NED frame are described by the three Euler angles ϕ, θ and ψ.

The motion of a rigid body is described by a translational and a rotational movement on the x, y and z axis. In figure 2.3, the notation u, v and w are the translational velocity, while p, q and r are the rotational velocity. The angle between the body frame and the NED frame are described by the three Euler angles ϕ, θ and ψ.

Chapter 3

Helicopter basics

3.1 Rotor properties

3.1.1 Cone angle

The lift force from a helicopters rotor system is created by the rotating rotor blades, which are assumed to be pitched. The lift force will change the rotor blades position from straight out to cone upwards. This creates an angle between the Shaft Normal Plane (SNP) and the rotor blade called "cone angle", which is depicted in figure 3.1.
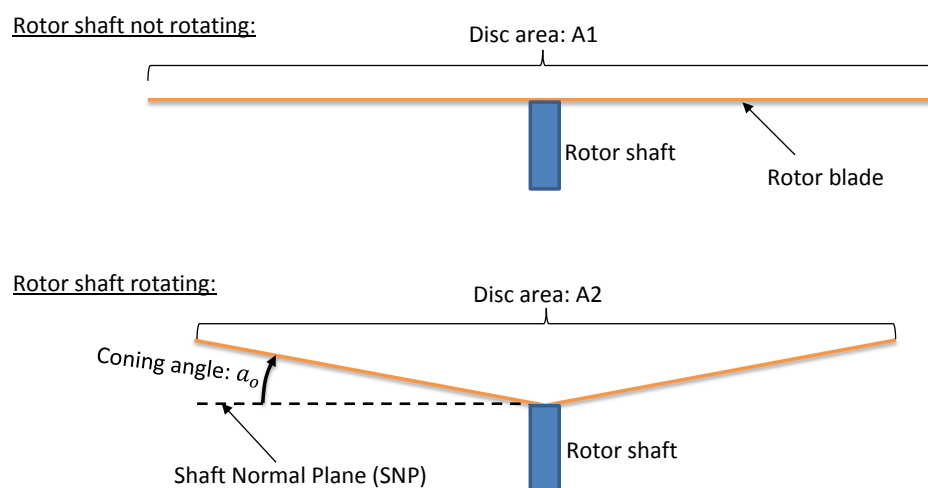
Figure 3.1: Rotor blade cone - The cone angle depends on; the rotor blades pitch angle and stiffness, the helicopter's overall weight and the G-forces it is subjected to during flight.

The cone angle is dependent upon the rotor blades pitch angle and stiffness, the helicopter's overall weight and the G-forces it is exposed to during flight. If the rotor blade pitch is constant, the cone angle will increase as the weight or G-forces increase. If the rotor blade pitch increment and the total weight and G-forces are consistent, the cone angle will increase. The cone angle directly affects the rotor disc area as depicted in figure 3.1.

3.1.2 Asymmetric lift

A helicopter's rotor blades can be turned 360 degrees, which creates a fictional "rotor disc". The rotor disc is divided into two parts, with respect to the helicopter's flight direction. In forward flight, the rotor disc is divided along the longitudinal axis of the helicopter. If the rotor blades are rotating clockwise, the right hand side is called the "Retreating blade area", while the left hand side is called the "Advancing blade area". This is depicted in figure 3.2. The opposite is true if the rotor blades are rotating counter clockwise.
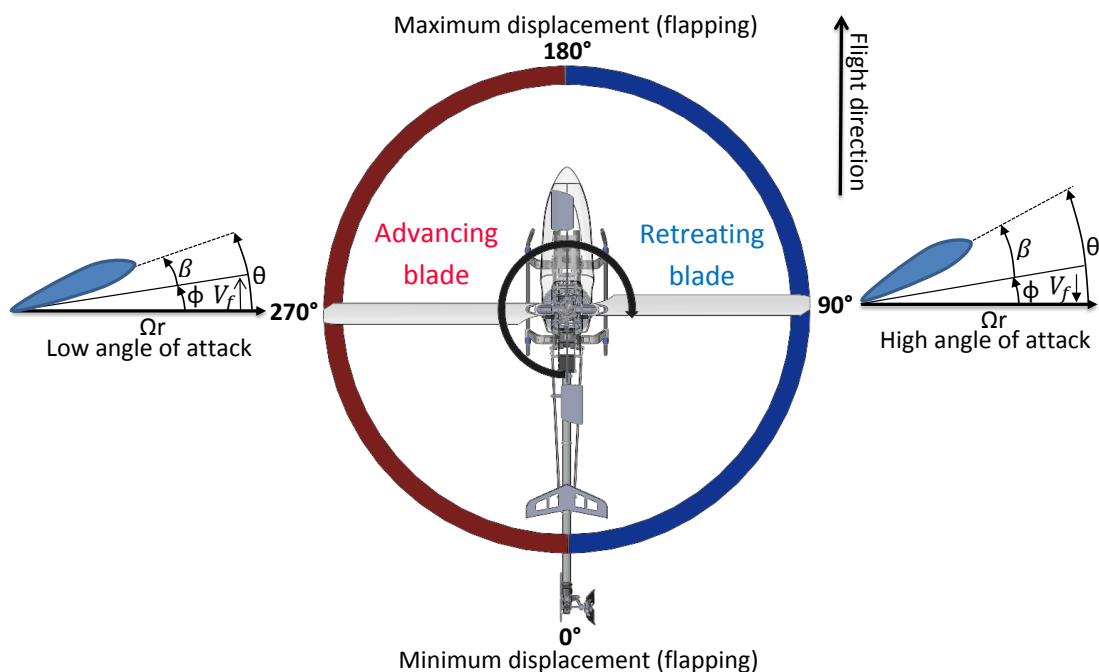
Figure 3.2: Advancing/Retreating blade - The blade advances in the red area, and retreats in the blue area.

When a helicopters rotor blades are rotating they switch between the two sides. A helicopter in hover creates equal amount of lift across the entire rotor disc, which makes the helicopter stable. When the helicopter is moving in any direction, the helicopter experience an asymmetry lift over the rotor disc.

The advancing blade (left hand side) creates more lift than the blade on the retreating side (right hand side), which causes the helicopter to become unstable. A dynamically unstable helicopter is impossible to fly, but there is a solution to the problem called "blade flapping".

3.1.3 Blade flapping

The rotor head is designed to allow the rotor blades to move up and down during flight. This function is called "blade flapping" and serves two purposes on a helicopter. The first function is to balance the amount of lift on the advancing and retreating area of the rotor disc. The second function allows the rotor blades to move in vertical direction independently, which allows the two blades to create an angled Tip Path Plane (TPP). The angled TPP makes the helicopter capable of flying in any horizontal directions with out tilting the helicopter. The angled TPP is shown in figure 3.3.
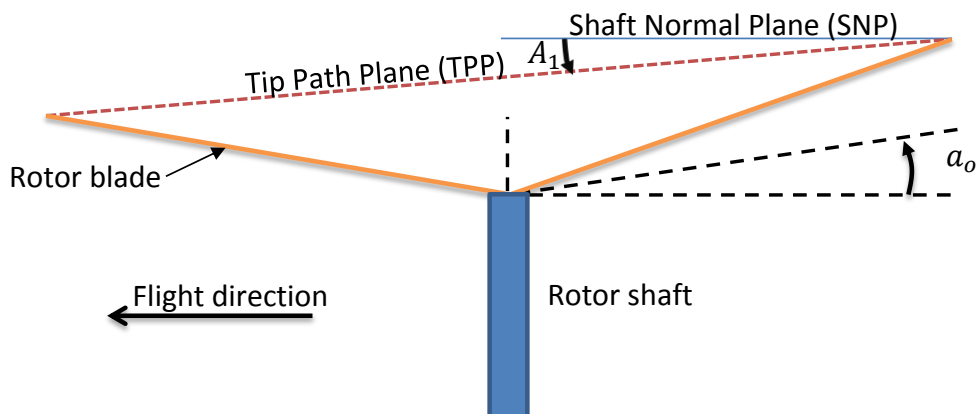
Figure 3.3: Blade flapping - The blade flapping stabilizes the lift over the rotor disc and allows the helicopter to fly in any horizontally directions without tilting the helicopter. The angle A_1 is the forward tilt angle while B_1 is the sideways tilt angle (not depicted)

In forward flight, the blade on the advancing area is subjected to an increase in the

air velocity, which creates more lift. To counteract this unbalance, the blade flapping allows the rotor blades to be pushed upwards (by the air resistance), and as a result, the angle of attack is reduced, and the lift is decreased. The opposite applies to the retreating side, and thereby keeping the lift balanced. This phenomenon also appear when the helicopter is flying side-ways.

An important thing to understand about blade flapping is that, in forward flight the flapping velocity V_f is at its maximum and minimum at 90° and 270° azimuth, respectively. This means that the blades will continue in the same vertical direction after they have passed 90° and 270°. In practice, the maximum displacement occurs 90° later, at 180° (front), and the minimum displacement occurs at 0° (back). The 90° offset is shown in figure 3.2.

The helicopter's rotor head is designed to compensate for the 90° offset, by adding the desired pitch angle 90° earlier. That is; if the swashplate is tilted forward in the longitudinal direction of the helicopter, the helicopter will fly forward.

3.1.4 Feathering shaft

The mechanical part that allows the blades to flap is called a "feathering shaft" and is located in the rotor head. The feathering shaft connects the rotor heads two blade grips and permits them to rotate along their center axis. The feathering shaft is not firmly attached to the rotor head, which allows the rotor blades a certain degree of movement called "blade flapping".

3.1.5 Disc angle of attack

The Disc Angle of Attack (DAoA) is the helicopter's pitch angle combined with the rotor's flapping angle. Since the helicopter has four independent rotors, it is possible to have different flapping angles on each rotor. In this project, it is assumed that the flapping angles are equal, which would be the case most of the time. A picture illustrating the disc angle of attack is shown in figure 3.4.
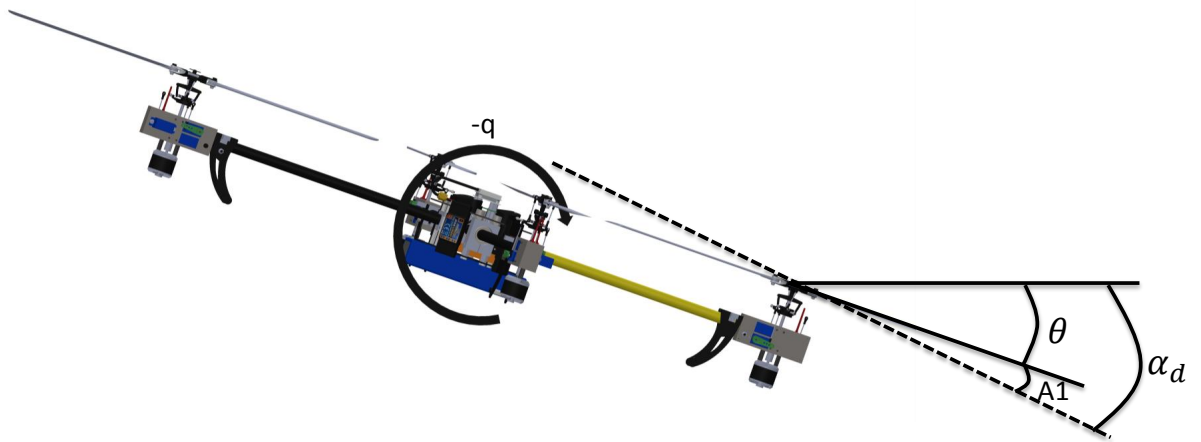
Figure 3.4: Disc angle of attack - The DAoA angle α_d consist of the helicopter's pitch angle θ and the flapping angle $A1$.

3.1.6 The swashplate

A helicopter swashplate is responsible for controlling a helicopter's collective pitch (up and down movements) and cyclic pitch (directional movement). When the swashplate is in a level position, the collective pitch can be controlled by raising or lowering the swashplate. The lowering and raising of the swashplate is shown in figure 3.5.

The cyclic pitch, or directional movement is controlled by tilting the swashplate in the direction the operator wants the helicopter to go. Tilting of the swashplate is depicted in figure 3.6.
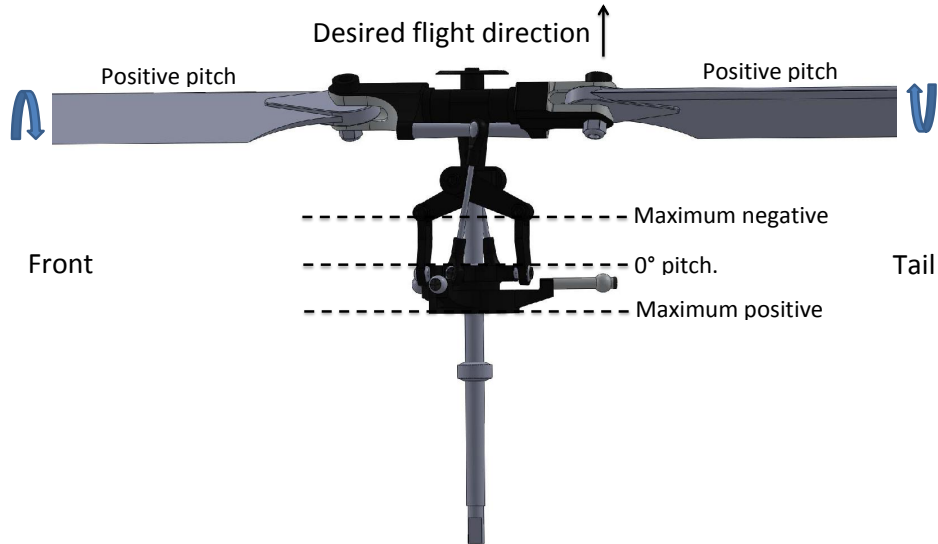
Figure 3.5: Swashplate - Collective pitch - The swashplate controls the up and down movements of the helicopter. The swashplate in the figure is at maximum pitch, and the movement will be upwards
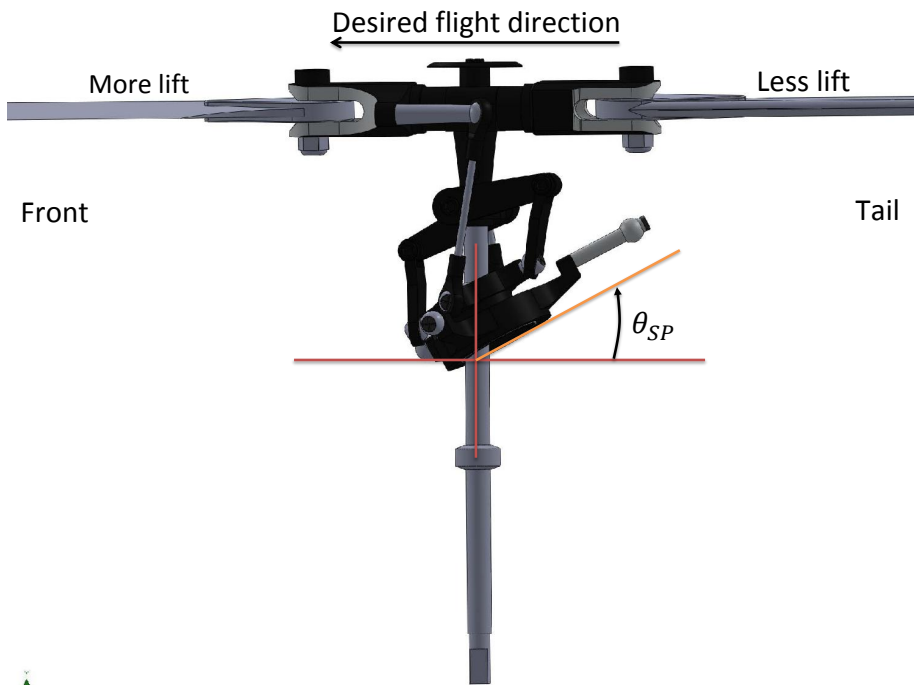
Figure 3.6: Swashplate - Cyclic pitch - The swashplate controls the directional movements of the helicopter. The swashplate is tilted with an angle θ_{SP}, which will make the helicopter fly forward.

3.2 Rotor Aerodynamics

The knowledge of helicopter dynamics has reached an exceptionally high level compared to a few decades ago, and as a result, the helicopter's performance has increased considerably. The use of analytic theories, experiments and numerical modeling has led to a better understanding of the helicopter's different aerodynamic problems.

The behavior of a helicopter's rotor blades is an important part of understanding a helicopter's dynamic behavior, and can be determined by using the two different theories; the Momentum Theory (MT) and the Blade Element Theory (BET). One of the more difficult aspects of rotor aerodynamic is modeling the air speed through the main rotor, called the "induced velocity". The induced velocity can be mathematical described by combining the two theories (BET and MT).

The two theories can also be used to compute how much power the helicopter's rotor system needs to fly. The rotor system requires a great deal of power, and most of it is used by the four BLDC (BrushLess Direct Current) motors. A more thorough explanation of the BET and MT can be found in the literature [11][15].

3.2.1 Momentum theory

The momentum theory is often referred to as the disc actuator theory and is used to analyze propellers, rotors and ducted fans. The theory uses mathematics to describe an infinitely thin actuator disc, which in this project is the helicopter's rotor disc. It uses the conservation laws of momentum, mass and energy on a control volume surrounding the rotor disc. The control volume is depicted in figure 3.7.

The laws are then used to prove a mathematical link between power, rotor radius, induced velocity and torque.

The rotor wake is a complex fluid dynamic air flow in 3 dimensions, and the conservation laws can only be used by making some assumptions:

- The flow must be incompressible, irrational and in viscid.

- The flow must be one-dimensional and uniform through the rotor disc and in the far wake.
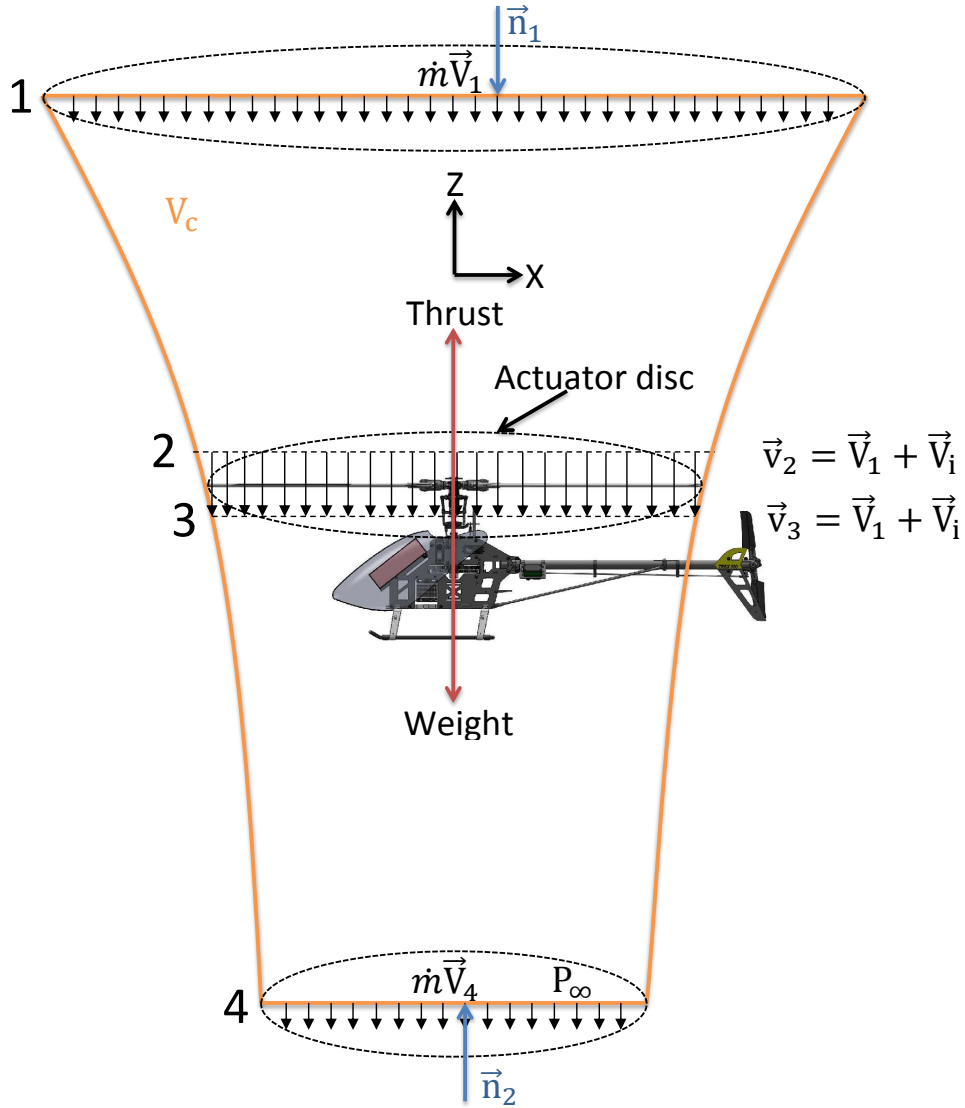
Figure 3.7: Rotor wake - A helicopter's rotor wake when the helicopter is hovering.

The linear momentum equation on the general form is given by [2]:

$$\sum \vec{F} = \frac{d}{dt} \int_{CV} \rho \vec{V} \, \mathrm{d}V + \int_{CS} \rho \vec{V} (\vec{V}_r \cdot \vec{n}) \, \mathrm{d}A \tag{3.1}$$

The momentum theory studies a special case within the control volume (V_c), where the flow is steady, and the amount of momentum is constant.

This special case makes the first term in equation 3.1 zero, and the equation becomes [2] :

$$\sum \vec{F} = \int_{CS} \rho \vec{V} (\vec{V}_r \cdot \vec{n}) \, \mathrm{d}A \tag{3.2}$$

Equation 3.2 can be rewritten to algebraic form, which makes it much more convenient to solve practical engineering problems [2]:

$$\int_A \rho \vec{V} (\vec{V} \cdot \vec{n}) \, \mathrm{d}A = \rho V_{avg} A \vec{V}_{avg} = \dot{m} \vec{V}_{avg} \tag{3.3}$$

The steady linear momentum equation for one-dimensional flow is given by [2]:

$$\sum \vec{F} = \sum_{in} \beta \int_A \rho \vec{V} (\vec{V} \cdot \vec{n}) \, \mathrm{d}A - \sum_{out} \beta \int_A \rho \vec{V} (\vec{V} \cdot \vec{n}) \, \mathrm{d}A \tag{3.4}$$

$$= \sum_{out} \beta \dot{m} \vec{V} - \sum_{in} \beta \dot{m} \vec{V} \tag{3.5}$$

The symbol β is the momentum-flux correction factor, which are used when the velocity is not uniform across the inlets or outlets. Note that the sign of the momentum flux in and out is dependent on the direction to the unity vector n_1 and n_2 in figure 3.7.

In this case where the flow is steady, equation 3.4 can be transformed to algebraic form by using equation 3.3 and $\beta = 1$.
This gives us:

$$F_{thrust} - F_{weight} = \dot{m}_2 \vec{V}_4 - \dot{m}_1 \vec{V}_1 \tag{3.6}$$

Where $\vec{V}_1$ and $\vec{V}_2$ are average velocities.

The mass conservation through the rotor disc gives us:

$$\dot{m} = \rho A (V_1 - v_2) = \rho A (V_1 - v_3) = \rho A_4 (V_1 - V_4) \tag{3.7}$$

This means that $v_2 = v_3$, and that there is no velocity jump through the rotor disc. In other words the induced velocity V_i is the same above and beneath the rotor disc.
The thrust from the rotor disc is generated by the rate of change in momentum, and can be calculated by using [15]:

$$T = \rho A V_i V_4 \tag{3.8}$$

$$= \dot{m} V_4 \tag{3.9}$$

The generated thrust can also be expressed by the pressure difference below and above the rotor disc[15]:

$$T = A(P_3 - P_2) \tag{3.10}$$

The pressure above and below the rotor disc can be found by applying Bernoulli's equation, but it cannot be used through the rotor disc. The Bernoulli's equation from far above (∞) the rotor disc to section point 2 is given by[2][15]:

$$P_\infty + \frac{1}{2}\rho V_4^2 + \rho g z_4 = P_2 + \frac{1}{2}\rho V_i^2 + \rho g z_1 \tag{3.11}$$

Solving for the pressure P_∞ gives us[15]:

$$P_\infty = P_2 + \frac{1}{2}\rho V_i^2 \tag{3.12}$$

While the pressure below the rotor is given by[15]:

$$P_3 + \frac{1}{2}\rho V_i^2 = P_\infty + \frac{1}{2}\rho V_4^2 \tag{3.13}$$

Since the pressure difference ΔP is assumed to be uniform across the actuator disc, it must be equal to the disc loading T/A [11]:

$$\Delta P = P_3 - P_2 = \frac{T}{A} \tag{3.14}$$

Inserting equation 3.12 into 3.13 and rearranging it, gives us[15]:

$$P_3 - P_2 = \frac{1}{2}\rho V_4^2 \tag{3.15}$$

Combining equation 3.8, 3.10, 3.15 gives us [15]:

$$V_4 = 2V_i \tag{3.16}$$

This means that the air speed far down the wake is twice the induced air speed.

If we now combine equation 3.14, 3.15 and 3.16, the induce velocity becomes:

$$V_i = \sqrt{\frac{T}{2\rho A}} = \sqrt{\frac{1}{2\rho}}\sqrt{\frac{T}{A}} \tag{3.17}$$

This shows that the induced velocity is dependent upon the disc loading term ($w_L = T/A$).

To see how the pressure above and below the rotor head depends on the disc loading term, equation 3.12 is combined with 3.17.

The pressure above the rotor head can then be written as:

$$P_2 = P_\infty - \frac{1}{2}\rho V_i^2 \tag{3.18}$$

$$= P_\infty - \frac{1}{4}\frac{T}{A} \tag{3.19}$$

Inserting equation 3.16 and 3.17 into equation 3.13 gives us the pressure below the rotor head:

$$P_3 = P_\infty + \frac{1}{2}\rho(2V_i)^2 - \frac{1}{2}\rho V_i^2 \tag{3.20}$$

$$= P_\infty + \frac{3}{2}\rho V_i^2 \tag{3.21}$$

$$= P_\infty + \frac{3}{4}\frac{T}{A} \tag{3.22}$$

This shows how important the disc loading factor is.

The ideal induced power required for a helicopter to hover is given by[15]:

$$P_i = TV_i \tag{3.23}$$

The equations 3.8 and 3.16 can now be inserted into equation 3.23, which give us:

$$P_i = TV_i = \rho AV_i V_4 V_i = 2\rho AV_i^3 \tag{3.24}$$

This proves that the ideal power required to hover increases with the cube of the induced velocity. Since the induced power is the majority of the power consumption in hover (shown later), the disc loading is one of the first items to be considered when designing a rotor system. A lower disc loading factor leads to a more efficient rotor with a higher performance.

3.2.1.1   Power requirement

The ideal induced power is the majority of the power needed for the helicopter to hover. To compensate for some of the other losses that exists a ratio is introduced. The ratio between the ideal induced power and the actual induced power is called "figure of merit" and denoted M.

The figure of merit is given by [11]:

$$M = \frac{Ideal\ induced\ power}{Actually\ induced\ power} = \frac{P_i}{k_i P_i + P_p} = \frac{P_i}{P_{hov}} \qquad (3.25)$$

In an ideal situation, the down-wash or induced velocity is constant. Since this is not true in reality, a factor called " induced power factor" k_i is introduced in equation 3.25.

The total required power for the helicopter to hover becomes:

$$P_{hov} = \frac{P_i}{M} \qquad (3.26)$$

3.2.2   Blade element theory

The blade element theory divides a rotor blade into thin sections and analyzes the forces acting on them. A rotor blade section is depicted in figure 3.8.
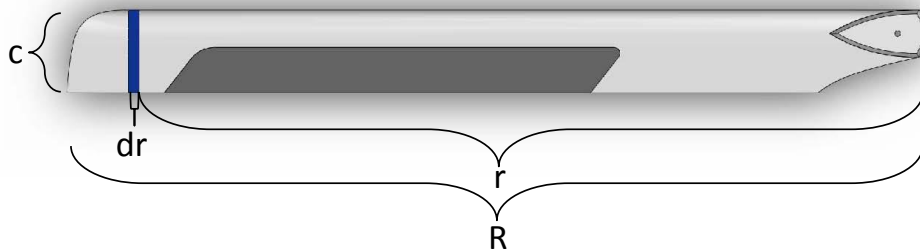
Figure 3.8: Rotor blade - The blade element theory analyze a small section of the rotor blade.

The forces acting on each section is divided into lift (dL) and drag (dD) forces as depicted in figure 3.9

The sum of the forces created by the rotor blades are found by integrating along the

blades and around one revolution.
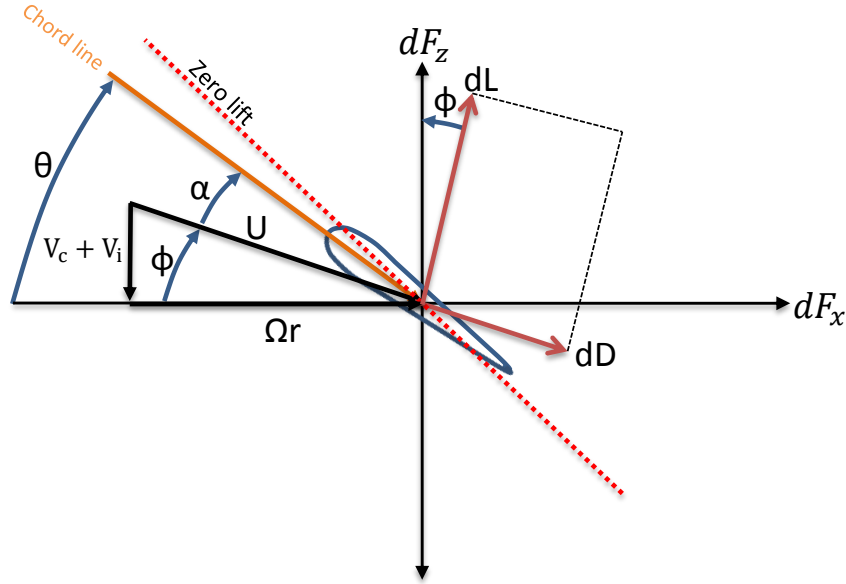
Figure 3.9: Blade element theory - Forces acting upon an infinitely small section of the propeller blade [11].

In figure 3.9; the velocity V_c is the helicopter's climb speed while V_i is the induced velocity. The angle θ is the pitch angle which has an upper critical value (dotted red), where the blade cannot produce lift anymore. The angle α is the Angle Of Attack (AoA), which is the angle between the blades chord line and the resultant line.

The angle of attack (AOA) is given by [15]:

$$\alpha = \theta - \phi = \theta - \frac{V_c + V_i}{\Omega r} \tag{3.27}$$

The air inflow angle ϕ is the angle between the resultant line and the x-axis and is described by[15]:

$$\phi = tan^{-1} \left| \frac{V_c + V_i}{\Omega r} \right| \underbrace{\approx}_{\phi \approx 0} \frac{V_c + V_i}{\Omega r} \tag{3.28}$$

The resultant velocity U is given by the rotor disc velocity (Ωr) and the perpendicular velocity ($V_c + V_i$) [15]:

$$U = \sqrt{(V_c + V_i)^2 + (\Omega r)^2} \tag{3.29}$$

The lift and drag forces for the section is given by [15]:

$$dL = \frac{1}{2}\rho U^2 C_L c \; dr \tag{3.30}$$

$$dD = \frac{1}{2}\rho U^2 C_D c \; dr \tag{3.31}$$

Where C_L and C_D are the lift coefficient and the drag coefficient, respectively, and c is the blade chord as depicted in figure 3.8.

The thrust for the small section of the propeller blade can now be written as[15][1] :

$$dT = dL \cos \phi - dD \sin \phi \tag{3.32}$$

And the elements blade torque is[15]:

$$dQ = (dL \sin \phi - dD \cos \phi)r \tag{3.33}$$

The air inflow angle ϕ can be assumed to be small. This might not be true near the root blade where Ωr is small, but the blade load it self is also quite small in this area. With this assumption, it is possible to do some approximation[15]:

$$U \simeq \Omega r \tag{3.34}$$

$$dT \simeq dL \tag{3.35}$$

$$dQ \simeq (\phi dL + dD)r \tag{3.36}$$

The blade element power can then be described by:

$$dP = dQ \cdot \Omega = (\phi dL + dD)\Omega r \tag{3.37}$$

Assuming that $\alpha = 0$ and $\sin \phi \approx \phi \approx \tan \phi = V_i/\Omega r$, gives us:

$$dP = (\phi dL + dD)\Omega r \tag{3.38}$$

$$= (dL \cdot \frac{V_i}{\Omega r} - dD)\Omega r \tag{3.39}$$

$$= V_i dT + \Omega r dD \tag{3.40}$$

The total power can now be found by integrating along the rotor blades and multiply it by the number of rotor blades [1]:

$$P = N \left(\int_0^R V_i \ \mathrm{d}T + \int_0^R \Omega r \ \mathrm{d}D \right) = P_i + P_p \tag{3.41}$$

The power is separated into the induced power P_i and the power needed to compensate for the drag of the propeller blades. The induced power can be approximated by using $P_i = k \ P_{i_{ideal}}$, where k is often set to 1.2 [1].

If we extract the equation for P_p and insert equation 3.31 we get [1]:

$$P_p = N \ \int_0^R \Omega r \ \mathrm{d}D \tag{3.42}$$

$$= N \ \int_0^R C_{d_r} \ \frac{1}{2} \rho (\Omega r)^3 \ c \, \mathrm{d}r \tag{3.43}$$

$$= \frac{1}{8} \bar{C}_{d_r} \rho \sigma (\Omega R)^3 \pi R^2 \tag{3.44}$$

The symbol $\bar{C}_{d_r}$ is the rotor blades mean drag coefficient, and σ is called "rotor solidity". The rotor solidity is a factor based on the difference between the surface area of the rotor blades (nRc) and the surface area of the actuator disc (πR^2) and is defined as [1]:

$$\sigma = \frac{NcR}{\pi R^2} = \frac{Nc}{\pi R} \tag{3.45}$$

3.2.2.1 Horizontal flight

In the previous subsection, an analysis was performed based upon the required power for helicopter to hover. In this section, the required power for a helicopter to fly horizontally in any direction, will be computed. The helicopter's horizontal flight direction is decided by the helicopter's swash plate (see section 3.1.6 for more information). In a forward flight with the rotor head rotating in the clockwise direction, the tilted swash plate makes the rotor blades increase their pitch as they pass 90° and lower the pitch as they pass 270°. This will generated more lift at the back of the helicopter then in the front of the helicopter. The lift generated is depicted in figure 3.10. When the lift difference is quite small, the flapping function allows the helicopter to move in any horizontal direction without tilting.
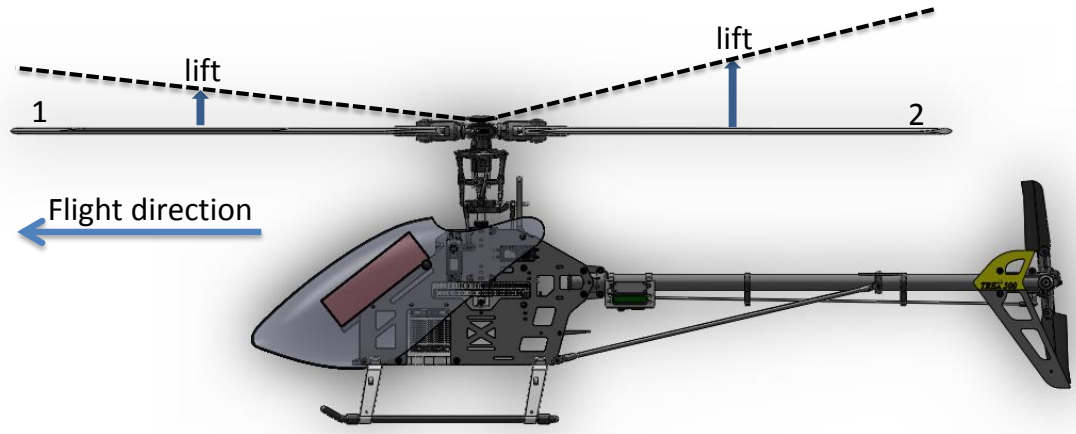
Figure 3.10: Forward flight - horizontal - When the helicopter's swashplate is tilted forward, the lift generated at the back of the helicopter is higher than the lift generated in front of the helicopter. The dotted lines represent the blades when the swashplate is tilted.

When the lift difference increase and the moment of inertia around the y-axis is overcome, the helicopter will tilt forward. This results in an increased forward velocity as depicted in figure 3.11. The rotor heads thrust is now divided into an x and z com-
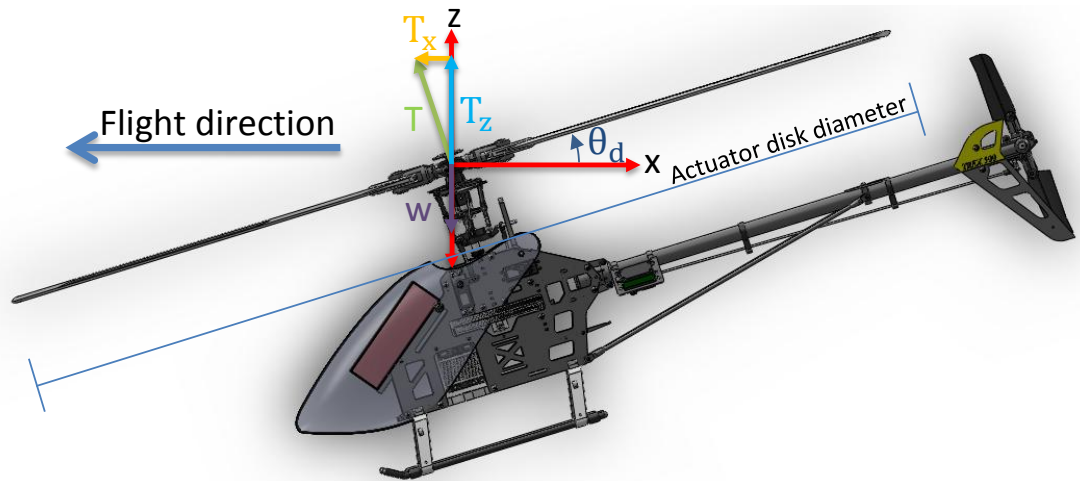
Figure 3.11: Forward flight - tilted - When the helicopter's cyclic pitch is increased at the tail and the inertia is overcome, the helicopter will tilt counter clock-wise and move forward. The opposite is true when increasing the cyclic pitch over the helicopter's nose.

ponent, which means that the thrust must be increased for the helicopter to maintain its altitude. In figure 3.11; the letter W is the helicopter's weight, T_z is the thrusts z-component, T_x is the thrusts x-component and the angle θ_d is helicopter's desired

48

pitch angle.

When the helicopter is hovering, it is subjected to drag forces acting on the fuselage, due to the rotor blades down-wash.

When the helicopter is moving, the helicopter is subjected to two additional drag forces. The first drag is the one acting upon the helicopter's fuselage and is called the "Parasite drag". The second drag force H_0 is the one acting upon the rotor disc.

The total amount of power required is given by [1]:

$$kTV_i + P_p + H_0V + D_{par}V = P_i + P_p + P_{drag} + P_{par} \tag{3.46}$$

Where P_i is the ideal power required to lift the helicopter, P_p is profile power required to overcome the profile drag of the rotor blades, P_{drag} is the power required to overcome the drag acting on the rotor disc and P_{par} is the power required to overcome the drag acting on the fuselage.

The profile drag P_p can be calculated using the "blade element theory", but there are now more elements to consider than just the distance from the center to the tip of the rotor blade. The velocity is also dependent on the azimuth angle ψ which is the angle between the back of the helicopter and the rotor blades position as depicted in figure 3.12.
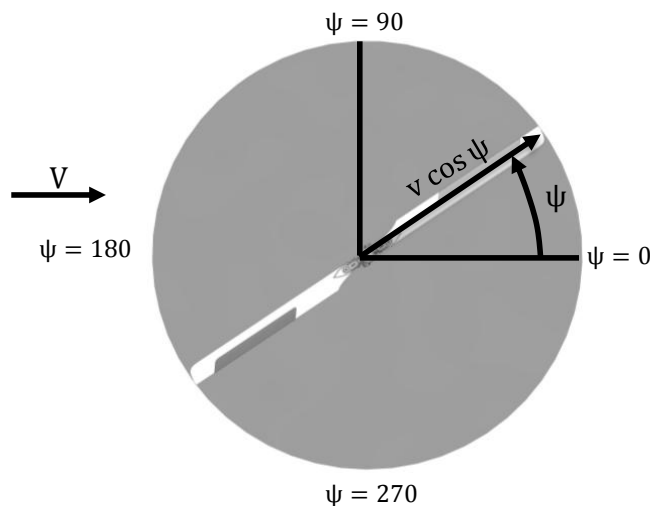
Figure 3.12: **Azimuth angle** ψ - The angle ψ is the angle between the back of the helicopter and the rotor blades position.

49

The velocity at the rotor tip is now given by:

$$V_r = \Omega R \pm V \cos \, \psi \tag{3.47}$$

Where the advancing blade use plus and retreating blade minus.

In general the formula can be written as [1]:

$$V_r = \Omega R \pm V \cos \psi_d \, \sin \mu \tag{3.48}$$

Where μ is called "the advance ratio", which is the ratio between the forward flight speed and the tip speed of the rotor blades. The maximum speed of the helicopter is reached when the pitch of the retreating rotor blade is at maximum. In practice μ is set to ≈ 0.3 [1].

$$\mu = \frac{V \cos \alpha_d}{\Omega R} \tag{3.49}$$

The power required to compensate for the profile drag P_p is given by [1]:

$$P_p = \frac{n}{2\pi} \int_0^{2\pi} \left(\int_0^R \frac{1}{2} C_{d_p} \rho (\Omega r + V \cos \alpha_d \sin \mu)^2 c \Omega r \, \mathrm{d}r \right) \mathrm{d}\psi \tag{3.50}$$

$$= \frac{1}{8} \bar{C}_{d_p} \sigma \rho (\Omega R)^3 \pi R^2 (1 + \mu^2) \tag{3.51}$$

$$= P_{p_{hov}} (1 + \mu^2) \tag{3.52}$$

This is actually the average profile power since it is divided by 2π. The required profile power in equation 3.44 is a part of equation 3.50, and can be written as:

$$P_{p_{hov}} = \frac{1}{8} \bar{C}_{d_p} \sigma \rho (\Omega R)^3 \pi R^2 \tag{3.53}$$

The complete set of equations derived in this chapter will be used to calculate the required power for the helicopter in chapter 4.

Chapter 4

Rotor power

The selection of the motors for the helicopter must be based upon the necessary required power. The BLDC motor that drives the main rotor system must be powerful enough so it is possible to fly the helicopter in a safe manner. The necessary power to operate the helicopter can be computed by using the formulas given in section 3.2.

The specified maximum mass for the helicopter in standard configuration (tilt system not active) is:

$$m_{max} = m_{heli} + m_{equip} = 1.4\,|kg| + 1.1\,|kg| = 2.5\,|kg| \tag{4.1}$$

Since the helicopter has four rotors, the mass per rotor becomes:

$$m_r = \frac{m_{tot}}{4} = 0.625\,|kg| \tag{4.2}$$

The weight pr rotor is then:

$$W_r = m_r g = 0.625\,|kg| \cdot 9.81\,\left|\frac{m}{s^2}\right| = 9.81\,\left|\frac{kg \cdot m}{s^2}\right| = 6.1313N \approx 6N \tag{4.3}$$

The diameter of the rotor disc is 460mm, which give us an induced velocity of:

$$V_i = \sqrt{\frac{W_r}{2\rho A}} = \sqrt{\frac{6.1313\,\left|\frac{kg \cdot m}{s^2}\right|}{2 \cdot 1.225\,\left|\frac{kg}{m^3}\right|\,(\frac{\pi \cdot 0.46^2 |m^2|}{4})}} = 3.8805\,\left|\frac{m}{s}\right| \approx 3.90\,\left|\frac{m}{s}\right| \tag{4.4}$$

4.1 The rotor's angular velocity

Some of the equations given in section 3.2 is dependent on the rotor's angular velocity, which means that the rotor's angular velocity must be computed first.

The rotor's lift force is given by:

$$L = \frac{1}{2}\rho C_L U^2 A \tag{4.5}$$

Rearranging equation 4.5 with respect to U gives us:

$$U^2 = \frac{2L}{\rho A C_L} \tag{4.6}$$

Inserting equation 3.29 into equation 4.6, which becomes:

$$(V_c + V_i)^2 + (\Omega R)^2 = \frac{2L}{\rho A C_L} \tag{4.7}$$

Rearranging equation 4.7 with respect to ΩR gives:

$$(\Omega R)^2 = \left(\frac{2L}{\rho A C_L}\right) - (V_c + V_i)^2 \tag{4.8}$$

Isolating Ω gives:

$$\Omega = \sqrt{\frac{\left(\frac{2L}{\rho A C_L}\right) - (V_c + V_i)^2}{R^2}} \tag{4.9}$$

Inserting the rotor blades area $A = 2Rc$ give us:

$$\Omega = \sqrt{\frac{\left(\frac{L}{\rho R c C_L}\right) - (V_c + V_i)^2}{R^2}} \tag{4.10}$$

Inserting $V_c = 0$ since the vertical climb speed is zero when the helicopter is hovering:

$$\Omega = \sqrt{\frac{\left(\frac{2L}{\rho R C_L c}\right) - V_i^2}{R^2}} \tag{4.11}$$

Exchanging L with W_r since they are equal when the helicopter is hovering:

$$\Omega = \sqrt{\frac{\left(\frac{2W_r}{\rho R C_L c}\right) - V_i^2}{R^2}} \tag{4.12}$$

The angular velocity can now be compute by using the following parameter setting; $W_r = 6.1313 \,|N|$, $R = 0.23 \,|m|$, $c = 0.021 \,|m|$, $C_L = 0.4$, $V_i = 3.8805 \,|m/s|$ and $\rho = 1.2 \,|kg/m^3|$.

The the lift coefficient C_L is it usually has a value between 0.4 and 0.8 [11].

The angular velocity becomes:

$$\Omega = \sqrt{\frac{\left(\frac{6.1313|N|}{1.225\left|\frac{kg}{m^3}\right| \cdot 0.23|m| \cdot 0.4 \cdot 0.021|m|}\right) - (3.8805\left|\frac{m}{s}\right|)^2}{(0.23\,|m|)^2}} = 220.6536\left|\frac{rads}{s}\right| \approx 220\left|\frac{rads}{s}\right| \tag{4.13}$$

The angular velocity in Rounds Per Minute (RPM) is given by:

$$\Omega = \frac{60 \cdot \Omega}{2 \cdot \pi} = \frac{60 \cdot 220.6536\left|\frac{rads}{s}\right|}{2 \cdot \pi} = 2107.0865\,|rpm| = 2107\,|RPM| \tag{4.14}$$

4.2 Power calculation - hover

Ideal power required to hover

Since $T_r = W_r$ in hover, the ideal power required for the helicopter to hover is given by:

$$P_{ideal} = V_i \cdot W_r = 3.8805\left|\frac{m}{s}\right| \cdot 6.1313N\,|N| = 23.7925\,|W| \approx 23.80\,|W| \tag{4.15}$$

For most modern helicopter's the figure of merit is 0.7 [1], and the real power required to hover becomes:

$$P_{hov} = \frac{P_{ideal}}{M} = \frac{23.7925\,|W|}{0.7} = 33.9893\,|W| \approx 34\,|W| \tag{4.16}$$

This is the power required for the helicopter to hover if drag forces are not part of the equation.

Power required to overcome drag forces in hover

The power required to overcome drag forces of the rotor blades are called "profile power", and can be computed by assuming a drag coefficient between 0.04 and 0.06 [11].

The following parameters are used to compute the drag force; $N = 2$, $R = 0.23\,|m|$, $c = 0.021\,|m|$, $\bar{C}_{d_r} = 0.06$ and $\rho = 1.2\,\big|kg/m^3\big|$. The rotor solidity is then given by:

$$\sigma = \frac{Nc}{\pi R} = \frac{2 \cdot 0.021\,|m|}{\pi \cdot 0.23\,|m|} = 0.05812 \tag{4.17}$$

and the required profile power becomes:

$$P_p = \frac{1}{8}\bar{C}_{d_r}\rho\sigma(\Omega R)^3\pi R^2 \tag{4.18}$$

$$= \frac{1}{8} \cdot 0.06 \cdot 1.225\,\left|\frac{kg}{m^3}\right| \cdot 0.05812 \left(220\,\left|\frac{rads}{s}\right|(0.23\,|m|)\right)^3 \pi \cdot (0.23\,|m|)^2 \tag{4.19}$$

$$= 11.4969\,|W| \approx 11.50\,|W| \tag{4.20}$$

The total power required to hover

The total power requirement is then given by:

$$P = P_i + P_p \tag{4.21}$$

$$= k \cdot P_{ideal} + P_p \tag{4.22}$$

$$= 1.2 \cdot 23.7925\,|W| + 11.4969\,|W| = 40.0479\,|W| \approx 50\,|W| \tag{4.23}$$

4.3 Power calculation - directional flight

The worst case scenario regarding power consumption is when the helicopter is flying in any direction.

Power required to overcome drag forces in direction flight

The required power to overcome the drag forces acting on the rotor blades (profile drag) in forward flight can be computed by using the result in 4.20:

$$P_p = P_{p_{hov}}(1 + \mu^2) = 11.4969\,|W|\,(1 + 0.3^2) = 12.5339\,|W| \approx 12.50\,|W| \tag{4.24}$$

The power needed to overcome the drag force H_0, which is acting on the rotor disc, is difficult to calculate and is most often approximated by[1]:

$$P_{drag} = H_0 V \cos \alpha_d \tag{4.25}$$

$$= P_{hov} 4.65 \mu^2 \tag{4.26}$$

$$= 33.9893 \left| W \right| \cdot 4.65 \cdot 0.3^2 \tag{4.27}$$

$$= 14.2245 \left| W \right| \approx 14.20 \left| W \right| \tag{4.28}$$

When the helicopter is in movement the helicopter body contributes with the highest drag. The power needed to overcome the parasite drag can be calculated according to:

$$P_{par} = D_{fus} V = \frac{1}{2} C_d \rho V^3 A \tag{4.29}$$

Where A is the area the drag is acting upon, and $C_{d_{fus}}$ is the drag coefficient for the helicopter's fuselage. The parasite drag can be computed by setting some of the parameters equal to the parameters for a big 450-size quadcopter. The average 450-size quadcopter has a maximum velocity of $15 \left| \frac{m}{s} \right|$, and can tilt at an angle of $50°$.

If the helicopter in this project is leveled and moving vertically, the drag force is acting on the top area of the helicopter. The top area of the helicopter is depicted in figure 4.1. The helicopter's top area is given by solidworks and is approximately $A_{top} \approx 0.686460 m^2$.

If the helicopter is moving side-ways (without tilting) the drag force is acting on the side area of the helicopter as depicted in figure 4.2. The area on the side of the helicopter is given by solidworks and is approximately $A_{side} \approx 0.220344 m^2$. The fuselage area beneath the rotor disc is given by solidworks and is approximately $A_{fus} = 0.01005 m^2$.

The helicopter's maximum velocity can then be set to $V = 15 \left| \frac{m}{s} \right|$ and the drag coefficient for the fuselage to $C_{d_{fus}} = 0.5$ [11].

The area the drag force act upon when the helicopter is tilted at an angle of $50°$ can
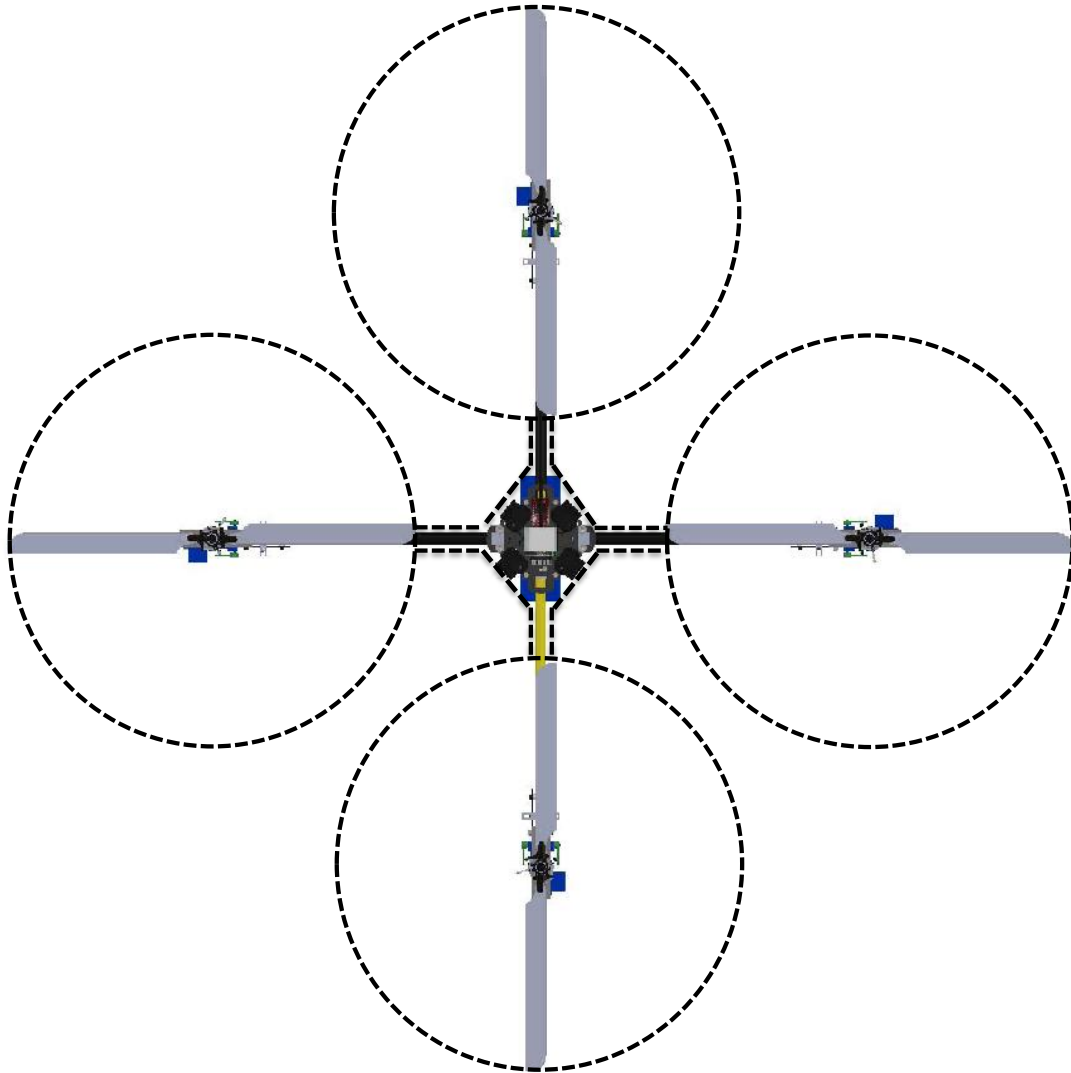
Figure 4.1: Drag force - vertical movement - When the helicopter is moving vertically, the drag force is acting on the area within the dotted line.
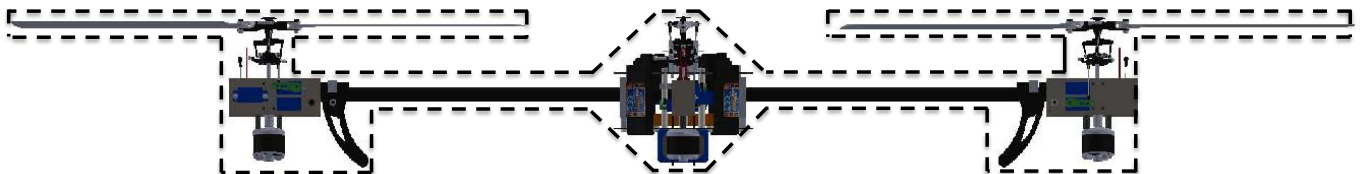
Figure 4.2: Drag force - horizontal movement - When the helicopter is moving horizontally, the drag force is acting on the area within the dotted line.

be computed by using:

$$A = \frac{(A_{top}\sin(50) + A_{side}\cos(50)}{4}) \tag{4.30}$$

$$= \frac{(0.686460\sin(50) + 0.220344\cos(50))}{4} \tag{4.31}$$

$$= 0.166873 \left|m^2\right| \tag{4.32}$$

The power needed to overcome the parasite drag becomes:

$$P_{par} = \frac{1}{2}C_d\rho V^3 A_{ref} \tag{4.33}$$

$$= \frac{1}{2} \cdot 0.5 \cdot 1.225 \left|\frac{kg}{m^3}\right| \cdot (15 \left|\frac{m}{s}\right|)^3 \cdot 0.166873 \left|m^2\right| \tag{4.34}$$

$$= 172.4789 \left|W\right| \approx 173 \left|W\right| \tag{4.35}$$

By using that $P_i = 1.2 \cdot P_{ideal}$ from earlier, the total required power becomes:

$$P_{forward} = P_i + P_p + P_{drag} + P_{par} \tag{4.36}$$

$$= (1.2 \cdot 23.7925 \left|W\right| + 12.5339 \left|W\right| + 14.2245 \left|W\right| + 172.4789 \left|W\right| \tag{4.37}$$

$$= 227.7888 \left|W\right| \approx 228 \left|W\right| \tag{4.38}$$

The conclusion is that the motor needs to deliver $228 \left|W\right|$ if the rotor system should lift a weight of 0.625kg.

Chapter 5

Rotor design

The helicopter's rotor system is an important part of the helicopter, and one of the major challenges in this project was to design a working rotor system. The rotor system had to be lightweight, small, rigid and powerful, to be able to lift the necessary load and withstand the forces that is acting upon it. In this project, proven technology from the RC community was used when designing the rotor system. The parts from existing RC helicopters are parts that were easily available and very reliable. Even though, the design is based on proven technology, the design of the rotor system is still custom made and very special.

One of the difficult choices that had to be done was the selection of a rotor head. It was difficult to identify the impact the different sizes could make on the outcome of this project. The two rotor heads that seemed most suitable for this helicopter was the 250 and 450 size rotor heads.

The 450 size rotor head was a strong rotor head made of aluminium and had a 5 mm shaft, which definitely could handle all the stress the rotor head would be subject too. The rotor head had a 3d model available, which would help speed up the design of the rotor system. The 450 size helicopter normally use 325 mm long rotor blades with a 32 mm chord (blade width), which would deliver more lift at lower RPM. The advantages can be summarized as; easier to assemble, produces more lift, is quieter and allows for a more compact design with enclosed motor and the gears. The disadvantages in using the 450 size rotor head were the blade length, which is quite bigger than the 250-size

rotor head. The helicopter would be larger and weigh a lot more compared to the 250-size rotor head. The higher weight is due to the parts, which was bigger than the parts on the 250-size rotor head.

The 250 size rotor head was also made of aluminium, but it was a lighter rotor head than the 450 size and had a 3.5 mm shaft. The typical rotor blades where 205 mm long and had a 21 mm chord. Although this was a smaller rotor head, it too could handle a great deal of stress. The advantages of using the 250 size rotor head were that the helicopter size would be smaller and weigh less when compared to the 450-size rotor head. The disadvantages of using the 250 size rotor head; it would be harder to assemble, it would produce less lift, be noisier and not so compact compared to the 450-size rotor head.

The conclusion of the comparison between the two rotor heads was that the 450-size rotor head had some advantages over the 250-size rotor head. The 450-size rotor head was quieter, and the compact design allowed for even further noise reduction. It had a 3d model available, was stronger and could lift more weight compared to the 250 size rotor head. It was therefore considered as the most suitable rotor head for this project.

5.1 Casing

The rotor system needed to have a surrounding case that allowed it to be attached to the end of the helicopter's leg boom. The casing needed to be light weight and rigid, which limited the choices of material to three alternatives; plexiglas, carbon fiber or aluminium.
Plexiglas is a light and flexible material, with a density of $1.17–1.20 g/cm^3$ [20]. It is easy to work with, but not as strong as carbon fiber or aluminium.
Carbon fiber is a strong material and a little heavier material, with a density of $1.75 - 1.93 g/cm^3$ [10]. It is fairly difficult to work with, but less rigid than aluminium.
Aluminium is the strongest and heaviest material with a density of $2.7 g/cm^3$ [19]. Aluminium is very rigid and is not easy to experiment with and must be processed in a tool shop. It is thereby not suitable for this project.
The lighter material carbon fiber, would probably be the best material to use, but since the carbon fiber dust is hazardous, it is not easy to experiment with.

In the end, plexiglas was chosen as the most suitable material to use and to make the casings rigid enough a 3 mm thick plate was used.

5.2   Rotor system - 450-size

In the beginning of this chapter, the advantages and disadvantages between the 250 and 450-size rotor heads where discussed, and it was concluded that the 450-size rotor head was the the most suitable rotor head for this prototype. The first step in designing a prototype was to make a 3d model of the 450-size rotor system. The prototype is depicted in figure 5.1.
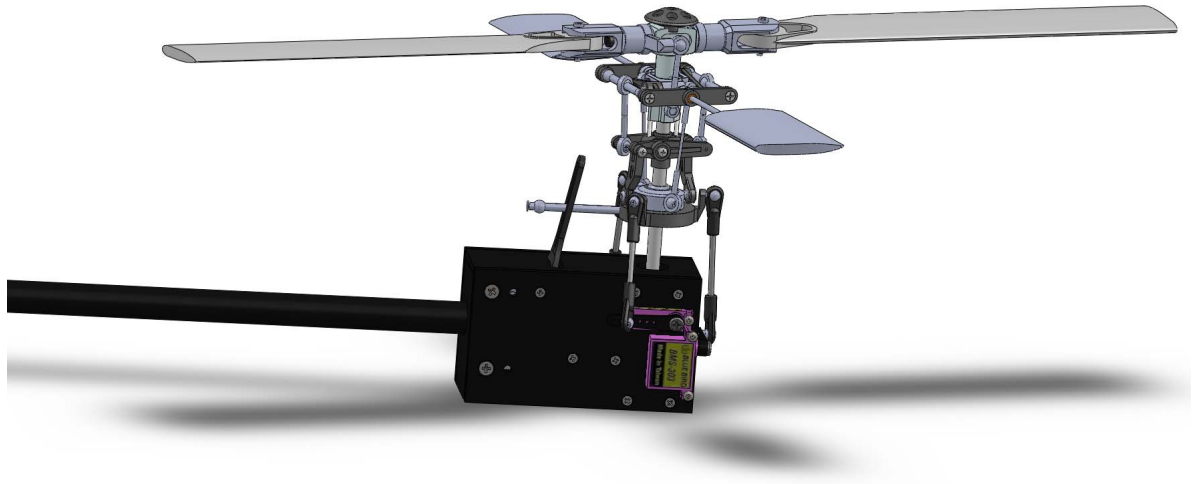
Figure 5.1: Rotor system (450-size) - 3d drawing - The rotor system consists of the motor and the gears, leaving only the rotor head exposed.

A more detailed description of the design is depicted in figure 5.2.

The model was subjected to a motion analysis in Solidworks, where it was confirmed that the rotor system would work as expected. The next step was to produce the casing for the rotor system. The casing was made of 3 mm plexiglas plates, which was cut on a contour saw. The plates where then sandpapered to achieve smooth lines and angles. The necessary holes where drilled, and the plates where then glued together with a special type of welding glue, which made the casings very robust. When the
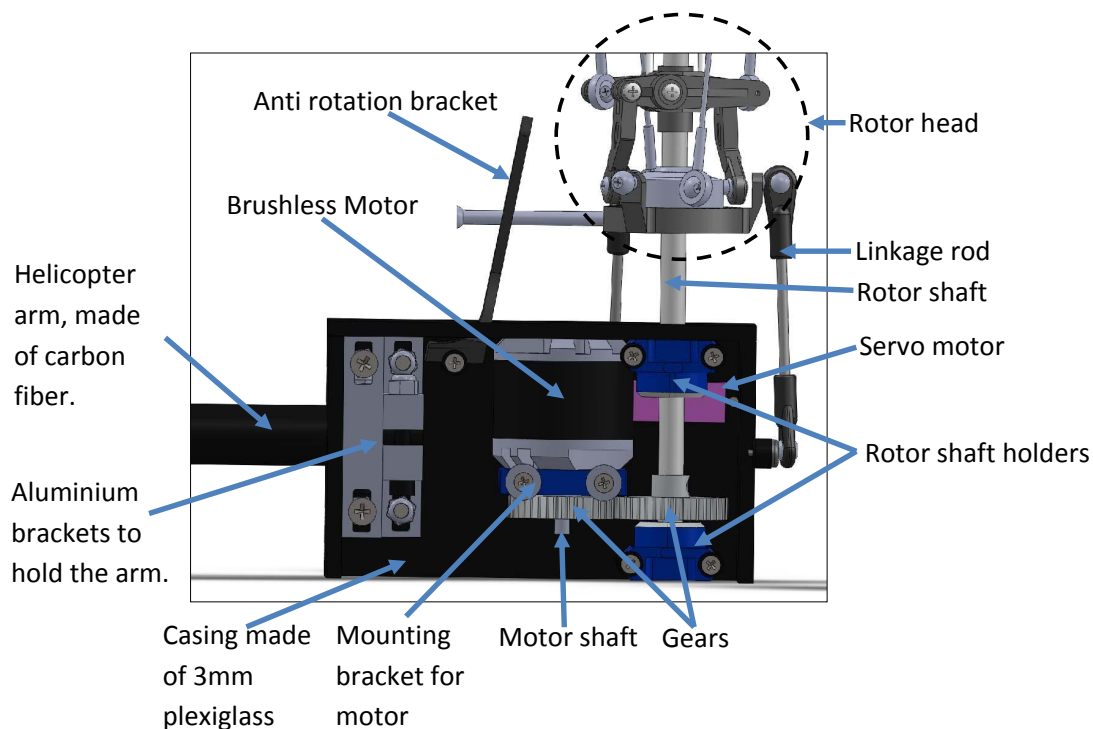
Figure 5.2: Rotor system (450-size) - detail view - The rotor system comprises more than just the motor and gears, and the figure shows all the parts included in the design.

first casing was produced, it was discovered that the casing needed to be made with higher precision if the parts should fit.

This problem could be solved, by using one of two different solutions. The casing could be made at the NTNU's workshop, which meant weeks on weeks in waiting, or the holes could be manipulated with a drill so that the parts would fit better. The latter allowed the casing to have some degree of errors, but still be functional. Since this project is carried out in Bergen, it would be very time consuming to make the parts at the NTNU's workshop. The workshop would need precise drawings and explanations, plexiglas plates and glue to carry it out. In the end, it seemed like a better solution to make the casings at my own workshop, and adjust the holes if necessary. After the casing had been manipulated, the parts where assembled. The first prototype of the 450-size rotor system is depicted in figure 5.3.

When the rotor system was assembled, another problem was detected. The gear connection between the motor and the rotor heads shaft did not align perfectly. When the

Figure 5.3: Rotor system (450-size) - prototype - The rotor system, made of 3mm plexiglas plates with all the parts assembled

rotor head was turned manually, it was possible to hear and feel the misalignment in the gear connection. This meant that the two gears had to be connected with greater precession than first thought. To achieve such precision between the two gears, the holes for the motor bracket would have to be very precise. If the gears where to fare from each other the gear connection would be too loose. If the gears where too close, there would be too much tension between the gears, causing heavy power loss and wear and tear. Another solution was to make adjustable holes for the motor bracket, leaving all the force on the screws holding it. This could work if the screws manage to keep the bracket in place.

It is important to keep in mind that the motor bracket only need to move a fraction of a millimeter before this becomes a problem.

All of the proposed adjustments were tested, in an effort to find the best solution.

5.2.1 Test - 450-size rotor system

The prototype of the 450-size rotor system was connected to the helicopter frame and strapped down by a dumb bell weighing 2.5 kg. The strapped down helicopter ensures that the helicopter would not take off from the test bench, damaging itself or nearby objects. The first test was done with fixed holes for the motor bracket. When the rotor head was turned by hand, it was not possible to detect any errors. The rotor head was

tested, but it did not take long before the two gears got misaligned. It seemed like the fixed holes where not precise enough and that adjustable holes might be a better idea. The holes were made adjustable, and this time it was easier to align the gears. The rotor system was tested again, but disappointedly the result was the same. After putting so much work into this prototype, it all depended on the gear connection between the rotor head shaft and the motor shaft.

It was then concluded that it would be very difficult to get the gear connection to work, because both gears have very small teeth that are very difficult to align. A standard RC helicopter do have a gear connection between the motor and the rotor, but the difference is that the gears are used to scale down the motors RPM. This is done by using a smaller gear with larger teeth's on the motor shaft, which makes it easier to adjust the two gears. Although the motion analysis in Solidworks showed that the prototype should work, it is difficult to see the impact of every little detail without testing it.

The conclusion was that the design needed to be altered, to avoid this problem. In the new design, the motor should be connected directly to the rotor head shaft, which meant that the motor would be exposed to the environment. This was one of the key arguments for using the 450-size rotor head. The new design meant that the already built prototype could not be modified to accommodate the needed modifications, and would have to be scraped. From this point on it seemed more natural to use the 250-size rotor head. The motor was about the same width as the casing and would fit nicely beneath it.

5.3   Rotor system - 250-size

One of the more popular 250-size helicopters is the t-rex 250, which is a fast and reliable helicopter. To ensure that the new prototype of the 250-size rotor system would fly, it is based on parts from the t-rex 250 helicopter. Two different designs were made of the prototype, to have some flexibility.

The first design uses a gear attached to the rear of the motor, which connects the motor and the rotor shaft. The design is very compact and is shown in figure 5.4.

This design could work, if the aluminium gear was strong enough to withstand the torque put upon it, and the mounting hole on the gear fits the rotor shaft.   The
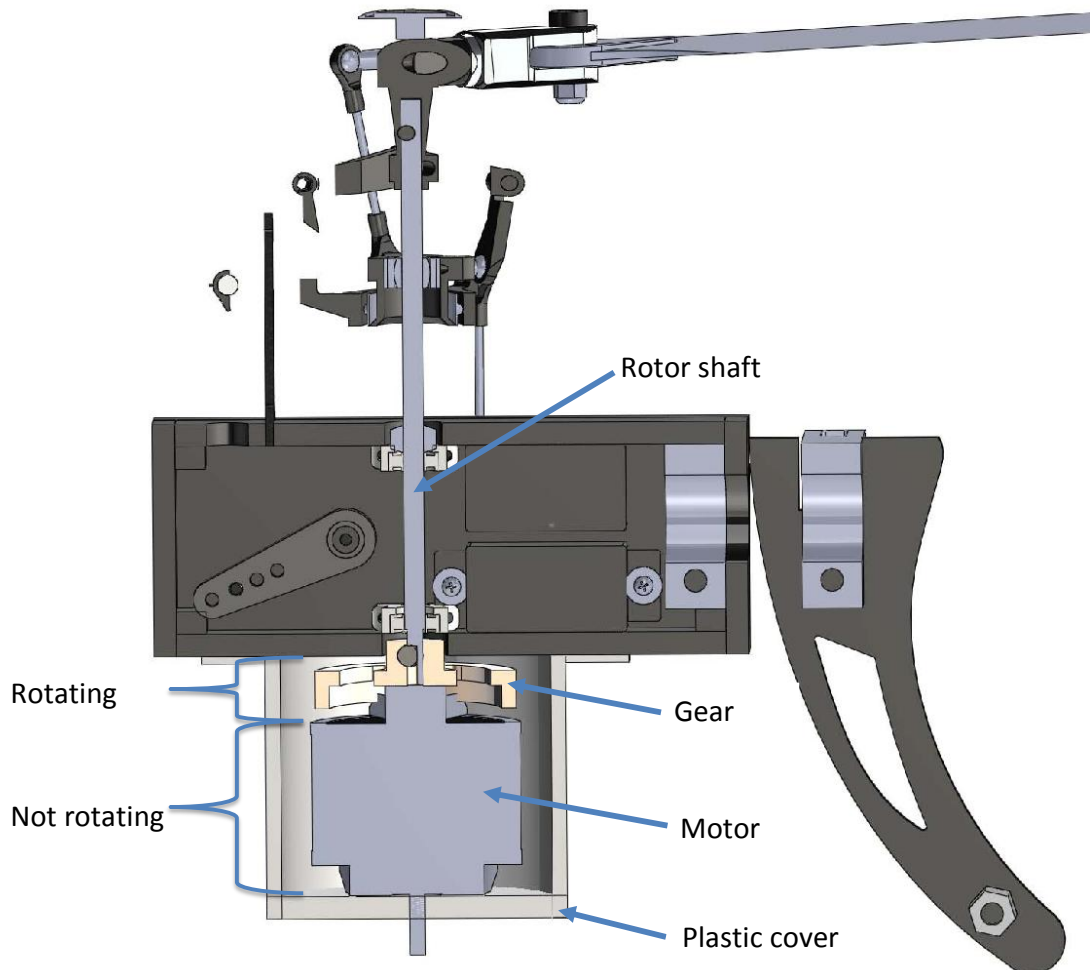
Figure 5.4: Rotor system 1 (250-size) - cut view - Detailed view of the first 250-size rotor system.

second design is based on a linkage between the motor shaft and the rotor shaft. This design was not as compact as the first design but created a very robust and firm linkage between the motor and the rotor, which were a big advantage compared to the first design.

The second design is shown in figure 5.5.
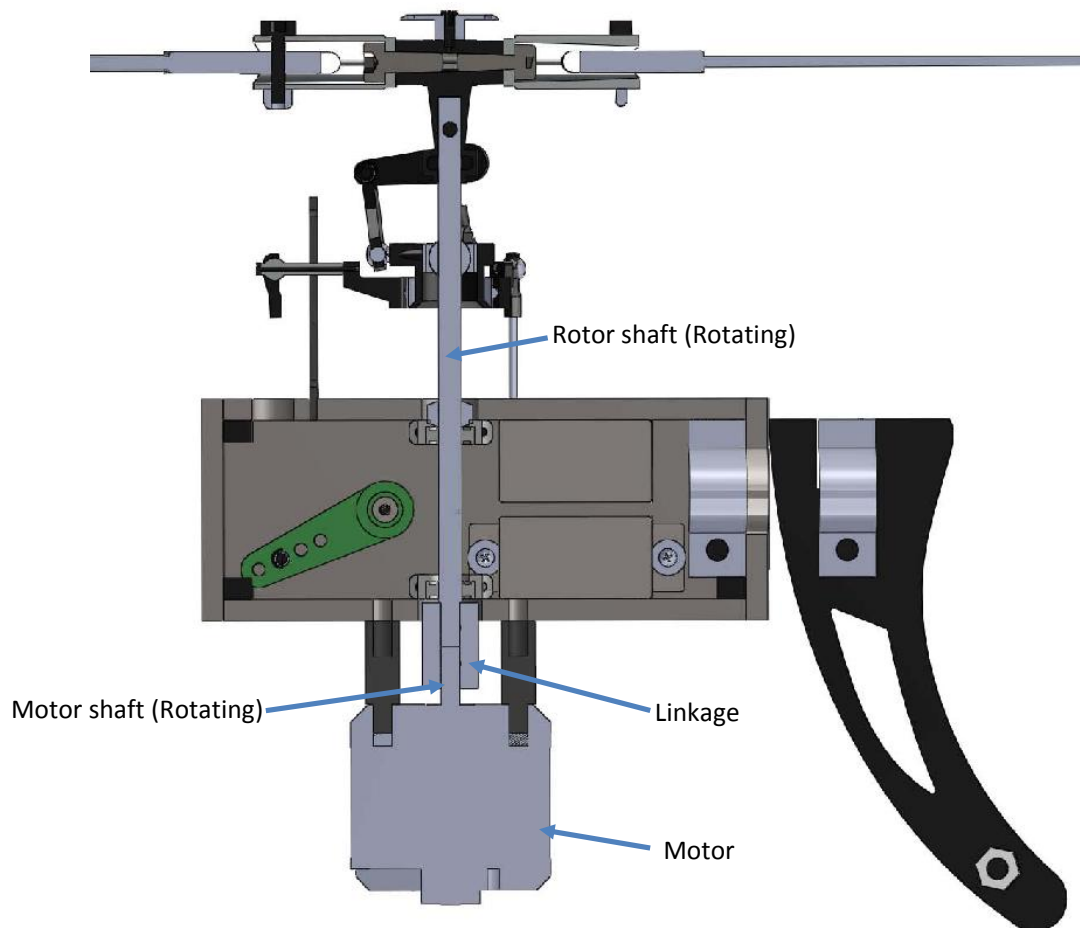
Figure 5.5: Rotor system 2 (250-size) - cut view - Detailed view of the second 250-size rotor system.

The motor has two hexagon brass spacers between the casing and the motor, to allow enough space for the linkage between the motor shaft and the rotor shaft.

5.3.1 Test - 250-size rotor system

A prototype of the first design was built and tested. A picture of the prototypes 3d drawing can be viewed in figure 5.6. When the rotor head was turned manually, there

Figure 5.6: Rotor system 1 (250-size) - 3d drawing - Picture of the first designs 3d drawing.

was no noticeable error in the design, but when tested at higher RPM a misalignment between the motor and the rotor shaft was detected. After examining what could have caused the misalignment, it was discovered that there was a difference between the diameter of the rotor shaft and the mounting hole on the gear. The mounting hole on the gear was 1/8" (3.175mm), and this was enough to create a noticeable misalignment. This is a good example of what kind of precession is needed for this project to succeed.

The attention now turned to the second design, which had a linkage between the motor and the rotor shaft. A picture of the prototypes 3d drawing can be viewed in figure 5.7. A prototype of the design was built and tested.
The test results were much better than the first design and finally a working prototype existed. It was now possible to test lifting properties of the helicopter's rotor system.

To test the helicopter's rotor system, a test bench was built. A picture of the test bench is shown in figure 5.8.
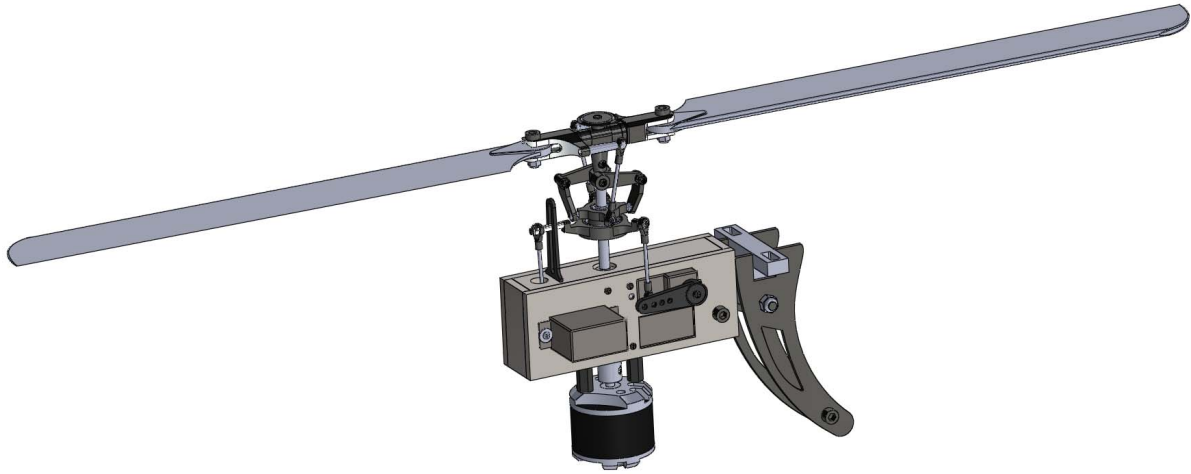
Figure 5.7: Rotor system 2 (250-size) - 3d drawing - Picture of the second designs 3d drawing.

The following equipment was used in the test:

- Portable Electronic Hanging Scale PRODUCT ID: OR013-09701

- Turnigy Multi-Blade Micro Tachometer PRODUCT ID: Tu-Tacometer

- Soft rotor blades (plastic) PRODUCT ID: GT250-111

- Hard rotor blades (carbon fiber) PRODUCT ID: CF205-3D

The rotor system was tested with two different types of rotor blades, one soft and one hard. The soft type of blade is much more flexible than the hard type and is made out of plastic. The hard type is a rigid blade and is made out of carbon fiber and weighs 10g less than the soft type.

If the blades are tighten too hard, the blade cannot be stretched out properly, when reaching high velocities, which will cause vibrations. If the blades are too loose, the blades will have problems resisting the air resistance and be bent backwards, which also will cause vibrations. The last parameter that affect the lifting properties is the speed of the rotor head. The transmitter's throttle curve was adjusted, such that the rotor heads RPM is constant regardless the blades pitch, and the blades pitch curve was adjusted to travel between 3° and 11°.
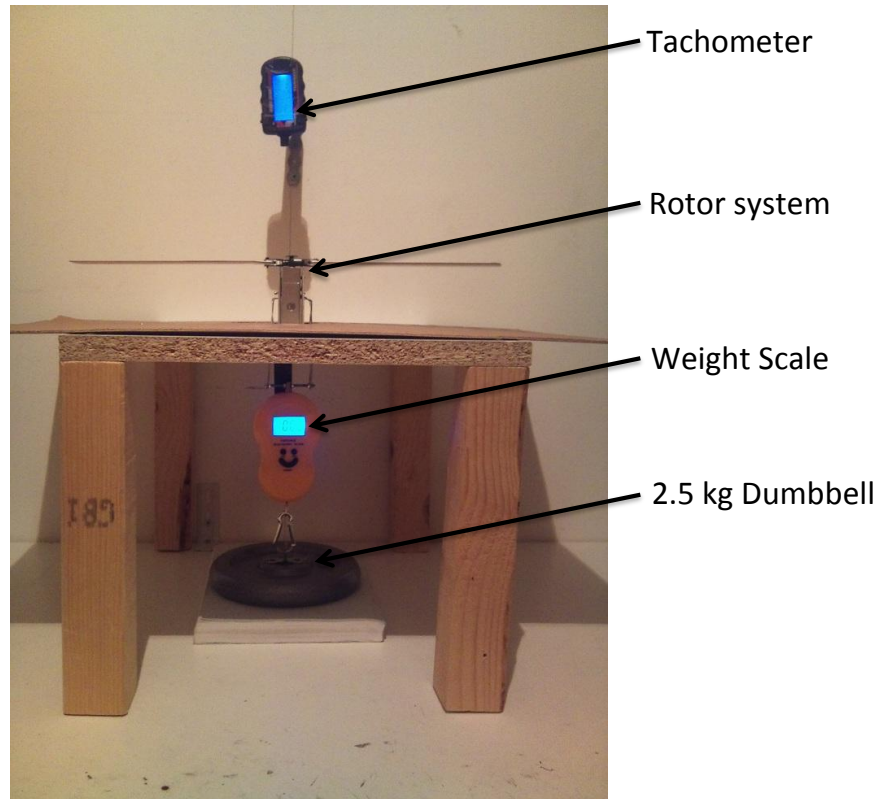
Figure 5.8: Test bench - The test bench is equipped with a tachometer to measure the rotor systems RPM and a weight scale to measure the amount of weight the rotor system can lift.

To determine what gave best effect during the test, it was experimented with how tight the blades should be fitted and how fast the rotor head should spin.

The first test was performed with the soft blades, and after some adjustments, the best result showed that the rotor system could lift 300g with a average rotor speed of ≈ 2100 RPM. The rotor speed was difficult to read, and is an approximately average based on many readings. Since the rotor system and the weight scale have a combined weight of 324g, it meant that the rotor system could lift a total of 624g.

In the second test, the hard carbon fiber blade was used. The same experiments were performed with regards to the settings, and the results were the same. The carbon fiber blades were able to lift more weight than the soft blades, but it also had a lot more vibrations when lifting more than 624g. The origin of the vibrations was hard

to find. Two plausible theories are that 624g was the rotor systems maximum lifting capacity, or it could be that when the rotor system lifted more than 624g it lifted it self fractions of millimeters above the test bench, which meant that it could move a little bit, which then evolved into vibrations.

The results from this test meant that the helicopter could lift a total of 2496g $\approx$ 2.5kg when all four rotor systems have a maximum pitch of 11° and a rotor speed of 2100 RPM. The results from these tests will be used as the rotor systems maximum lifting capacity for the remaining of this thesis.

Chapter 6

Dynamic model

The helicopter's dynamic model is very important and can be used in simulations and control designs. The helicopter's dynamic model will be derived in the Body frame, and the NED frame will be used as inertial frame. The two frames are explained in chapter 2.1.

The NED frame $(\cdot^n)$ is the tangent plane on the earth's surface. It has the x-axis pointing towards true north, the y-axis pointing towards east and the z-axis pointing towards the center of the earth. The body frame $(\cdot^b)$ is attached to the helicopter, where the x-axis is pointing forward, the y-axis is pointing to the right and the z-axis is pointing downwards.

The helicopter's position in the NED frame given in standard notation is:

$$\boldsymbol{p}_{b/n}^n = \begin{bmatrix} x_n & y_n & z_n \end{bmatrix}^T \tag{6.1}$$

The angles between the two frames are given by the Euler angles depicted in figure 2.3. The Euler angles are also called the helicopter's attitude and are described by:

$$\boldsymbol{\Theta}_{b/n} = \begin{bmatrix} \phi & \theta & \psi \end{bmatrix}^T \tag{6.2}$$

Where ϕ is the rotation angle around the x-axis, θ is the rotation angle around the y-axis and ψ is the rotation angle around the z-axis.

By combining equation 6.1 and 6.2, the helicopter's position and orientation vector

becomes:

$$\boldsymbol{\eta} = \begin{bmatrix} \boldsymbol{p}^n_{b/n} & \boldsymbol{\Theta}_{b/n} \end{bmatrix}^T \qquad (6.3)$$

The body-fixed linear velocity vector is given by:

$$\boldsymbol{v}^b_{b/n} = \begin{bmatrix} u & v & w \end{bmatrix}^T \qquad (6.4)$$

The three linear velocities u, v and w are perpendicular to each other and works along the x, y and z axis, respectively. Similar to the linear velocities, the body-fixed angular velocity vector is given by:

$$\boldsymbol{\omega}^b_{b/n} = \begin{bmatrix} p & q & r \end{bmatrix}^T \qquad (6.5)$$

The three angular velocities p, q and r are also perpendicular to each other and works around the x, y and z axis, respectively.

By combining equation 6.4 and 6.5 the helicopter's linear and angular velocity vector becomes:

$$\boldsymbol{\nu} = \begin{bmatrix} \boldsymbol{v}^b_{b/n} & \boldsymbol{\omega}^b_{b/n} \end{bmatrix}^T \qquad (6.6)$$

6.1 Rigid body dynamics

A description of the helicopter's dynamics can be made by using the equation of motion for a rigid body ($\cdot_{RB}$) given by [4]:

$$\boldsymbol{M}_{RB}\dot{\boldsymbol{\nu}} + \boldsymbol{C}_{RB}(\boldsymbol{\nu})\boldsymbol{\nu} = \boldsymbol{\tau}(\boldsymbol{u}) \qquad (6.7)$$

Where the $\boldsymbol{M}_{RB}$ matrix is unique and satisfies:

$$\boldsymbol{M}_{RB} = \boldsymbol{M}^T_{RB} > 0, \ \dot{\boldsymbol{M}}_{RB} = \boldsymbol{0}_{6\times6} \qquad (6.8)$$

The $\boldsymbol{M}_{RB}$ matrix is given by:

$$\boldsymbol{M}_{RB} = \begin{bmatrix} m\boldsymbol{I}_{3\times3} & -m\boldsymbol{S}(r^b_g) \\ m\boldsymbol{S}(r^b_g) & \boldsymbol{I}_b \end{bmatrix} \qquad (6.9)$$

The skew symmetric matrix $\boldsymbol{S}$ is defined in appendix C.1.

The $\boldsymbol{M}_{RB}$ matrix can be simplified by putting the Center of Origin (CO) to coincide with the Center of Gravity (CG), the cross-axis moments of inertia can then be neglected [6], and the inertia matrix becomes:

$$\boldsymbol{M}_{RB} = \begin{bmatrix} m\boldsymbol{I}_{3\times3} & \boldsymbol{0}_{3\times3} \\ \boldsymbol{0}_{3\times3} & \boldsymbol{I}_g \end{bmatrix} \tag{6.10}$$

The inertia matrix $\boldsymbol{I}_g$ is defined in appendix C.2.

The Coriolis matrix is represented by to vector terms; the Coriolis vector term $\boldsymbol{\omega}^b_{b/n} \times \boldsymbol{v}^b_{b/n}$ and the centripetal vector term $\boldsymbol{\omega}^b_{b/n} \times (\boldsymbol{\omega}^b_{b/n} \times \boldsymbol{r}^b_g)$. The simplified inertia matrix leads to a simpler Coriolis matrix, and is given by:

$$\boldsymbol{C}_{RB} = \begin{bmatrix} \boldsymbol{0}_{3\times3} & -\boldsymbol{S}(\boldsymbol{M}_{11}\boldsymbol{\nu}_1) \\ \boldsymbol{S}(\boldsymbol{M}_{11}\boldsymbol{\nu}_1) & \boldsymbol{S}(\boldsymbol{M}_{22}\boldsymbol{\nu}_2) \end{bmatrix} \tag{6.11}$$

The vector $\boldsymbol{\tau}$ in equation 6.7 comprises forces and moments acting on the helicopter, and is given by:

$$\boldsymbol{\tau} = \begin{bmatrix} \boldsymbol{f}^b_b & \boldsymbol{m}^b_b \end{bmatrix}^T = \begin{bmatrix} X & Y & Z & L & M & N \end{bmatrix}^T \tag{6.12}$$

The X, Y and Z components are the translational forces along the x, y and z axis, respectively. The L, M and N components are the moments around the x, y and z axis, respectively.

The different elements in the force and moment vector are defined as [7]:

$$\boldsymbol{\tau} = \begin{bmatrix} \boldsymbol{f}^b_b & \boldsymbol{m}^b_b \end{bmatrix}^T = \begin{bmatrix} X_{mr} + X_{fus} \\ Y_{mr} + Y_{fus} + Y_{tr} + Y_{vf} \\ Z_{mr} + Z_{fus} + Z_{ht} \\ L_{mr} + L_{vf} + L_{tr} \\ M_{mr} + Mht \\ -Q_e + N_{vf} + N_{tr} \end{bmatrix} + \begin{bmatrix} \boldsymbol{f}^b_g \\ \boldsymbol{0}_{3x1} \end{bmatrix} \tag{6.13}$$

The subscript are defined as; $(\cdot)_{mr}$ is the main rotor, $(\cdot)_{fus}$ is the fuselage, $(\cdot)_{tr}$ is the tail rotor, $(\cdot)_{ht}$ is the horizontal tail, $(\cdot)_{vf}$ is the vertical fin.

The gravitational force vector $\boldsymbol{f}^b_g$ in equation 6.13 is expressed in body frame and is

6. DYNAMIC MODEL

given by:

$$\boldsymbol{f}_g^b = \boldsymbol{R}_b^n(\boldsymbol{\Theta})^{-1}\boldsymbol{f}_g^n \tag{6.14}$$

The gravitational force vector $\boldsymbol{f}_g^n$ expressed in NED frame is:

$$\boldsymbol{f}_g^n = \begin{bmatrix} 0 & 0 & mg \end{bmatrix}^T \tag{6.15}$$

The gravitational force vector in the body-frame can be derived by using the rotation matrix given in appendix A.3:

$$\boldsymbol{f}_g^b = \begin{bmatrix} c\theta c\psi & c\theta s\psi & -s\theta \\ -c\phi s\psi + s\phi s\theta c\psi & c\phi c\psi + s\phi s\theta s\psi & s\phi c\theta \\ s\theta s\psi + c\phi s\theta c\psi & -s\phi c\psi + c\phi s\theta s\psi & c\phi c\theta \end{bmatrix} \begin{bmatrix} 0 \\ 0 \\ mg \end{bmatrix} = mg \begin{bmatrix} -s\theta \\ s\phi c\theta \\ c\phi c\theta \end{bmatrix} \tag{6.16}$$

The helicopter in this project is not equipped with tail fins, tail rotors, vertical fins or horizontal tails, but has instead four main rotors and four leg booms. The elements in the force and moment vector given in 6.13 is adapted to this project's helicopter and becomes:

$$\boldsymbol{\tau} = \begin{bmatrix} \boldsymbol{f}_b^b & \boldsymbol{m}_b^b \end{bmatrix}^T = \begin{bmatrix} X_{mr1} + X_{mr2} + X_{mr3} + X_{mr4} + X_{fus} \\ Y_{mr1} + Y_{mr2} + Y_{mr3} + Y_{mr4} + Y_{fus} \\ Z_{mr1} + Z_{mr2} + Z_{mr3} + Z_{mr4} + Z_{fus} \\ L_{mr1} + L_{mr2} + L_{mr3} + L_{mr4} \\ M_{mr1} + M_{mr2} + M_{mr3} + M_{mr4} \\ -Q_e \end{bmatrix} + \begin{bmatrix} \boldsymbol{f}_g^b \\ \boldsymbol{0}_{3x1} \end{bmatrix} \tag{6.17}$$

All the elements in the equation of motion are now defined.

If the equation of motion is rearranged with respect to $\dot{\boldsymbol{\nu}}$ it becomes:

$$\dot{\boldsymbol{\nu}} = M_{RB}^{-1}\left(\boldsymbol{\tau}(\boldsymbol{u}) - C_{RB}(\boldsymbol{\nu})\boldsymbol{\nu}\right) \tag{6.18}$$

If the matrices are inserted with all its elements the equation becomes:

$$
\begin{bmatrix} \dot{u} \\ \dot{v} \\ \dot{w} \\ \dot{p} \\ \dot{q} \\ \dot{r} \end{bmatrix} = \begin{bmatrix} \frac{1}{m} & 0 & 0 & 0 & 0 & 0 \\ 0 & \frac{1}{m} & 0 & 0 & 0 & 0 \\ 0 & 0 & \frac{1}{m} & 0 & 0 & 0 \\ 0 & 0 & 0 & \frac{1}{I_{xx}} & 0 & 0 \\ 0 & 0 & 0 & 0 & \frac{1}{I_{yy}} & 0 \\ 0 & 0 & 0 & 0 & 0 & \frac{1}{I_{zz}} \end{bmatrix} \left(\begin{bmatrix} X_{mr1} + X_{mr2} + X_{mr3} + X_{mr4} + X_{fus} \\ Y_{mr1} + Y_{mr2} + Y_{mr3} + Y_{mr4} + Y_{fus} \\ Z_{mr1} + Z_{mr2} + Z_{mr3} + Z_{mr4} + Z_{fus} \\ L_{mr1} + L_{mr2} + L_{mr3} + L_{mr4} \\ M_{mr1} + M_{mr2} + M_{mr3} + M_{mr4} \\ -Q_e \end{bmatrix} - \right.
$$

$$
\left. \begin{bmatrix} 0 & 0 & 0 & 0 & mw & -mv \\ 0 & 0 & 0 & -mw & 0 & mu \\ 0 & 0 & 0 & mv & -mu & 0 \\ 0 & -mw & mv & 0 & -I_{zz}r & I_{yy}q \\ mw & 0 & mu & I_{zz}r & 0 & -I_{xx}p \\ -mv & mu & 0 & -I_{yy}q & I_{xx}p & 0 \end{bmatrix} \begin{bmatrix} u \\ v \\ w \\ p \\ q \\ r \end{bmatrix} \right) \tag{6.19}
$$

The equation of motion can now be written on component form as:

$$
\dot{u} = \frac{1}{m} \left(vr - wq - g\sin\theta + (X_{mr1} + X_{mr2} + X_{mr3} + X_{mr4} + X_{fus}) \right) \tag{6.20}
$$

$$
\dot{v} = \frac{1}{m} \left(wp - ur - g\sin\phi\cos\theta + (Y_{mr1} + Y_{mr2} + Y_{mr3} + Y_{mr4} + Y_{fus}) \right) \tag{6.21}
$$

$$
\dot{w} = \frac{1}{m} \left(uq - vp - g\cos\phi\cos\theta + (Z_{mr1} + Z_{mr2} + Z_{mr3} + Z_{mr4} + Z_{fus}) \right) \tag{6.22}
$$

$$
\dot{p} = \frac{1}{I_{xx}} \left(qr(I_{yy} - I_{zz}) + (L_{mr1} + L_{mr2} + L_{mr3} + L_{mr4}) \right) \tag{6.23}
$$

$$
\dot{q} = \frac{1}{I_{yy}} \left(pr(I_{zz} - I_{xx}) + (M_{mr1} + M_{mr2} + M_{mr3} + M_{mr4}) \right) \tag{6.24}
$$

$$
\dot{r} = \frac{1}{I_{zz}} \left(pq(I_{xx} - I_{yy}) + Q_e \right) \tag{6.25}
$$

6.2 Forces and moments

The thrust force created by the helicopter's rotor system is a vector in the x, y and z-axis. The components of the thrust vector are dependent on the Euler angles and on the flapping angles A1 and B1. If the helicopter is leveled in the NED frame, the magnitude of the flapping angles A1 and B1 will decide if the helicopter moves horizontally in the x or y direction. If the helicopter is not leveled, the thrust vector is dependent on both the Euler angles and the flapping angles A1 and B1. The thrust vector in NED frame is described by:

$$\boldsymbol{T}^n_{b/n} = T_{mr} \begin{bmatrix} \sin(A1 + \theta) \\ \sin(B1 + \phi) \\ \cos(A1 + \theta)\cos(B1 + \phi) \end{bmatrix} \tag{6.26}$$

Where T_{mr} is the rotor thrust given by [11]:

$$T_{mr} = -\frac{1}{2}C_T\rho A(\Omega R)^2 \tag{6.27}$$

Where C_T is the thrust coefficient. The motor thrust T_{mr} is negative since z-axis in the NED frame is positive in the downward direction.

The thrust vector in NED frame can be transformed to the body frame by using:

$$\boldsymbol{T}^b_{n/b} = \begin{bmatrix} X_{mr} \\ Y_{mr} \\ Z_{mr} \end{bmatrix} = (\boldsymbol{R}^n_b(\boldsymbol{\Theta}_{nb}))^{-1}\boldsymbol{T}^n_{b/n} \tag{6.28}$$

The inverse rotation matrix is given in appendix A.3.

The rotor torque vector $\boldsymbol{Q}$ behaves exactly like the thrust vector, and can be rotated the same way, which gives:

$$\boldsymbol{Q}^n_{b/n} = Q_e \begin{bmatrix} \sin(A1 + \theta) \\ \sin(B1 + \phi) \\ \cos(A1 + \theta)\cos(B1 + \phi) \end{bmatrix} \tag{6.29}$$

Where Q_e is the rotor torque given by:

$$Q_e = \pm\frac{1}{2}C_Q\rho A(\Omega R)^2 \tag{6.30}$$

Where C_Q is the torque coefficient. The sign of the rotor torque Q_e is dependent on

the rotor's direction of rotation. Transforming it to the body frame give us [11]:

$$\boldsymbol{Q}_{n/b}^b = (\boldsymbol{R}_b^n(\boldsymbol{\Theta}_{nb}))^{-1}\boldsymbol{Q}_{b/n}^n \qquad (6.31)$$

The force and moment vector $\boldsymbol{\tau}$ can now be described in the body frame by combing equation 6.28 and 6.31:

$$\boldsymbol{\tau} = \begin{bmatrix} \boldsymbol{T}_{n/b}^b \\ \boldsymbol{Q}_{n/b}^b \end{bmatrix} \qquad (6.32)$$

If the helicopter's drag forces were not accounted for, this would be correct. In the next section the force and moment vector $\boldsymbol{\tau}$ will be extended to incorporate the helicopter's drag force called "parasite drag".

6.3   Drag forces

When a helicopter is flying forward it is subjected to two drag forces; one is acting on the helicopter fuselage (parasite drag) and one is acting on the rotors.

The helicopter's drag forces can be modeled by combining the drag forces with the helicopter's tilt angle.

The parasite drag vector created when the helicopter is moving through the air is given by:

$$\boldsymbol{D}_{par_{top}} = \frac{1}{2}C_d\rho\boldsymbol{V}_{heli}\boldsymbol{A}_{heli} \tag{6.33}$$

where

$$\boldsymbol{V}_{heli} = \begin{bmatrix} u^2 & 0 & 0 \\ 0 & v^2 & 0 \\ 0 & 0 & w^2 \end{bmatrix}$$

and

$$\boldsymbol{A}_{heli} = \begin{bmatrix} A_{side} \\ A_{side} \\ A_{top} \end{bmatrix}$$

The drag force acting on the helicopter is caused by the down wash from the rotor disc onto the fuselage. This drag force is dependent on the induced air velocity, which can be computed by using equation 3.17.

$$V_i = \sqrt{\frac{T}{2\rho A}} = \sqrt{\frac{1}{2\rho}}\sqrt{\frac{T}{A}}$$

The drag force acting on the area beneath the rotor disc is then given by:

$$\boldsymbol{D}_{par_{fus}} = \frac{1}{2}C_{d_{fus}}\rho\boldsymbol{V}A_{fus} \tag{6.34}$$

where

$$\boldsymbol{V} = \begin{bmatrix} 0 \\ 0 \\ V_i \end{bmatrix}$$

The total parasite drag can then be described by combining equation 6.33 and 6.34:

$$\boldsymbol{D} = \boldsymbol{D}_{par_{top}} + \boldsymbol{D}_{par_{fus}} \tag{6.35}$$

The parasite drag vector can be transformed from NED frame to the body frame by using:

$$\boldsymbol{D}^b_{n/b} = (\boldsymbol{R}^n_b(\boldsymbol{\Theta}_{nb}))^{-1}\boldsymbol{D}^n \tag{6.36}$$

When computing the parasite drag an estimate of the drag coefficient can be very difficult to find. To simulate a worst case scenario the drag coefficient is set to $C_{d_{fus}} = 0.5$.

Now that a parasite drag vector exists it is possible to derive the force and moment vector $\boldsymbol{\tau}$ by combining equation 6.32 and 6.36:

$$\boldsymbol{\tau} = \begin{bmatrix} \boldsymbol{T}^b_{n/b} + \boldsymbol{D}^b_{n/b} \\ \boldsymbol{Q}^b_{n/b} \end{bmatrix} \tag{6.37}$$

The complete force and moment vector $\boldsymbol{\tau}$ is given in body frame, which will be used in later simulations.

6.4 Swashplate

The swashplate is an essential part of a helicopter's dynamic's and controls the helicopter's collective pitch (up and down) and cyclic pitch (forward/backward and left-/right). A detailed description on how the swashplate works is given in section 3.1.6. The cyclic pitch is very complex and difficult to model, but for simulation and control design, some of the complexity can be neglected. The model can be simplified by only including the rotor's tilt angle and the movement of the servos.

The flapping angles can be modeled as [14]:

$$\dot{A}_1 = \frac{1}{T_f}(-lu_{Servo_1} \cdot \theta_{SPmax} - A_1) \tag{6.38}$$

$$\dot{B}_1 = \frac{1}{T_f}(-lu_{Servo_{2,3}} \cdot \theta_{SPmax} - B_1) \tag{6.39}$$

6. DYNAMIC MODEL

Where the time constant T_f covers the dynamics of the servos and rotor head while the l is a scaling factor. The angle θ_{SPmax} is the swashplates maximum tilt angle.

The rotor disc angles A_1 and B_1 are the angles between the TTP and SNP, longitudinal and lateral to the helicopter, respectively. This is explained and illustrated in subsection 3.1.3.

The two flapping angles can only be adjust to a few degrees, and are set to $\theta_{SPmax} \pm 2°$ in the simulation.

The flapping angle A_1 is controlled by Servo 1 while the flapping angle B_1 is controlled by Servo 2 and 3. The Servo positions and the swashplate are depicted in figure 6.1, and the flapping angles are depicted in figure 3.3
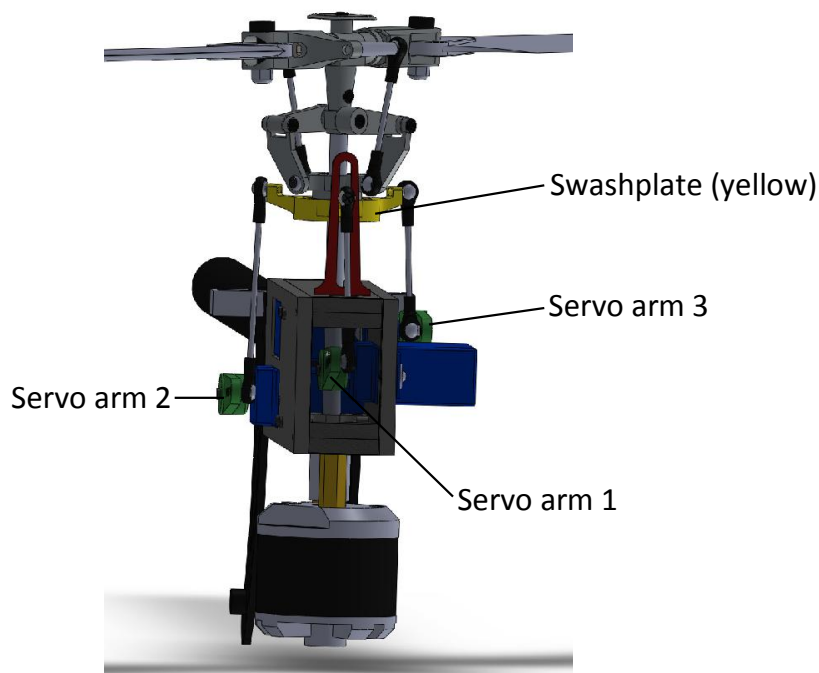

Figure 6.1: Servo motors - location - The figure shows the Servo motors and the swashplates location.

6.5 Electric motor and gear

The electric BLDC motor is controlled by an Electronic Speed Controller (ESC), without any electronic feedback signal. A BLDC motor and its properties are depicted in figure 6.2.
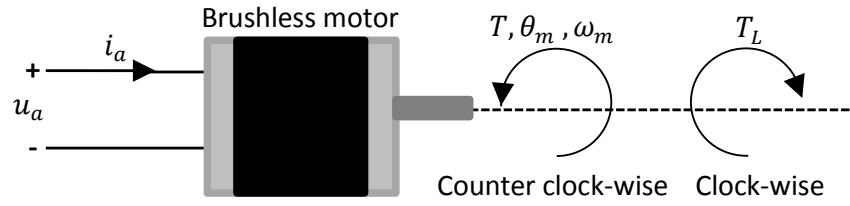

Figure 6.2: BLDC motor - properties - A Brushless DC motor properties; u_a is the supply voltage, i_a is the supply current, R_a is the motors resistance, L_a is the motors inductance, J_m is the motors moment inertia, ω_m is the motors angular velocity, θ_m is the shaft angle and , T_L is the load torque.

The dynamic model for the motor can be derived by using the equation of motion for the motor shaft and the voltage law given by [3]:

$$L_a \frac{d}{dt} i_a = -R_a i_a - K_E \omega_m + u_a \tag{6.40}$$

$$J_m \dot{\omega}_m = K_T i_a - T_L \tag{6.41}$$

$$\dot{\theta}_m = \omega_m \tag{6.42}$$

In equations above, K_T is the torque constant while K_E is the field constant. The rest of the parameters are explained in figure 6.2.

If equation 6.40 is inserted into equation 6.41 the model becomes:

$$J_m \dot{\omega}_m = K_T \left(\frac{u_a - K_E \omega_m - L \frac{d}{dt} i_a}{R_a} \right) - T_L \tag{6.43}$$

Since the motor speed is equal to the rotor speed $\omega = \Omega$ the model becomes:

$$J_m \dot{\Omega} = K_T \left(\frac{u_a - K_E \Omega - L \frac{d}{dt} i_a}{R_a} \right) - T_L \tag{6.44}$$

Where T_L is the rotor's drag torque. If the rotor system connects the motor and rotor

through a gear, the gear needs to be described by a dynamic model.

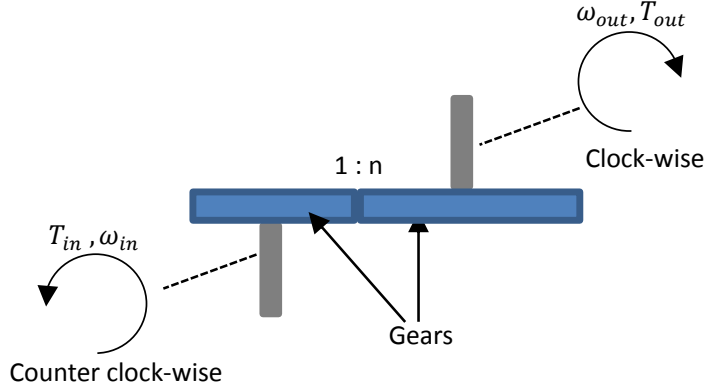The gear connection between the motor and rotor and its properties is depicted in figure 6.3.

Figure 6.3: Gear connection - The two gears is connected together and rotates in the opposite direction of each other.

A model of a gear connection where the two gears spin in the same direction is given by [3]:

$$\omega_{out} = n\omega_{in} \tag{6.45}$$

$$T_{out} = \frac{1}{n}T_{in} \tag{6.46}$$

In this project, the gears between the motor and rotor spin in the opposite direction of the each other, and the modified model becomes:

$$\omega_{out} = -n\omega_{in} \tag{6.47}$$

$$-T_{out} = \frac{1}{n}T_{in} \tag{6.48}$$

The subscript $(\cdot)_{out}$ can be replaced with $(\cdot)_e$ (external), and the subscript $(\cdot)_{in}$ can be replaced with $(\cdot)_L$ (load). The gear connection is depicted in figure 6.4.

The modified model gives us:

$$\omega_L = -n\omega_m \tag{6.49}$$
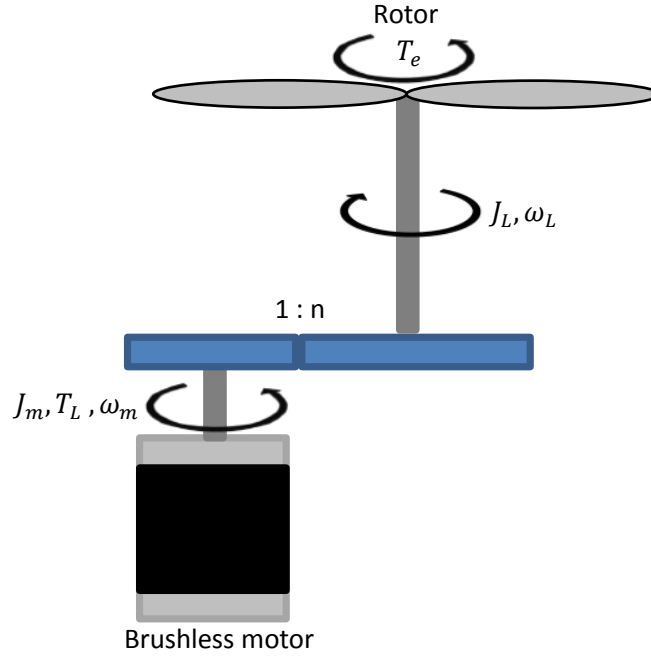
$$-T_e = \frac{1}{n}T_L \tag{6.50}$$

Figure 6.4: Gear connecting motor and rotor - The motor and the rotor are connected through a gear, and rotate in the opposite direction of each other.

The equation of motion for the motor is given by [3]:

$$-J_m\dot{\omega}_m = T_L - T \tag{6.51}$$

While the equation of motion for the load is given by [3]:

$$J_L\dot{\omega}_L = \frac{1}{n}T_L - T_e \tag{6.52}$$

Rewriting equation 6.51 yields:

$$\frac{1}{n}T_L = \frac{1}{n}T - \frac{1}{n}J_m\dot{\omega}_m \tag{6.53}$$

Inserting equation 6.53 into equation 6.52 yields:

$$J_L\dot{\omega}_L = \frac{1}{n}T - \frac{1}{n}J_m\dot{\omega}_m - T_e \tag{6.54}$$

6. DYNAMIC MODEL

Rewriting equation 6.54 yields:

$$nJ_L\dot{\omega}_L + J_m\dot{\omega}_m = T - nT_e \tag{6.55}$$

Inserting equation 6.49 into equation 6.55 yields:

$$nJ_L\dot{\omega}_L + J_m(-\dot{n}^{-1}\omega_L - n^{-1}\dot{\omega}_L) = T - nT_e \tag{6.56}$$

$$nJ_L\dot{\omega}_L - \frac{1}{n}J_m\dot{\omega}_L = T - nT_e \tag{6.57}$$

$$\left(J_L - \frac{1}{n^2}J_m\right)\dot{\omega}_L = \frac{1}{n}T - T_e \tag{6.58}$$

Inserting $T = K_T i_a$ from equation 6.41 gives us:

$$\left(J_L - \frac{1}{n^2}J_m\right)\dot{\omega}_L = \frac{1}{n}K_T i_a - T_e \tag{6.59}$$

Inserting equation 6.40 yields:

$$\left(J_L - \frac{1}{n^2}J_m\right)\dot{\omega}_L = K_T\left(\frac{u_a - K_E\omega_m - L\frac{d}{dt}i_a}{nR_a}\right) - T_e \tag{6.60}$$

Inserting equation 6.49 yields:

$$\left(J_L - \frac{1}{n^2}J_m\right)\dot{\omega}_L = K_T\left(\frac{u_a + \frac{1}{n}K_E\omega_L - L\frac{d}{dt}i_a}{nR_a}\right) - T_e \tag{6.61}$$

And since the load's angular velocity is equal to the rotor's angular velocity $\omega_L = \Omega$ equation 6.61 becomes:

$$\left(J_L - \frac{1}{n^2}J_m\right)\dot{\Omega} = K_T\left(\frac{u_a + \frac{1}{n}K_E\Omega - L\frac{d}{dt}i_a}{nR_a}\right) - T_e \tag{6.62}$$

Where T_e is the rotor shaft torque Q, which is given by [11]:

$$Q = \frac{1}{2}C_Q\rho\pi\Omega^2 R^5 \tag{6.63}$$

Inserting equation 6.63 into equation 6.62 gives us the model for the electric motor and

gear:

$$\left(J_L - \frac{1}{n^2}J_m\right)\dot{\Omega} = K_T\left(\frac{u_{op}u_{motor} + \frac{1}{n}K_E\Omega - L\frac{d}{dt}i_a}{nR_a}\right) + \frac{1}{2}C_Q\rho\pi\Omega^2 R^5 \tag{6.64}$$

Where u_{op} is the motors operating voltage and u_{motor} is the control input.

6.6 Control input and state vectors

In the previous sections, the helicopter's dynamics has been modeled. The complete model has a control input vector given by:

$$\boldsymbol{u} = \begin{bmatrix} u_{motor} & u_{Servo1} & u_{Servo2,3} \end{bmatrix}^T \tag{6.65}$$

Where the control inputs are bounded by:

$$u_{motor} \in \{0,1\}, \ u_{Servo1} \in \{-1,1\}, \ u_{Servo2,3} \in \{-1,1\}$$

And a complete state vector given by:

$$\boldsymbol{X} = \begin{bmatrix} \boldsymbol{\nu} & \boldsymbol{\eta} & \boldsymbol{A1} & \boldsymbol{B1} & \boldsymbol{\Omega_{mr}} \end{bmatrix}^T \tag{6.66}$$

Where $\boldsymbol{\eta}$ is given in 6.3 and $\boldsymbol{\nu}$ is given in 6.6 and:

$$\boldsymbol{A1} = \begin{bmatrix} A1_1 \\ A1_2 \\ A1_3 \\ A1_4 \end{bmatrix}, \ \boldsymbol{B1} = \begin{bmatrix} B1_1 \\ B1_2 \\ B1_3 \\ B1_4 \end{bmatrix}, \ \boldsymbol{\Omega_{mr}} = \begin{bmatrix} \Omega_{mr_1} \\ \Omega_{mr_2} \\ \Omega_{mr_3} \\ \Omega_{mr_4} \end{bmatrix}$$

Chapter 7

Simulation

The helicopter's stability properties and behavior can be examined by simulating it Simulink/MATLAB, where the simulation model is based upon the mathematical models derived in chapter 6. When simulating the helicopter, some important knowledge can be gained about the helicopter's when it is affected by weather. In this simulation, some of the unknown parameters are set to values that match the properties detected when testing the rotor head. The rest of the parameters affect the rotor heads dynamic time constants, which are set to values close to their actual value. This should create a realistic simulation that will give us a good understanding of how this helicopter will behave in the real world.

In this simulation, three different PID controllers are used to control the helicopter's altitude and speed. The helicopter has two speed controllers; one that controls the helicopter's speed by controlling the rotor discs flapping angles, and one that controls the helicopter's forward speed by controlling the helicopter's pitch angle. The controllers set point are adjusted manually and is dependent upon the test that is about to be performed.

This simulation will detect the helicopter's stability properties in pitch and roll and show how the helicopter will behave when subjected to winds and downdrafts.

The Simulink diagram of the simulation is depicted in figure 7.1. The Simulink subsystems are shown in appendix D.
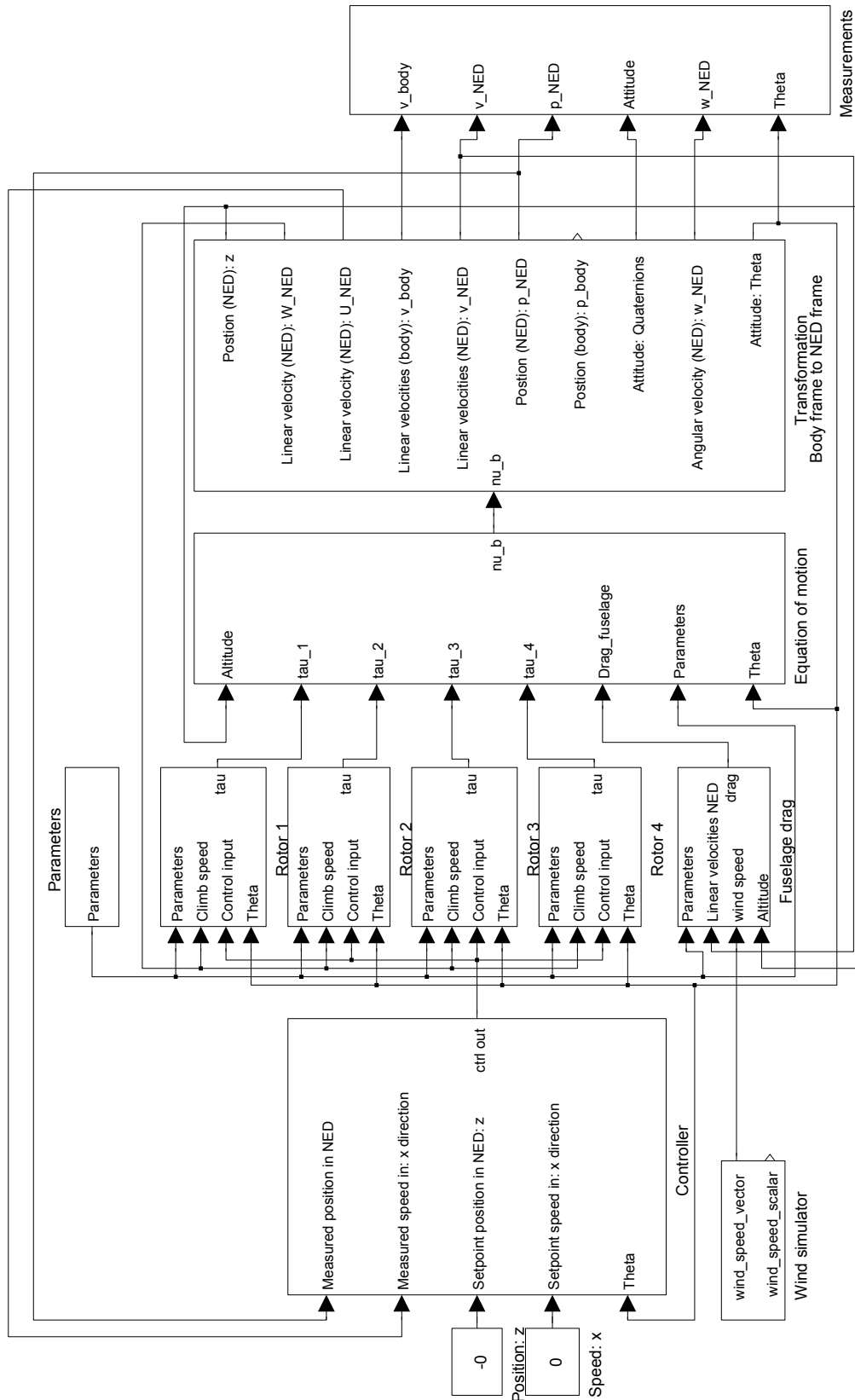
Figure 7.1: Simulation - Simulink diagram - The Simulink diagram comprises the complete dynamics of the helicopter

7.1   Stability in pitch and roll

The helicopter's stability property in pitch is detected by increasing the helicopter's pitch angle until it no longer can maintain its present altitude. The same principle can also be used in roll, but since the helicopter is symmetric, it is only necessary to check one of the angles; that is $\theta_{crit} = \phi_{crit}$. The helicopter's body frame is defined with; the x-axis towards the front, the y-axis towards the right hand side and z-axis pointing downwards (see figure 2.2). The helicopter's pitch angle is the angle around the helicopter's y-axis.

The helicopter's critical DAoA angle θ is the sum of the flapping angle $A1$ (when tilting forward) and the helicopter's pitch angle θ_0 (see figure 3.4).

Since the critical DAoA angle is dependent on the flapping angle $A1$, the flapping angle was set to maximum to simulate worst case scenario. The critical DAoA angle is also dependent upon the helicopter's weight, and the first simulation was performed to detect the relationship between the two. The result is shown in figure 7.2.
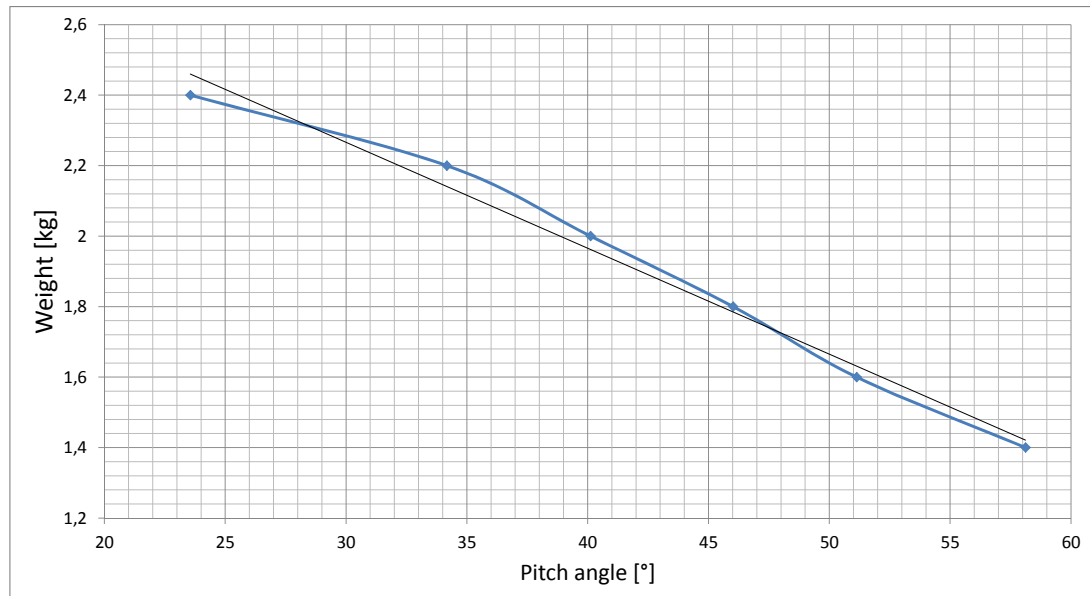

Figure 7.2: Helicopter - stability - The blue line is the relationship between the helicopter's weight and the critical DAoA angle. The black line is a linear curve through the sampled points.

Throughout this simulation, the helicopter will be assumed to weigh $1.4kg$, which means

that according to figure 7.2 the helicopter can have a critical DAoA angle of $\theta_{crit} \approx 58°$, but a safety margin is necessary and θ_{crit} is set to $50°$.

7.2 Stability - crosswinds and downdrafts

Helicopters are very often subjected to crosswinds and downdraft, and it is important to get a better understanding on how the helicopter will behave in these situations.
In the first simulation, the helicopter was subjected to a downdraft. A downdraft is often a big problem for a helicopter when it comes too close to a steep mountain side or a tall building.

The basis for the first test is a levelled (not tilted) helicopter at an altitude of 100 meters moving slowly in the x-direction. The helicopter is then subjected to an increasing downdraft until it cannot maintain lift anymore. The result from this simulation is shown in figure 7.3.
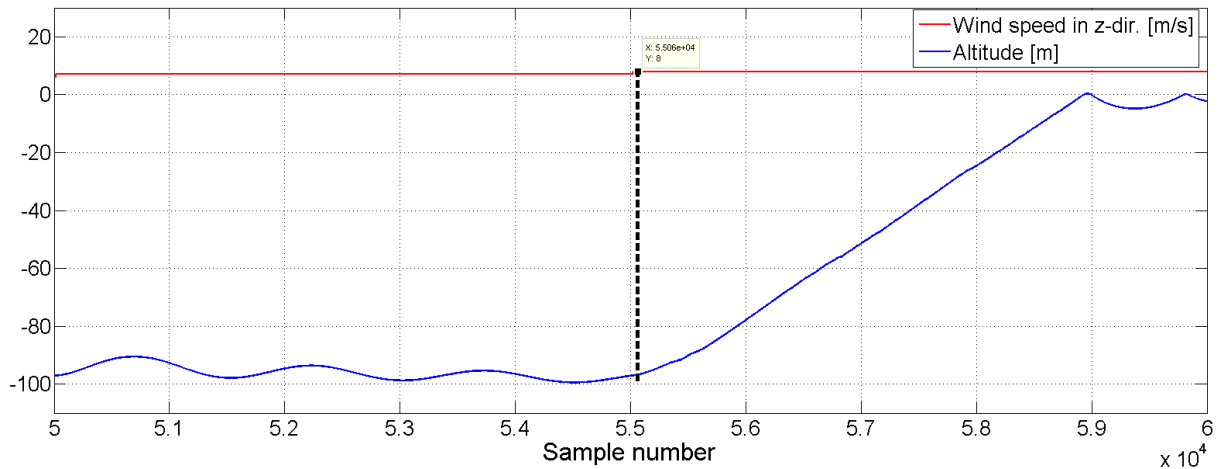

Figure 7.3: Helicopter levelled - downdraft - The plot shows that when the speed of the downdraft is larger than 8 m/s the helicopter cannot maintain its altitude anymore

In the next test, the helicopter will have the same settings as previous, but the helicopter will be tilted at a DAoA angle $\theta = 50°$. The result from this simulation is shown in figure 7.4

In the second simulation the helicopter was subjected to a wind to establish how fast the wind must be, before the helicopter is not able to hold its position anymore. The
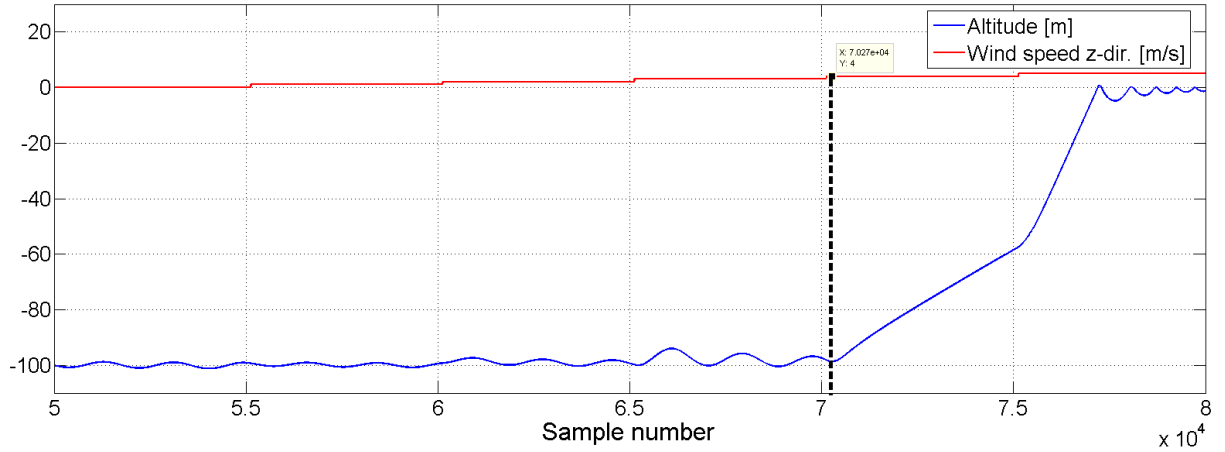
Figure 7.4: Helicopter tilted - downdraft - The plot shows that when the speed of the downdraft is larger than 4 m/s the helicopter cannot maintain its altitude anymore

maximum thrust that the helicopter can output in any direction is dependent on the helicopter's disc angle of attack. When the force of the wind is equal to the helicopter's thrust force in the direction of the wind, the helicopter cannot correct its position anymore.

To determine the maximum speed of the wind, the helicopter is tilted at a DAoA angle $\theta = 50°$ and moves at an altitude of 1000 meter (to create more visible plots). The wind speed is then increased in negative x-direction until the helicopter stops. The plots from this test are shown in figure 7.5.
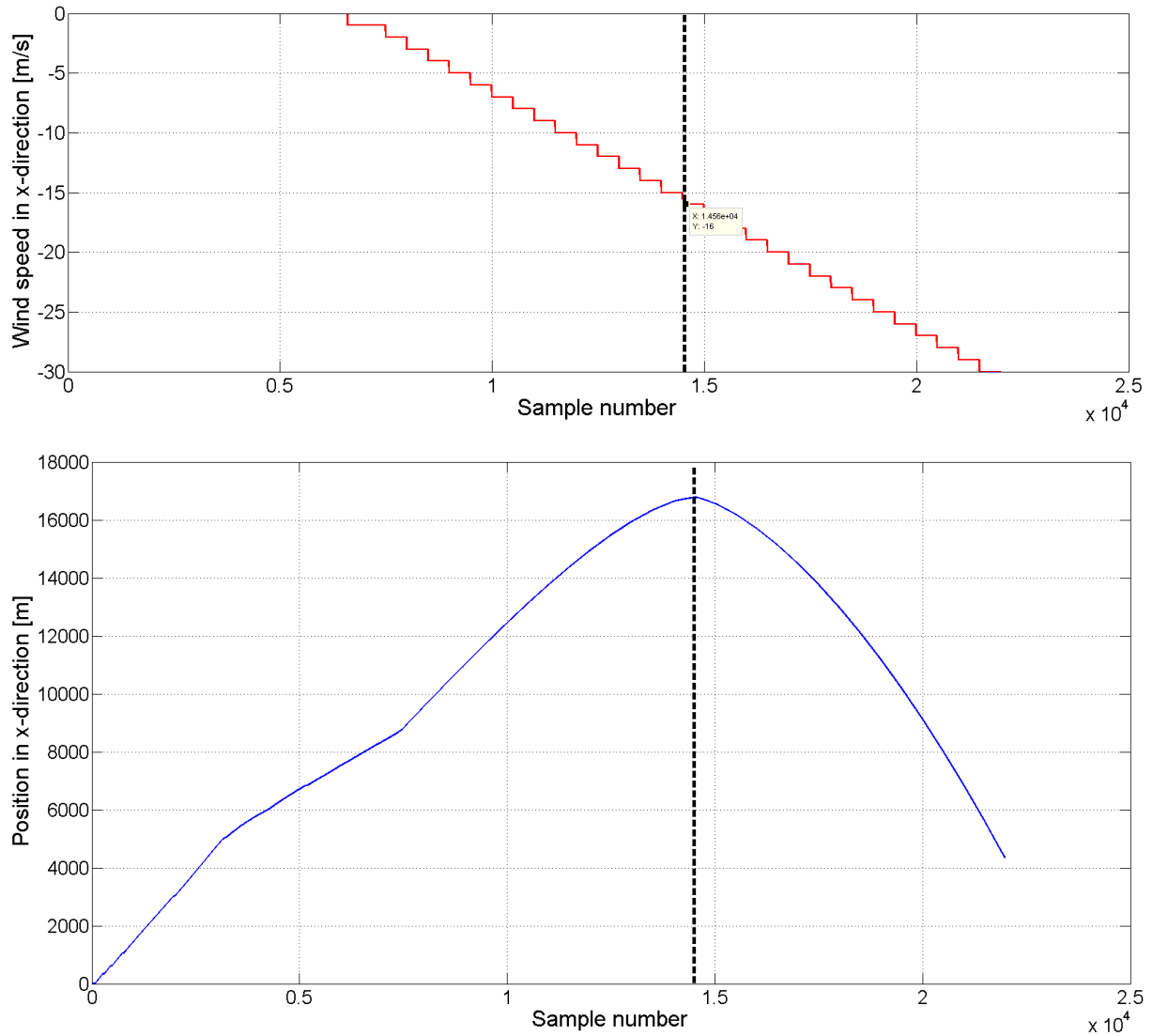
Figure 7.5: Wind stability - The helicopters stability while subjected to wind.

The plot shows that when the helicopter is subjected to wind speeds excessive of $16[m/s]$ the helicopter is not capable of maintaining its position. Since the helicopter is symmetric about the x and y-axis, this result will also be true when subjected to crosswind from the y-direction.

7.3 Speed test

The helicopter has three methods of creating forward thrust. The first method is to use the flapping angles to achieve thrust. The second method is to use the flapping angles and tilt the helicopter while the third method is to use the tilt rotor system. The helicopter will be simulated to detect its maximum forward velocity when using the three methods.

In the first test, the helicopter will use the flapping angle $A1$ to achieve maximum thrust in the x-direction. In this simulation, the flapping angles have been set to maximum $A1 = 2°$ [11]. The result from this simulation is shown in figure 7.6.
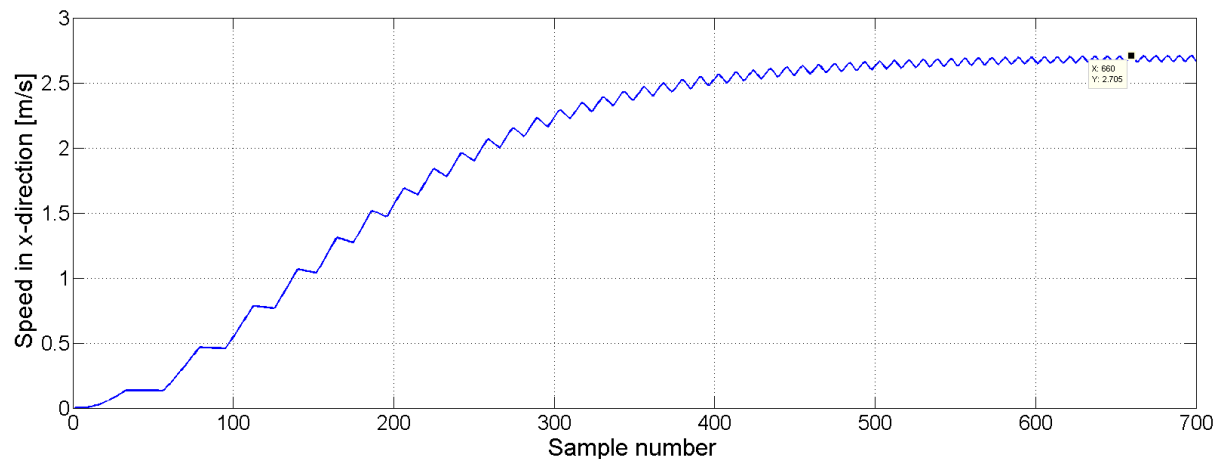

Figure 7.6: Maximum speed - flapping angle - The plot shows the helicopters maximum speed when using the flapping angle $A1$. The maximum speed is according to the plot 2.7 m/s

In the second test, the helicopter will be tilted and the flapping angle at maximum to achieve thrust in the x-direction. The result from this simulation is shown in figure 7.7.

In the third and final test, the helicopter will use the tilt rotors to achieve maximum thrust in the x-direction. The result from this simulation is shown in figure 7.8.
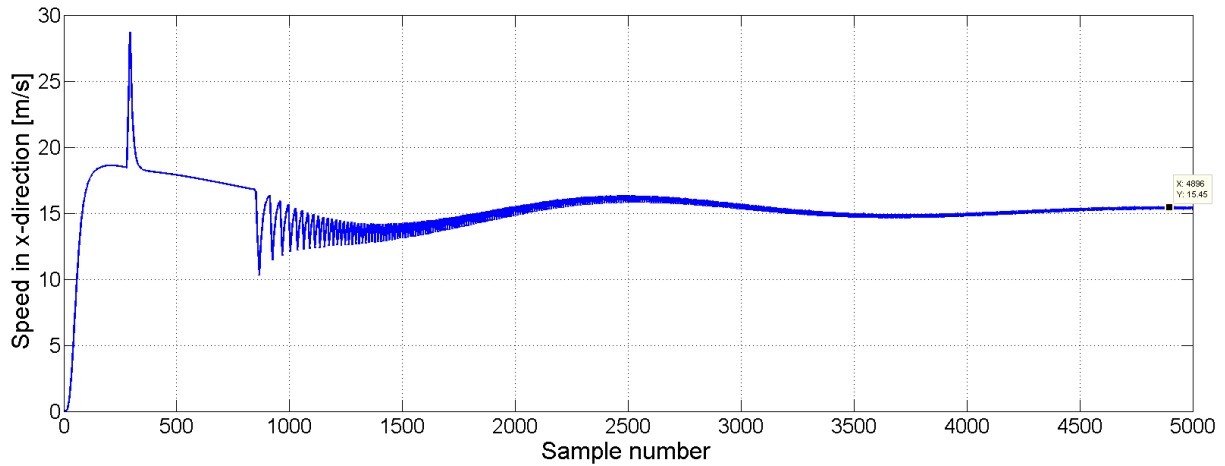
93

Figure 7.7: Maximum speed - flapping angle and tilt - The plot shows the helicopters maximum speed when using the flapping angle and tilting the helicopter. The maximum speed is according to the plot $\approx 15 \ m/s$. The spike on the curve is due to the altitude controller, which controls the helicopters thrust.
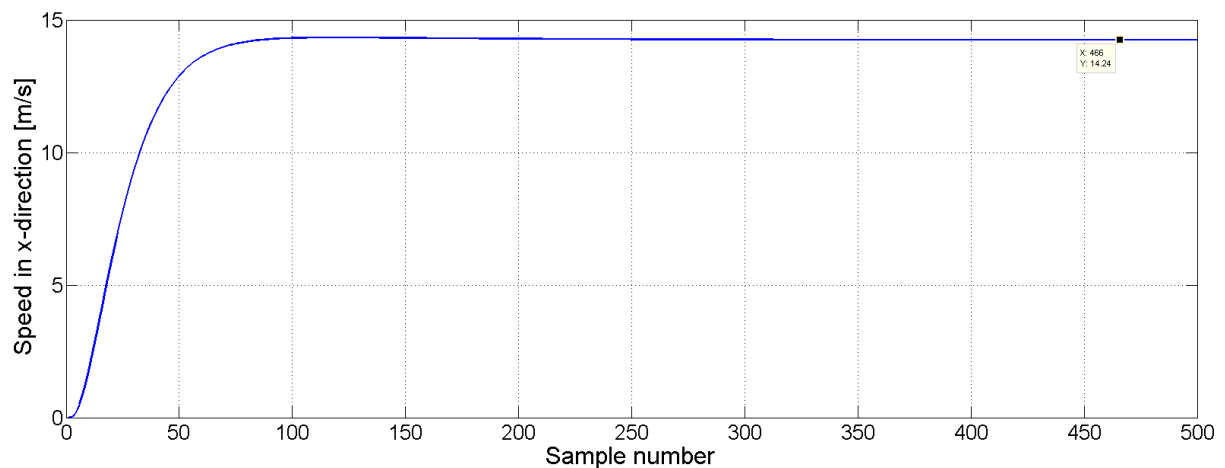

Figure 7.8: Maximum speed - tilt rotors - The plot shows the helicopters maximum speed when using the tilt rotors. The maximum speed is according to the plot $\approx 14 \ m/s$.

7.4 Conclusion of the simulation

The result of the stability tests shows that the helicopter has a critical DAoA angle of 58°, which is a reasonable result compared to a standard big size quadcopter. Many of the standard quadcopters operate from a maximum tilt angle between $45 - 60°$. To establish a safety margin and achieve a good response from the helicopter, the maximum DAoA angle was set to 50° for the rest of the tests.

The results from the wind tests shows that the helicopter can resist downdraft with speeds up to 8 m/s when it is levelled and 4 m/s when it is tilted. The helicopter can also resist crosswinds with speeds up to $16[m/s]$ which is "High wind" according to Beaufort's wind scale.

The results from the last test shows that this helicopter can move at a speed of $\approx 15m/s$ both tilted and levelled. The advantage of having a helicopter that can fly while levelled is the opportunity to equip the helicopters with wings, which would create extra lift and thereby reduce fuel/battery consumption.

The conclusion when all the results have been reviewed is that the helicopter performed very well and within the borders of what could be expected of it.

Chapter 8

Architecture

The helicopter's architectural design is divided into three different sub-architectures, a system architecture, a hardware architecture and a software architecture. The three architectures gives a better understanding on how the different parts are connected and how they interact.

8.1   System architecture

The helicopter's system architecture is an overview on how the software and hardware operate together, and is depicted in figure 8.1.   The software modules are a proposal on how the software can be constructed such that the helicopter can operate in autonomous and manual mode.

To understand this section better, three of the used terms will be explained. The term "waypoint" is defined as a set of coordinates that identifies a point in space while the term "path" is defined as a set of waypoints which is a geometrical description of the helicopter's movement. The term "trajectory" is defined as the path which the helicopter will follow through space as a function of time.

The helicopter's system architecture is designed to operate in two different operation modes. The helicopter can either operate in Unmanned Aerial Vehicle (UAV) mode or in manual mode.
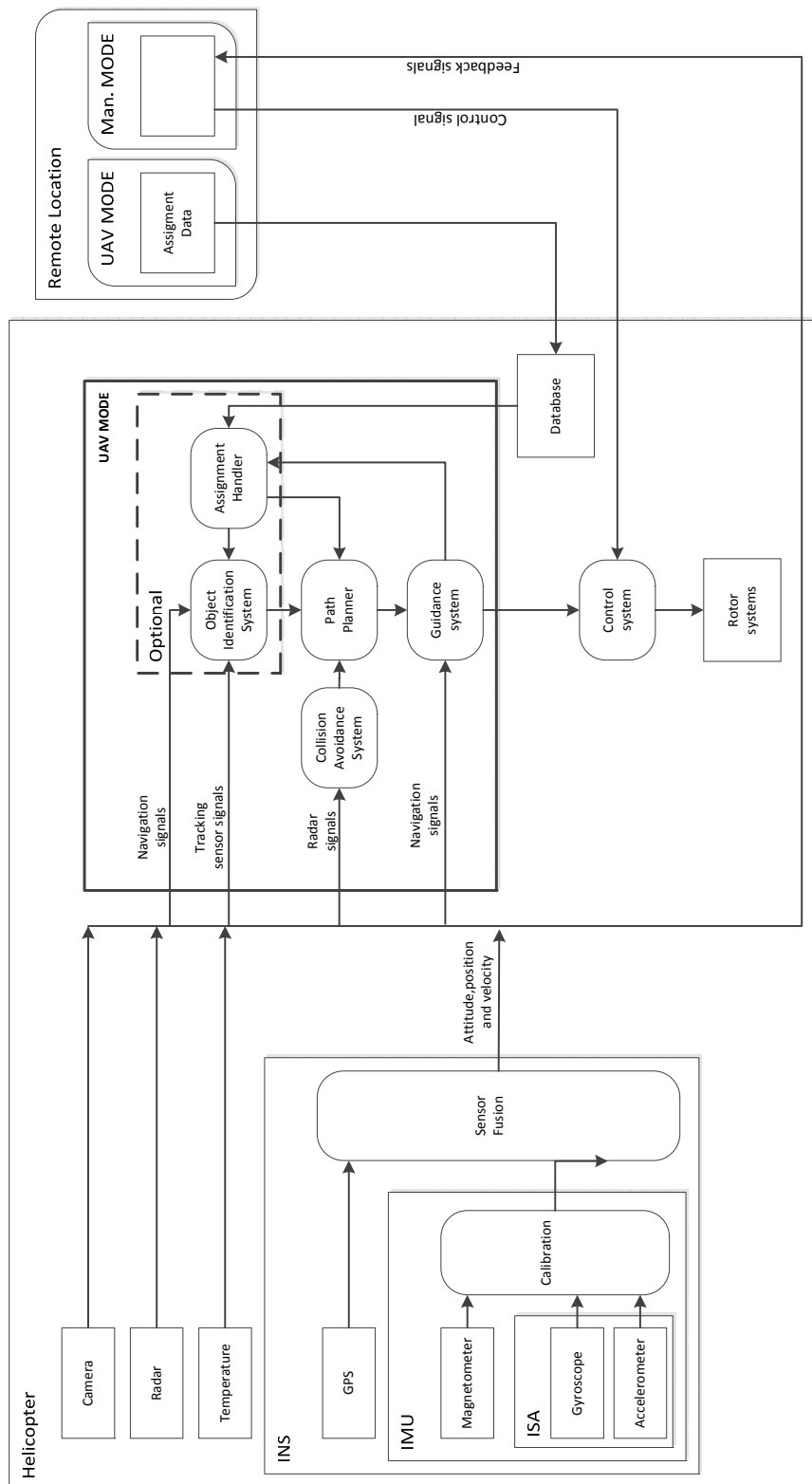
Figure 8.1: System architecture - block diagram for the control system.

8.1.1 UAV mode

When the helicopter is in UAV mode, the assignment data can be uploaded from a remote location to the helicopter's database. The assignment data consists of desired waypoints, objects to track, priorities and so on. The waypoints are represented by a Cartesian coordinate, a speed and a heading.

The Assignment Handler (AH) extracts the information from the database and sends data to the Path Planner (PP) and the Object Identification System (OIS). The path planners task is simple and consists only of deciding if the desired path is possible or not, and deals with the request of next waypoint from the guidance system. If the path planner is not interrupted by the Collision Avoidance System (CAS) or the object identification system, the path is sent to the Guidance System (GS) which then generates set points to the control system. When the helicopter reaches the desired waypoint, the guidance system will ask the assignment handler for the next waypoint. The assignment handler will then fetch the next waypoint from the database and send it to the path planner which will pass it on to the guidance system as long as there are no messages from the OIS or the CAS. This loop will continue to the end of the assignment. If the path planner receives an input from the CAS system, it will compare the proposed waypoints from the CAS with the priorities given in the assignment file and incorporate the one with the highest priority in the path. To ease the complexity of this project, better and more advanced methods of obstacle avoidance will not be a part of this project.

The OIS system receives data from the assignment handler about the object and its priority. If the OIS system detects and object of interest it will interrupt the path planner by sending a new waypoint and a priority, which the path planner will matches against the priority of its existing waypoint, and choose the one with the highest priority.

8.1.2 Manual mode

When the helicopter is in manual mode, the helicopter can be controlled from a remote location. One way of controlling the helicopter in real-time is by satellite communication. Satellite communication is a two way communication channel, which could also

be used to deliver feedback from cameras and other sensors. To limit the extent of this project it is used traditional radio frequency to control the helicopter.

8.2 Hardware architecture

The helicopter's hardware architecture explains how the hardware is connected together and how they communicate through different interfaces. All the different types of hardware and its properties are explained later in this section. The hardware's architecture is shown in figure 8.2.
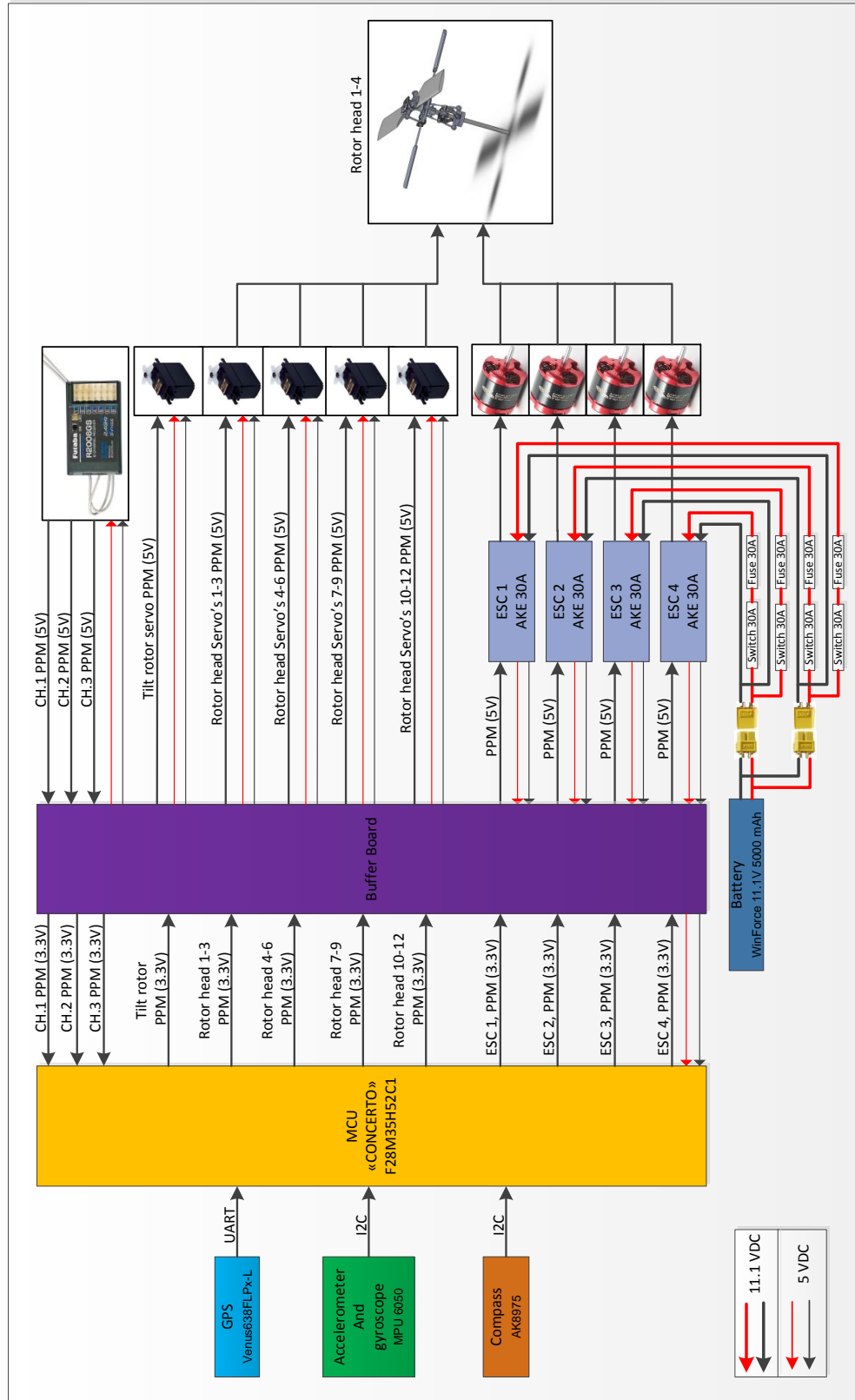
Figure 8.2: Hardware architecture - The Hardware architecture comprises the MCU, accellerometer, gyroscope, magnetometer, GPS, speed controllers, battery, RC receivers and the buffer card.

8.2.1 Micro-controller unit

The Micro-Controller Unit (MCU) selected for this project is the "F28M35H52C1" with the codename "Concerto". The MCU is developed by Texas Instruments and belongs to the c2000 "real-time" micro-controllers, which has a unique construction. The MCU comprises a dual-subsystem technology, with a master subsystem (ARM Cortex-M3 core) and a control subsystem (C28x core). The development card for the concerto is depicted in figure 8.3.
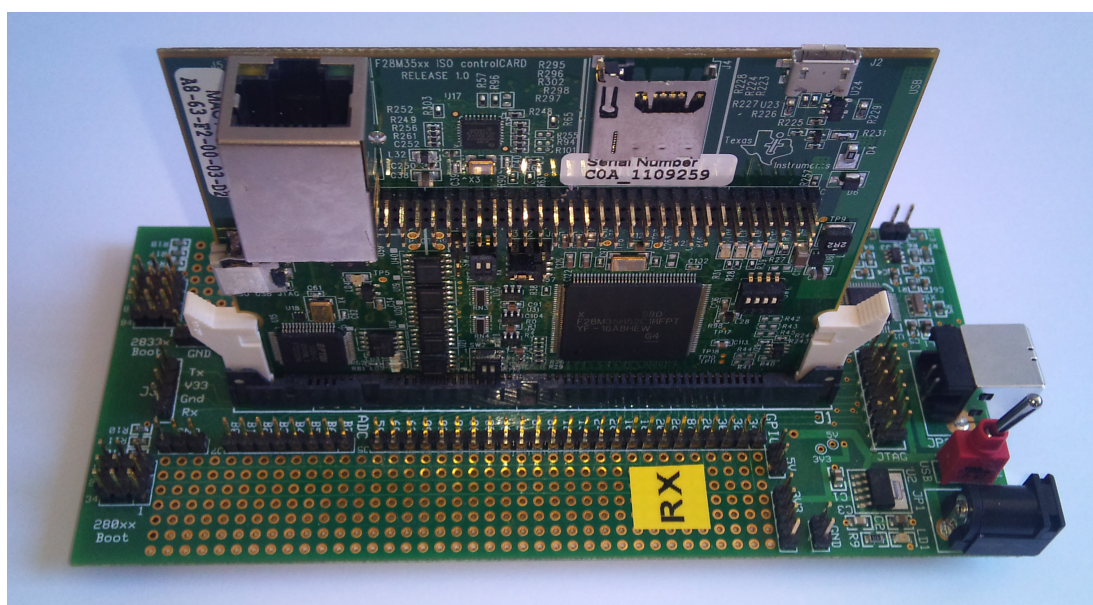

Figure 8.3: MCU Concerto - F28M35H52C1 - The development card is divided in two; the bottom part is a shared platform that is used on many different micro-controllers, while the top part is the card for the Concerto MCU

The ARM Cortex-M3 core is optimized to run an operating system (scheduling), non-real-time tasks and handle all external communication, while the C28x core is designed to run all time critical real-time tasks for control. The advantage of this dual-subsystem is that there is no need to compromise between communication and control. The two subsystems communicate through an Inter-Processor Communication (IPC), which is based on shared memory. The F28M35Hx series C28x core can operate up to 100 MHz and contain up to 512KB flash memory while the ARM Cortex-M3 core can operate up to 150 MHz and contain up to 512KB flash memory. The master subsystem

have five Universal Asynchronous Receiver/Transmitters (UARTs), two I^2C interfaces, four Serial Peripheral Interface (SPI) and one 10/100 Ethernet interface. The control subsystem have a Floating Point Unit (FPU) unit, six-channel Direct Memory Access (DMA), one SPI interface, one I^2C interface and nine Enhanced Pulse Width Modulation (EPWM) modules with two outputs A and B resulting in a total of 18 EPWM outputs. The Concerto MCU's is selected because of its unique construction, which have all the necessary inputs and outputs required for this project, and the flexibility needed with regards to future expansions.

8.2.2 Inertial sensors

The inertial navigation chip selected for this project is the MPU6050 developed by InvenSense. The MPU6050 is the world's first integrated 3-axis accelerometer and 3-axis gyroscope where the gyroscope/accelerometer cross-axis misalignment associated with discrete solutions is eliminated through embedded sensor fusion technology. The MPU6050 is depicted in figure 8.4.
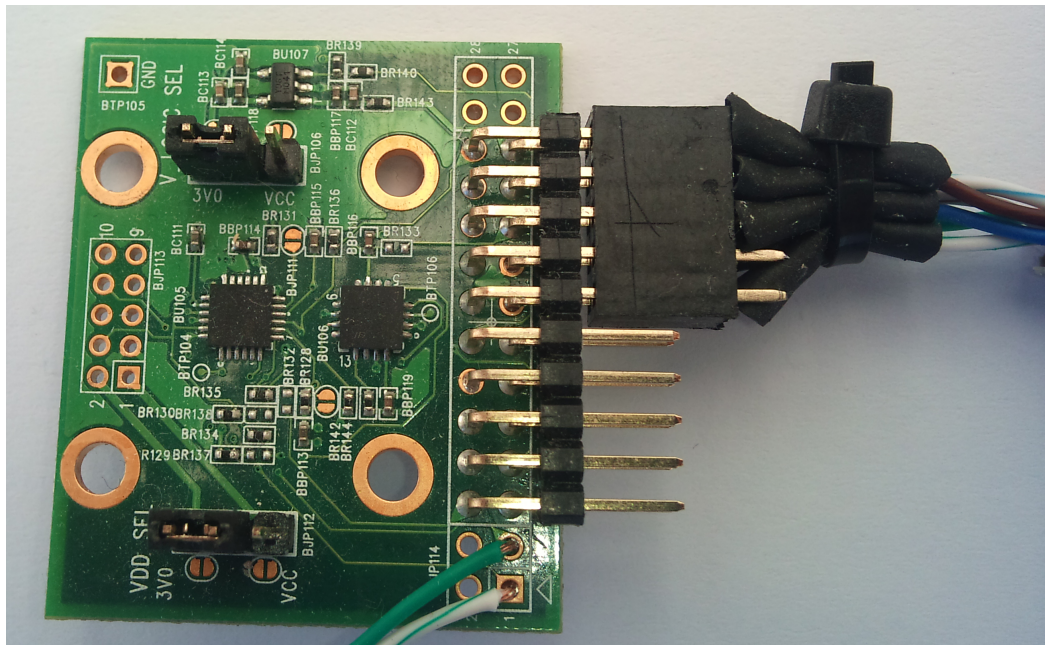

Figure 8.4: Inertial sensor - MPU6050 development card - The MPU6050 development card comprises a 3-axis accelerometer, a 3-axis gyroscope and an external chip with a 3-axis magnetometer

Even though, it only incorporates two of the sensors (accelerometer and gyroscope) it is possible to connect a magnetometer to it through an auxiliary master I^{2}C bus. This allows for a full data set without intervention of the micro-controller. The MPU6050 communicates through I^{2}C and can deliver digital-output of 6 or 9-axis motion fusion data in rotation matrix, quaternion, Euler Angle, or raw data format. It has a dynamic range for both the accelerometer and the gyroscope and even a low power mode. In this project, the Development Board (DB) for the MPU6050 is used, which has an on-board magnetometer AK8975 developed by AKM. This means that the MPU6050 DB can output a complete data set needed for navigation. The inertial sensor has many unique features, which made this a preferable choice.

8.2.3 GPS

The GPS system selected for this project is a breakout board of the Venus638FLPx GPS. The GPS shall provide accurate position data, which is used to calibrate the inertial system. The Venus638FLPx is depicted in figure 8.5.
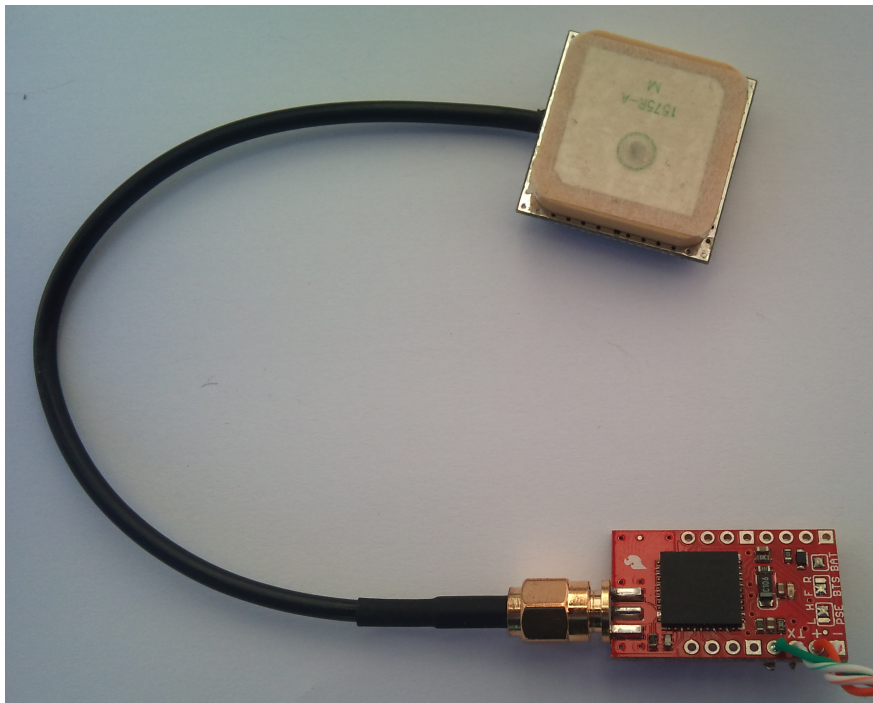

Figure 8.5: GPS - Venus638FLPx breakout board - The Venus638FLPx is equipped with an antenna that has a SubMiniture version A (SMA) connector

The Venus638FLPx has a maximum update rate of 20Hz, which is fast compared to other GPS's on the market, and outputs standard NMEA-0183 or SkyTraq Binary on a UART at a selective speed between 9600-115200 bps. The accuracy of the GPS is about $2.5m$, and requires a 3.3 volt supply to operate. It only uses 60 mA at reduced power and 90mA at full power. The GPS board can be outfitted with a super capacitor, which provides ultra-fast restart after a power cycle. If the helicopter is not to fare off from its actual position, the GPS receiver can use the INS's current position to "hot-start" the search for satellites, and thus speeding up the reacquisition time. The GPS's fast update time, powerful antenna and NMEA output, made this GPS favorable compared to other GPS's.

8.2.4 Buffer card

The buffer card has three different tasks to perform. The first is to convert 3.3V PWM output from the MCU to 5V PWM, which is connected to the electronic speed controller and servo motors. The second task is to convert 5V PWM input from the RC receiver to 3.3V PWM, which is connected to a high impedance input on the micro-controller. The last task is to supply the MCU and the servo motors with 5V power.

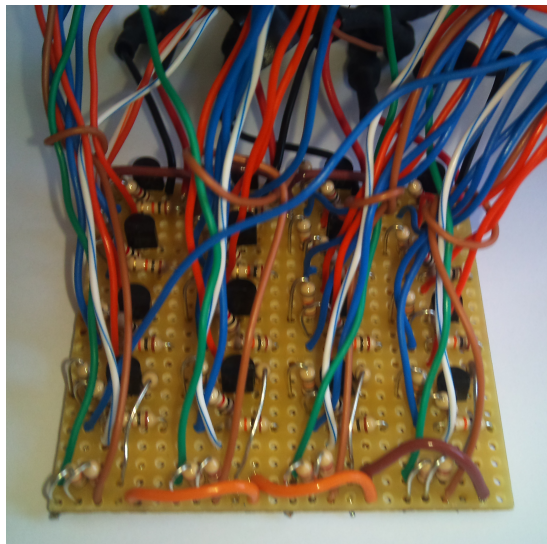The complete buffer card is shown in figure 8.6.

Figure 8.6: Buffer card - The buffer card is made from a experimenter circuit board and has support for sixteen 3.3V to 5V PWM and four 5V to 3.3 PWM

8. ARCHITECTURE

The conversion of 3.3V PWM to 5 PWM is done by using a NPN switching transistor. The 5V PWM is used to control the servo motors and the motors for the rotor heads. The servo motors must have a signal that lasts no more than 1-2ms, or else it can get damaged. To prevent this from happening, a pull-up resistor R1 is connected to the base of the transistor.

The purpose of R1 is to open the transistor when there is no input signal, such that the output is zero and the servo motors do not get any signal. The conversion circuit from 3.3 V PWM to 5V PWM is shown in figure 8.7.
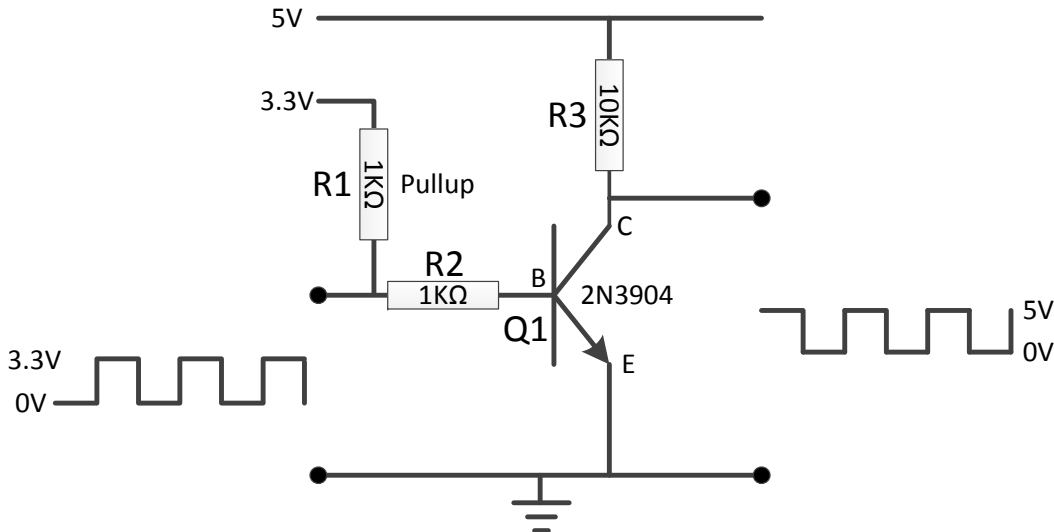

Figure 8.7: Buffer card - 3.3V PWM to 5V PWM - The conversion from 3.3V PWM to 5V PWM is done by using a transistor.

The Base-Emitter current in figure 8.7 is given by:

$$I_{BE} = \frac{3.3\,|V| - 0.7\,|V|}{1000\,|\Omega|} = 2.6\,|mA| \tag{8.1}$$

Since the transistors Base cut-off current is 50nA (listed in the datasheet [17]), this transistor will open when a 3.3V signal is applied.

The conversion from 5V PWM to 3.3V PWM is done by using a voltage divider as shown in figure 8.8.

106

The voltage is computed by using:

$$U_2 = \left(\frac{U_{in}}{R1 + R2} \right) \cdot R2 = \left(\frac{5\,|V|}{1000\,|\Omega| + 5100\,|\Omega|} \right) \cdot 10000\,|\Omega| = 3.31\,|V| \qquad (8.2)$$

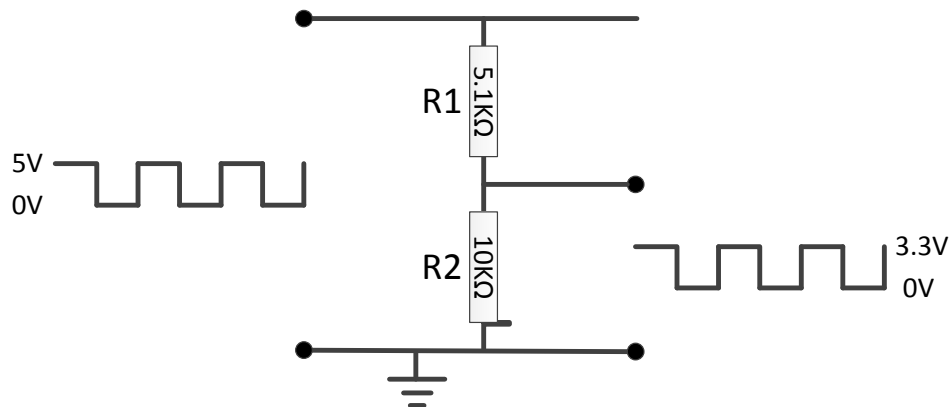The 3.3V PWM is input to the MCU, which interprets the control signals from the RC receiver.

Figure 8.8: Buffer board - 5V PWM to 3.3V PWM - The conversion from 5V PWM to 3.3V PWM is done by using two resistors.

8.2.5   RC Transceiver

The transceiver selected for this project is a Futaba "T6J" transmitter and a Futaba "R2006GS" receiver. The Futaba transceiver is a 2.4 GHz with Futaba Advanced Spread Spectrum Technology (FASST) system, which holds many important advantages compared to other 2.4 GHz systems [5]. The transmitter and receiver are depicted in figure 8.9.

Figure 8.9: Futaba transmitter and receiver - The T6J transmitter and R2006GS receiver

The Futaba's FASST system changes frequencies hundreds of times per second to prevent interference with other transceiver systems and applies sophisticated error techniques to the incoming data to ensure an error free connection between transmitter and receiver. The transmitter is linked to a receiver with a unique factory code, which guarantees that the receiver will only respond to this particular transmitter. To ensure a good reception and prevent signal loss, the receiver can also switch between two different antennas.

Another remarkable advantage with this system is its minimum latency which ensures real-time fast response of the control subject. The Futaba's transceiver system was selected because of its uniqueness compared to other brands on the market, which made this choice easy.

8.2.6 Gear

A big challenge when designing the rotor system was finding a suitable gear that would fit the 3 mm motor shaft and the 5 mm rotor shaft. Finding a gear for the 5 mm shaft was a lot easier, because it is not limited to the RC community. Most of the RC parts are usually related to a specific car, helicopter or air plane, where its dimensions are not important. This made it more difficult to find a suitable gear for the motor. In general, gears are identified by the pitch, number of teeth and pressure angle. In the RC community, the pitch angle is usually 48 or 64 and has a pressure angle of 20 degree. The pitch is the distance between the teeth's along the gears circumference, and the pressure angle is the angle between the slope of the teeth and the teeth's perpendicular axis. A typical gear and its properties are shown in figure 8.10. When the rotor system
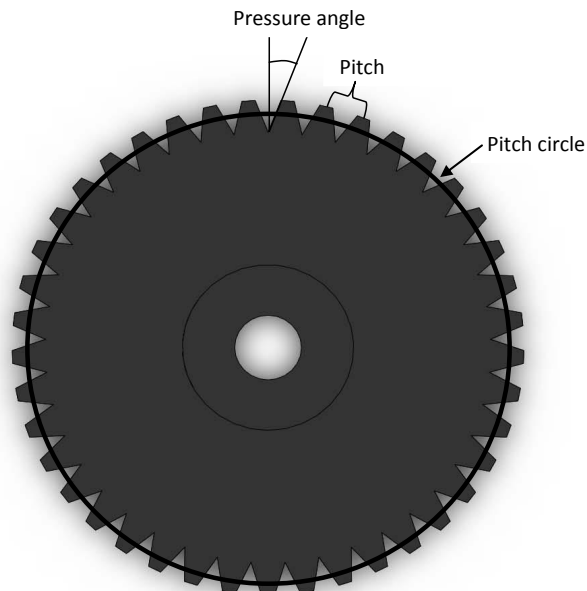

Figure 8.10: Gear properties - The three most important properties on a gear are the number of teeth's, pitch angle and pressure angle.

was designed, the gears where selected from parts where the outer diameter was given. This restricted the number of pinion gears that would fit this project. Later in the project it was discovered a formula that could compute the gears outer diameter based on the pitch angle and the number of teeth [16].

$$D_0 = \frac{N + 2}{P} \tag{8.3}$$

Where D_0 is the outer diameter (inch), N is the number of teeth and P is the pitch angle.

If this information would have been available earlier the gears for the 450-size design could have been selected with a larger diameter, such that the gears would have been easier to connect. Even so, the teeth size would still have been the same, which was the main issue, and the result would not have been different.

8.2.7 Motor

The selection of the BrushLess Direct Current (BLDC) motor is dependent on the outcome of the computation derived in chapter 4. The required power for one rotor

Figure 8.11: BLDC motor - The selected BLDC motor for this project

system was computed (worst case) to 228 Watt. Many different motors where evaluated, but the required power, reliability and recognition, made the selection a little easier. The motor selected is the 250 Watt NTM Prop Drive Series 28-26A, which is depicted in figure 8.11.

8.2.8 Speed controller

The helicopter's rotor speed is controlled by an Electronic Speed Controller (ESC), which converts a PWM signals duty cycle to motor power. The ESC selected for this project is the 20A ESC produced by Hobbyking, which was recommended for the selected motor. The ESC is depicted in figure 8.12.
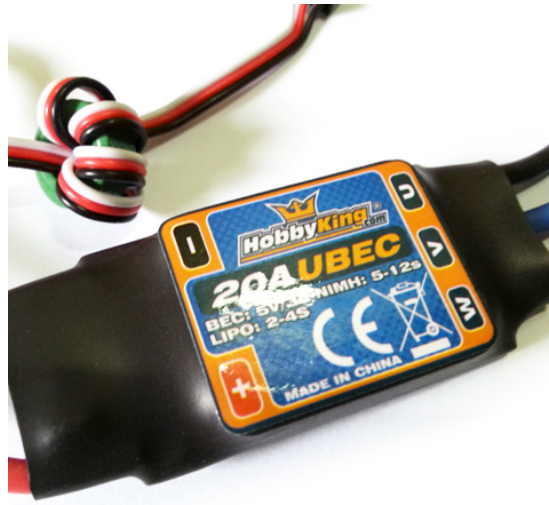

Figure 8.12: **ESC - Hobbyking** - The specified ESC for this project

The ESC is connected between the motor and the battery and in addition to controlling the motor, it also delivers a 5 Volt DC to drive additional circuits like the microcontroller, servo motors and so on. A detailed sketch on how the ESC is connected to the motor is depicted in figure 8.13.

The duty cycle can be computed by using:

$$D = \frac{\tau}{T} \tag{8.4}$$

Where τ is the duration of the pulse, and T is the period. The PWM control signal must have a maximum duration of 1 - 2ms, or else the speed controller could get damaged.

PWM signal to
ESC (5V)

Power out of
ESC (5V)

Power from
battery (11.1V)

Speed controller

AKE
20 AMP
ESC

Brushless motor

Duty cycle = 10% (2ms)
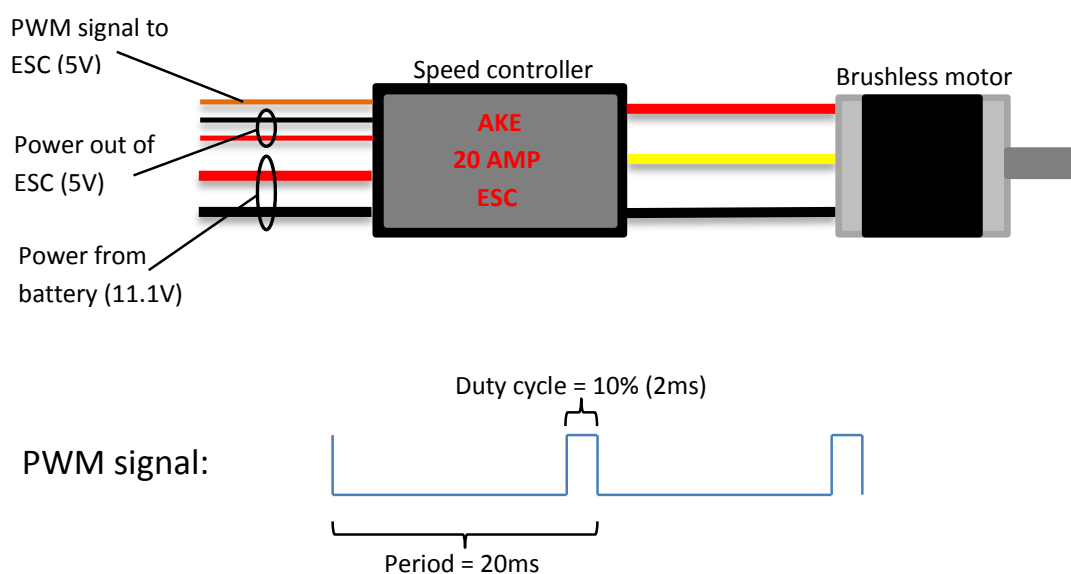
PWM signal:

Period = 20ms

Figure 8.13: ESC - PWM duty cycle - The figure shows how the ESC is connected
to the motor and battery, and explains the term "duty cycle"

8.2.9 Servo motor

The servo motor selected for this project is the DS65HB digital high speed servo. Up
to a few years ago, the only servo existed was the analog servo. The analog and the
digital servo are very much alike, and comprise a casing, motor, gears and a feedback
potentiometer. The main difference between these two types of servos is how the
feedback from the receiver is processed, and how this information is utilized to control
the servo motor.

The analog servo controls the motor by sending pulses to it. The pulses has a constant
voltage and is sent to the motor with a frequency of 50Hz. The movement of the motor
is dependent on the signals duty cycle (how long it is on), and the duration is usually
between 1-2 ms. The higher duty cycle, the faster the motor turns and the more torque
it produces.

In contrast to the analog servo, the digital servo has a microprocessor inside that ana-
lyzes the receiver signal and converts them into high frequency pulses. The servo motor
is now receiving pulses with a frequency close to 300Hz instead of 50Hz. This guar-
antees that the motor speed up faster and delivers a constant torque. The advantages
are a much smaller dead-band, faster response, quicker and smoother acceleration and

better holding power. The servo motors dead-band is the area of sluggish response when the servo motor is given a small movement command. A picture of the digital servo motor DS65HB is shown in figure 8.14.

Figure 8.14: Digital servo motor - DS65HB - The digital servo motor DS65HB

8.3   Software architecture

The helicopter's software architecture is a proposal on how the software can be constructed such that the helicopter can operate in autonomous and manual mode. The architecture give an overview of the software's modular structure and describes the purpose of the different modules and how they interact. The software architecture is depicted in figure 8.15

The Communication module takes care of communication to and from the helicopter. The communication to the database and to the control system module is separated on two different communication ports. When the helicopter is in manual mode, the communication module receives remote input to control the helicopter and sends back video data (not part of this project). When the helicopter is in UAV mode, the assignment data is downloaded to the database through the communication port assigned for the database.

The collision avoidance module uses the radar signals to detect objects it wish to avoid. If an object emerges that block the path, the system will calculate a new safe waypoint according to priorities given in the assignment data and sends it to the path planner.

The path planners job is to evaluate if the helicopter should follow the desired path in the assignment data or if there is a new path that has higher priority. In the latter case, it will include a new waypoint to the path, and the path is then sent to the guidance system module. Once the guidance module has got the reference path from the path planner module it will use a guidance scheme called Line Of Sight (LOS) to make sure that the helicopter follows the reference path as close as possible. More literature on the line of sight scheme can be found in [4].

The output from the guidance system module is used as input to the control system module which controls the helicopter through its rotor systems. The control system module comprises an on-line system identification scheme that is used to create an on-line model of the system. This model is used as a black-box model for the Model Predictive Controller (MPC). More on this can be found in chapter 10.

The inertial navigation module calibrates the measurement data from the inertial sensors and produces more accurate measurement data through sensor fusion. The ac-
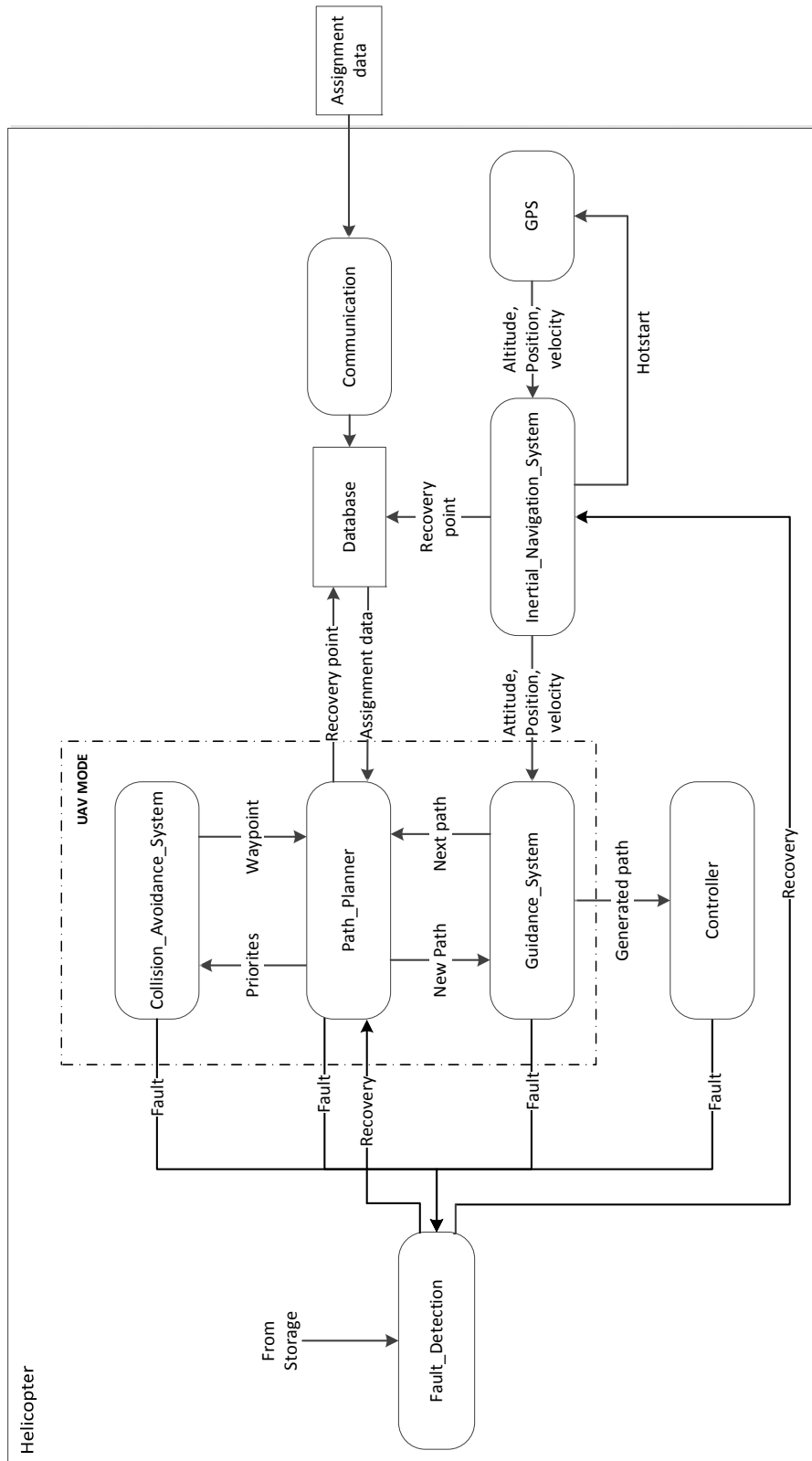
Figure 8.15: Software architecture - The figure shows the modular structure of the software architecture

celerometer, gyroscope and magnetometer are very temperature dependent, and their measurements drift if they are not calibrated when the temperature change. The accelerometer has a built in temperature sensor, and since all three inertial sensors are within proximity, the temperature measurement from the accelerometer is used to calibrate all three sensors. The calibrated measurements are then fused together with the data from the GPS sensor, to produce an accurate attitude, position and velocity.

Chapter 9

Final design and assembly

When designing a helicopter it is crucial that all the important details like; weight, rigidity, power consumption, response time, drag forces, clearances and space, are considered. The main part of a helicopter is the frame, and this chapter will start by reviewing the selected frame and the necessary modifications that needs to be done.

9.1 Helicopter frame

The helicopter's body frame selected for this project is a "X-450" quadcopter frame. The X-450 frame is made of carbon fiber and aluminum, which makes this frame very light and strong. The frame is very suitable for this project due to the fact that it is very easy to modify and assemble.

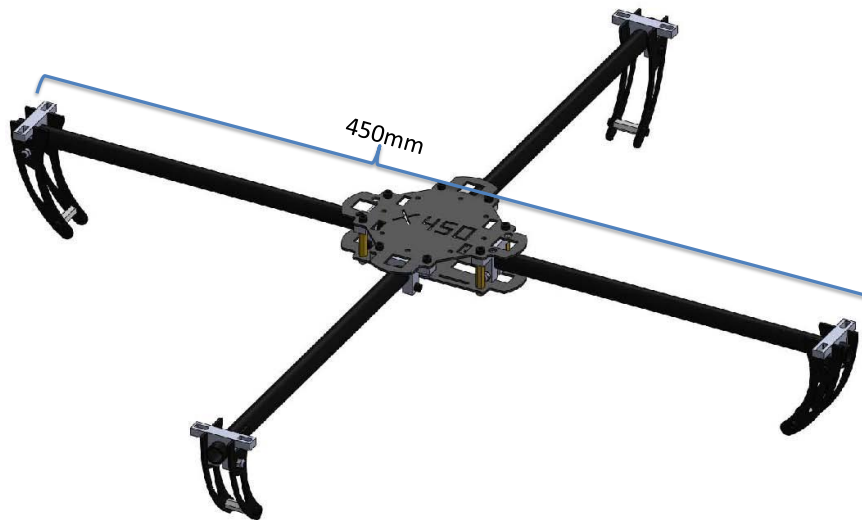The X-450 frame is depicted in figure 9.1.

Figure 9.1: Helicopter frame - The helicopter frame is a X-450 frame, which means that the diagonal distance between the leg booms are 450mm

The center part of the frame has a top and a bottom plate as depicted in figure 9.2. The disadvantage with the X-450 frame is the bottom plate, which only supports two
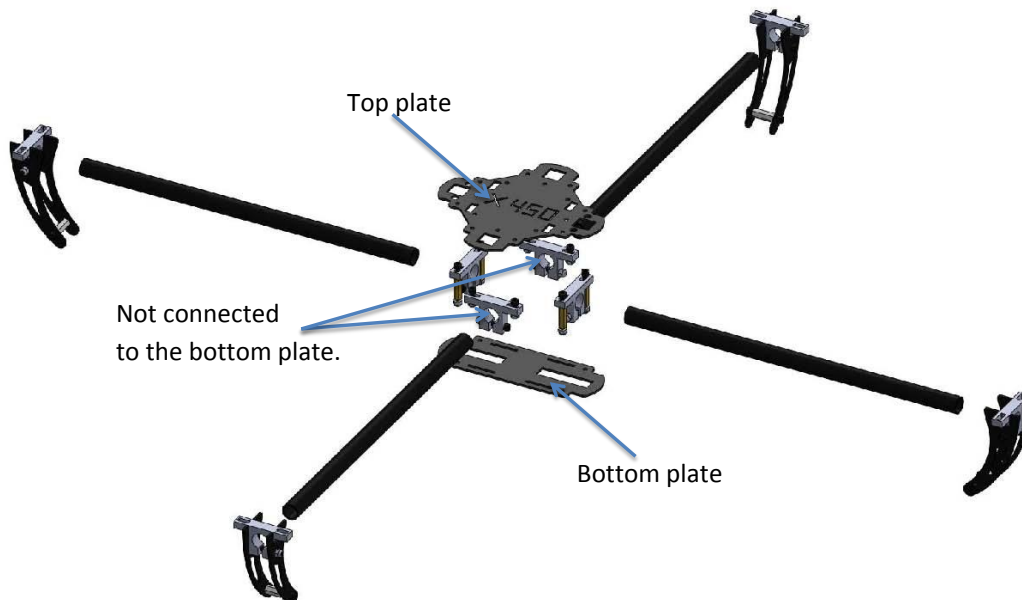

Figure 9.2: Helicopter frame - exploded view - The helicopter frame is shown in exploded view.

of the leg booms. This makes the body frame too flexible to be used in this project (see figure 9.2). The solution to this problem is to exchange the bottom plate with a top plate. This would make the frame very rigid and suitable for this project.

Since the helicopter is specified with tilt rotor function, two of the aluminum brackets have to be redesigned and equipped with ball bearings. The ball bearings for this project are depicted in figure 9.3.
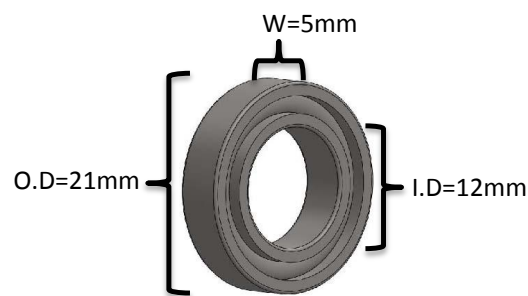

Figure 9.3: Tilt rotor ball bearing - The ball bearing has an inner diameter of 12mm, an out diameter of 21mm and a width of 5mm.

The easiest and fastest way to manufacture the aluminum bracket's is by modifying an existing and available product. The disadvantage is that it will weigh a little more than necessary. Compared to weight of the helicopter this will not be noticeable. A suitable product is the high quality 20mm Aluminum Shaft Support Pillow, which is depicted in figure 9.4.
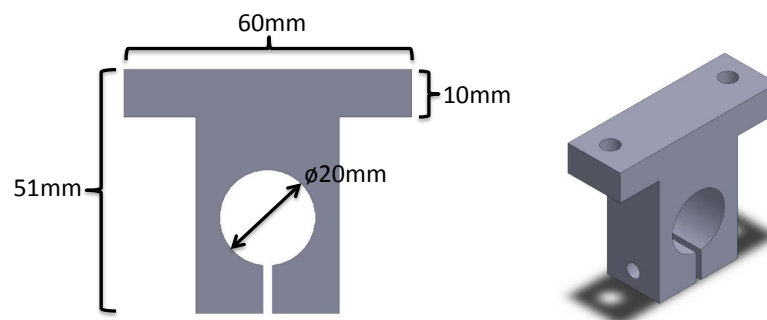

Figure 9.4: Commercial available support pillow - The picture shows a commercial available support pillow.

The support pillow needs to be modified to fit the helicopter frame, and is shown in
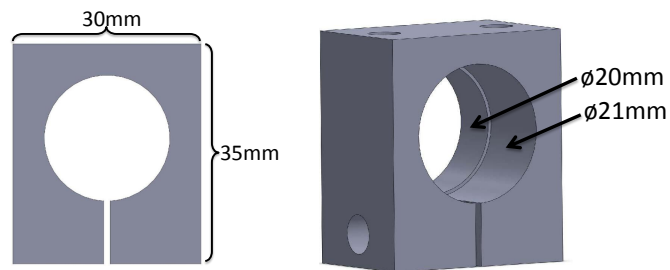
figure 9.5.

Figure 9.5: Modified support pillow - The picture shows the modified support pillow.

The modified helicopter frame with the new support pillows, ball bearings and the new bottom plate is depicted in figure 9.6.
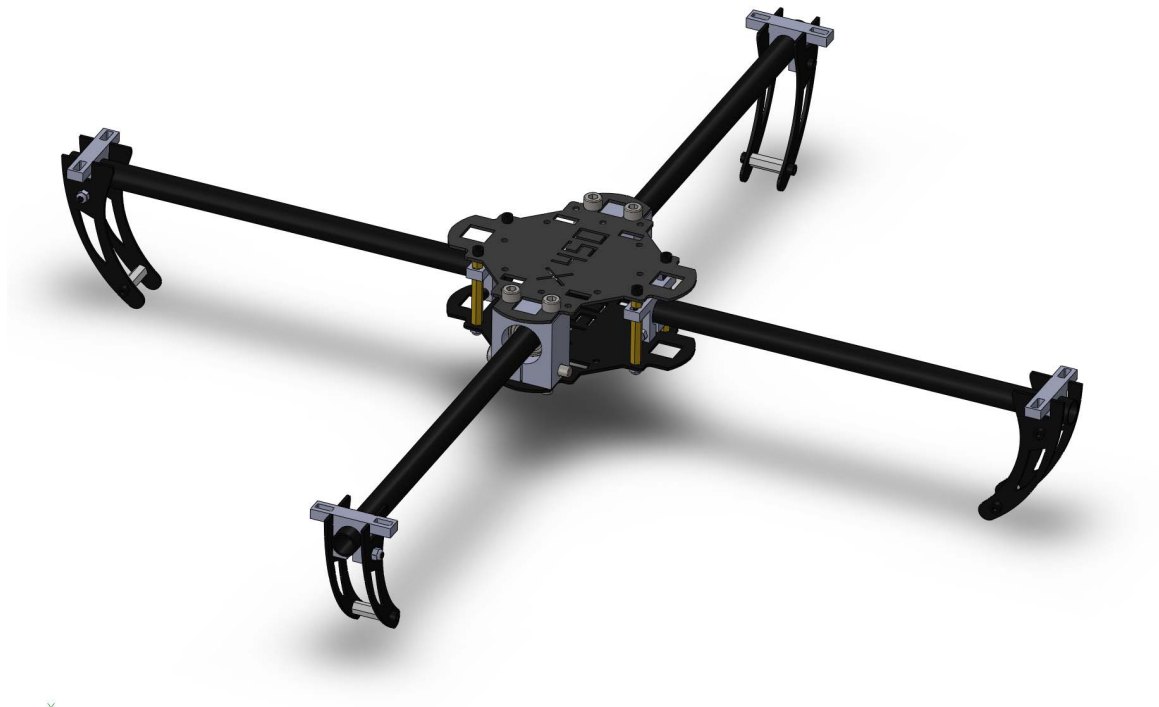
Figure 9.6: Modified helicopter frame - The modified helicopter frame with the new support pillows, ball bearings and bottom plate.

9.2 Final build

The final design of the helicopter is shown in figure 9.7.

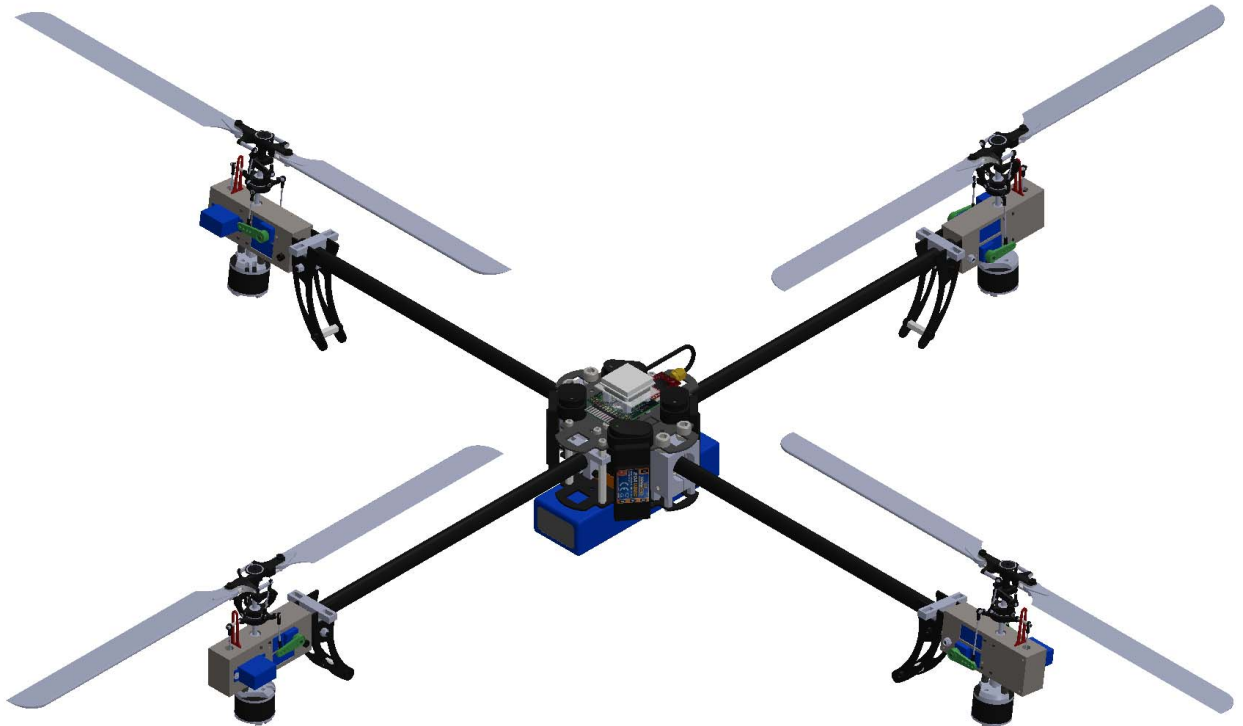Figure 9.7: **Complete helicopter - design** - Picture of the complete helicopter.

A more detailed view of the components attached to the body frame is depicted in figure 9.8, and the working rotor system is depicted in figure 9.9.
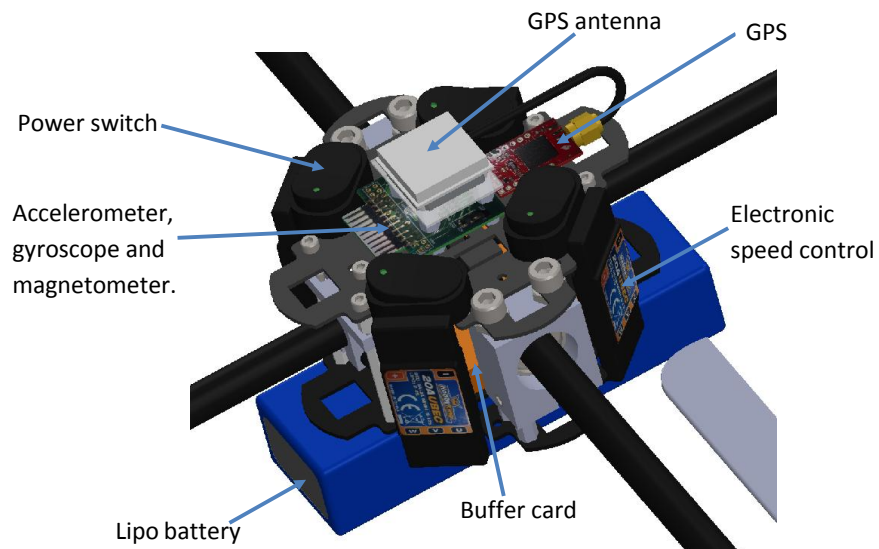
Figure 9.8: Main body design - detailed view - Detailed view of the main body assembly
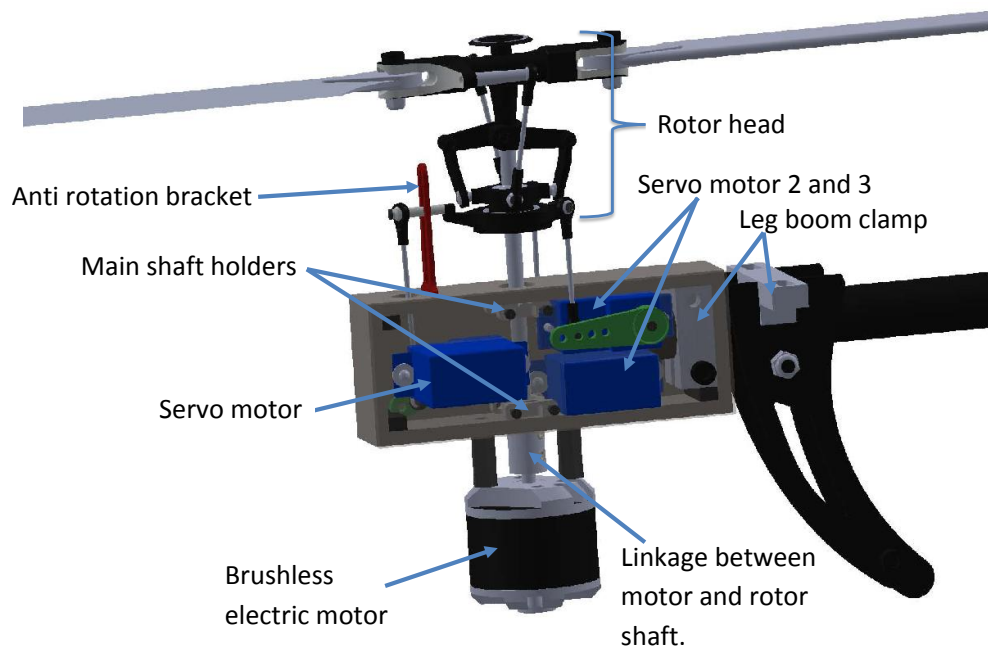
Figure 9.9: Rotor system design - detailed view - Detailed view of the working rotor system

After the helicopter was designed in Solidworks, all the necessary sub assemblies were built, and finally assembled to become a complete helicopter.

The complete helicopter with standard configuration is shown in figure 9.10.

Figure 9.10: Helicopter - standard configuration - The helicopter is depicted in the standard configuration.

The complete helicopter with tilt configuration is shown in figure 9.11.

Figure 9.11: Helicopter - tilt configuration - The helicopter is depicted in tilt configuration

A close-up picture of the helicopter's main body is shown in figure 9.12.

Figure 9.12: Rotor system - main body - Close-up picture of the main body.

Chapter 10

Control theory

The helicopter's control system can be quite difficult to design since the helicopter comprises so many control variables. A helicopter can be controlled based on altitude, speed along the x, y and z-axis, attitude and position.

In this chapter, a more suitable control strategy called Model Predictive Controller (MPC) will be proposed to optimize the helicopter's fuel/battery consumption. The MPC controller has its most successful niche in replacing the ad-hoc layer above the local loop controllers, which in the first place is not a very optimized solution. A typical control hierarchy is shown in figure 10.1.
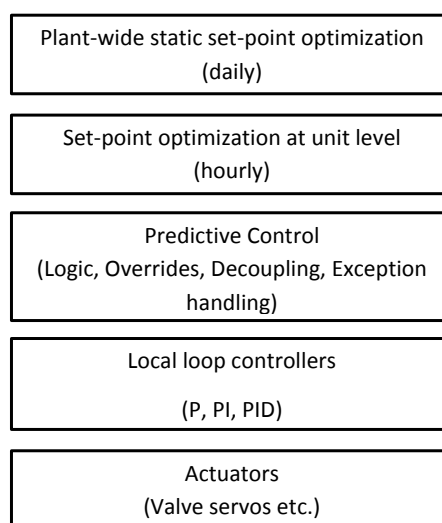

Figure 10.1: Control Hierarchy - MPC - Typical use of a MPC controller[12]

The MPC controller can achieve a more optimum solution with regards to the helicopter's fuel/battery consumption. Since the MPC controller provides a more integrated solution to handle all the problems, it can increase the performance dramatically in comparison to the ad-hoc solution.

10.1 Working principle

The basic concept of a discrete MPC controller used on a Single Input Single Output (SISO) process is depicted in figure 10.2. In this case, there is only one coincidence

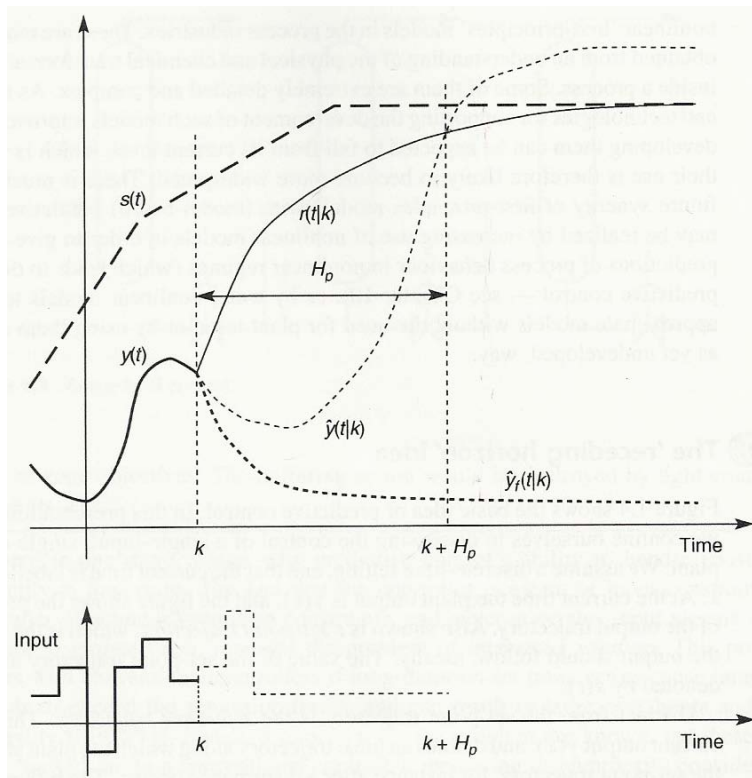**Figure 10.2: MPC basic concept** - [12]

point (where $\hat{y}(t|k)$ crosses $r(t|k)$) and one parameter. The dotted line s(t) on the figure is the controller's "setpoint trajectory", $r(t|k)$ is the "reference trajectory" and H_p is the "prediction horizon". The reference trajectory is often chosen to be an exponential function as it is often desired that it approaches the set-point exponentially.

At sample time k, the controller estimates the processes future behavior over the prediction horizon (free response of the system $\hat{y}_f(t|k)$), based on its internal model of the process, and an assumed input trajectory. Since there are many different input trajectories which give the same result, only the input trajectory that gives the best predicted behavior is chosen. From this input trajectory, only the first element is applied to the process.

The same horizon length is used at each time step, and it slides along one step at the time. This is why it is often called "receding horizon strategy"[12].
Usually there are more coincidence points than there are parameters, which means that there are more equations than number of variables, and this solution cannot be used. In these cases, only an approximation can be used, such as a "recursive least squares" method that minimizes the sum of squares of the errors.

$$\sum_{i\epsilon p}[r(k+i|k) - \hat{y}(k+i|k)]^2 \tag{10.1}$$

Where p is the set of indices's i, which are coincidence points.

When dealing with constraints the problem becomes an optimization problem with the objective function of the form:

$$min\frac{1}{2}\theta^T\Phi\theta + \phi^T\theta \tag{10.2}$$

Which is minimized with respect to θ. The inequality formulation of the constraints is given by:

$$\Omega\theta \leq \omega \tag{10.3}$$

This problem is more difficult to solve, and the use of *Quadratic Programming* is needed. More profound details will not be explained in this chapter.

10.2   Implementation

The MPC controller can be implemented as shown in figure 10.3. The mathematical model of the helicopter is often an off-line model of the helicopter, which means that

a mismatch between the model and the actual helicopter can exist. If a mismatch between the off-line model and the actual helicopter is too great, the closed loop stability analysis for the helicopter will not be valid.

To eliminate this problem, the proposed implementation could use online system identification scheme. This means that the model parameters are identified on the fly, which gives a very accurate model of the helicopter. The disadvantages of the adaptive mechanism are related to the transient effects it involves, which can affect the helicopter's performance, and the computational power needed to compute the parameters fast enough.
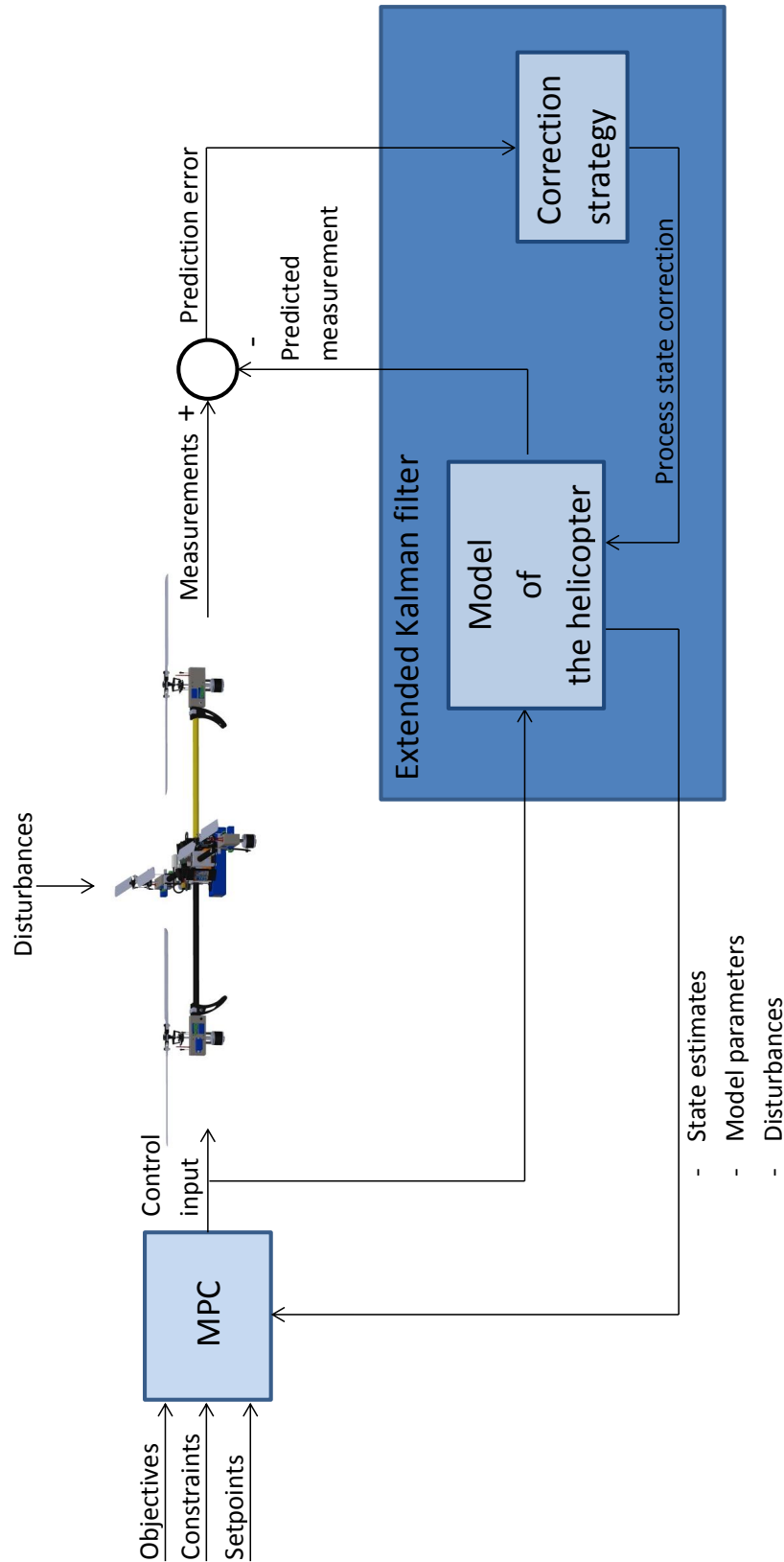
Figure 10.3: MPC implementation - implementation of the MPC controller on the rotorcraft [13].

Chapter 11

Discussion

The test results of the new type of helicopter illustrates the benefits of combining different types of modern helicopter technology, to make an advanced helicopter that can perform tasks that never before has been possible. In this chapter, some of the results and the challenges of designing and constructing the helicopter will be highlighted and discussed. The first part of this chapter will discuss the selection of the rotor size and the build of the rotor system. This was a big challenge in this project, and took a lot of time to complete. The second part of this chapter will discuss the test results, both practical and from the simulations done in Simulink.

11.1 Selection of the rotor head size

In the beginning of this project, a 450-size prototype of the rotor system was built. The rotor head size was selected based on pros and cons compared to a 250-size rotor head. In the end, the 450-size prototype failed due to problems with the gear connection between the motor and the rotor shaft. The solution to this problem was to connect the motor directly to the rotor shaft eliminating the needs for a gear connection. Simultaneously it was decided that the 250-size rotor head was more suitable to use instead of the 450-size rotor head. This was mainly because of the design change, which meant that the motor had to be located beneath the rotor systems casing. Since the 450-size rotor head needs more space between the shaft holders, than the 250-size

rotor head, the whole construction would have been very tall. The disadvantages by changing the design, were more noise and less thrust. The advantages were a smaller, lighter helicopter that could be tested indoor. The main concern of changing the rotor head size was the amount of lift that it produced. The 250-size rotor head needed to produce enough lift so that the helicopter could be operated safely. From the test results of the rotor head, the rotor head can lift a total of 634g without any penalties like vibrations. The problem with this test was identifying where the vibrations came from, and it is not concluded if they will appear when the rotor system is attached to the helicopter. If this test result is the maximum lift capacity when the tilt function is activated, it would seem a bit low. With the tilt function activated the helicopter's altitude is only maintained by two rotors that delivered a total thrust a little higher than the helicopter's weight. On the other hand, when the tilt function is active, the helicopter is moving fast forward, and if it needs to adjust its altitude it can do so by adjusting the angle of the tilt rotors. Another solution to create more lift is to put wings on the tilt rotors leg boom or extending the rotor blades to larger blades.

11.2 Problems during construction

The casings for the rotor systems were produced out of 3mm plexiglas plates, which is an easy material to work with and very light. One of the big challenges when making the plates for the casings, was the lack of precision that was needed for the parts to fit. This problem cost a lot time as the parts needed to be manually customized. Another solution to this problem would have been to make the parts at NTNU's workshop. This would have taken a lot of time as every little detail would have needed explanation and materials would have to be purchased. Another problem that might arise is the danger of misunderstandings. If this would have occurred the total project could be delayed for weeks, and in the worst case jeopardized. The decision to make the casings in my own workshop was a bit challenging. The casing for the 450-size prototype was quite easy to make, but the precision of the drilling of the holes was still a problem. The 450-size prototype had larger clearings between the different holes, which made it easier to drill the holes and made the plates stronger.

When constructing the 250-size plates, the holes were much closer to each other, which made the plates much more fragile. This made it more problematic to adjust the holes and some of the plates cracked during production. These problems became more apparent after the first prototype had been made, which is partially due to luck and a fraction higher precision. If the problems had been discovered earlier, it could have been a better solution to make them at the NTNU's workshop or used another material. Either way, this would have been a time consuming process.

11.3 Test of rotor system

The rotor system was tested in subsection 5.3.1, where it was established that the rotor system could lift 624g and a total lift capacity of 2.5kg. When the tilt function is not activated, the helicopter can lift approximately twice its own weight, but when the tilt function is active it can only lift its own weight. This is not a huge problem since the helicopter can use its tilt rotors to adjust its altitude during flight and it is possible to attach wings to the tilt rotor leg booms, which will create lift when they are tilted in the forward direction. Another solution is to make the helicopter lighter by replacing the large and heavy battery with a smaller one.

11.4 Simulation

The simulation of the helicopter is performed under ideal circumstances and incorporate many unknown parameters. Some of these parameters are set to recommended values while others are adjusted such that the performance in the simulation is equal to the performance in real life. A good example of this is the rotor systems thrust coefficient, which was adjusted such that it was capable of lifting the same amount of weight at the same rotational velocity as the real rotor system (tested in 5.3.1). The more unreliable parameters are the recommended values. If the recommended values are not correct, the performance of the helicopter during the simulation will not be correct, but there exists some suggestions that these parameters are not far from the real value. If the results from the simulation is compared to performance data from a big size quadcopter, it can be seen that they are not too far apart. Even though, the simulation results

are similar to the test results of a quadcopter,there are differences that makes this helicopter superior. Both helicopters can tilt approximately 60°, and has a forward speed of 15 m/s (tilted), but the main difference is how this is achieved. The helicopter in this project uses cyclic and collective pitch to achieve the same performance as the quadcopter. This makes this helicopter more suitable to operate over vast areas, in cold environments, over a long time frame and even perform high precision positioning. The simulation also showed that this helicopter can fly forward in horizontal position at speeds up to 14 m/s. If wings were attached it can operate as a plane, and thus create additional lift, which helps save fuel. These advantages makes a huge difference when it is supposed to perform operation tasks for the industry, either by performing high precision inspection tasks or operate over vast areas in cold climate were a long operation time is required.

Chapter 12

Conclusion

The helicopter is one of the most complex flying machines ever created, and the helicopter developed in this thesis is without exception. At the start of this project, I was fairly new to remote controlled helicopters and its dynamics, and it has taken some time and effort to understand its functionality. The number of challenges in this project has been many, and some of them were quite difficult and tedious to solve. In addition, it has been difficult to combine the practical and the theoretical work, which constantly interfered with the continuity of this project. The new earned knowledge of; helicopter dynamics, RC control systems, micro-controllers, navigational systems (accelerometer, gyroscope, magnetometer) and GPS systems have increased tremendously. The knowledge and the "know how" gained in this project will be a great asset in the future and will be used in other planned helicopter projects.

In this master thesis, it has been derived equations based upon the two aerodynamic theories, the "Momentum theory" and the "Blade element theory", to compute the required power necessary for the helicopter to fly. It has been developed software for testing the rotor system and a buffer card that is used to transform the signals to and from the micro-controller. In addition it has been developed and built a test bench, which can measure the rotor system's maximum lifting capacity and rotational velocity. Further, it have been developed three different designs of the helicopter's rotor system and all of them have been built and tested. Among the three rotor systems, one of them was established as a working prototype, and additional tested to detect its lifting properties.

A mathematical model of the helicopter has been derived and used in simulations to detect the helicopter's stability properties and behavior when subjected to crosswinds and downdrafts. To create a realistic simulation, the test results of the rotor system was used as parameters for the helicopter model.

Three different architectural designs have been proposed; a system architecture, a hardware architecture and a software architecture. The architectures give an overview on how the hardware and software are connected and how they interact. In addition, it is proposed how the software can be constructed such that the helicopter can operate in autonomous and manual mode.

Based on the good results from the simulation, a complete helicopter with the desired tilt function was designed and constructed. In the end of this thesis, a model predictive controller was proposed as a control strategy, which would optimize the helicopter's fuel/battery consumption.

The test results from the simulation showed that this helicopter can be tilted 58° without losing altitude, and can reach speeds up to 15 m/s (14 m/s levelled). It can also withstand downdrafts up to 8 m/s when levelled (4 m/s tilted) and crosswinds up to 16 m/s. The conclusion is that this helicopter's performance is about the same as for bigger quadcopters, but it has many additional advantages. The helicopter can be equipped with petrol driven motors instead of the electric ones, which makes it capable of operating over vast distances and in cold environments. It can be positioned with high accuracy during inspections tasks and perform 3d maneuvers, due to its cyclic and collective pitch control. It can be equipped with fixed wings to the tilt rotor system which will serve two purposes; It will compensate for the reduced lift capacity caused by the tilted rotors and help minimize the fuel/battery consumption. The many unique features of this helicopter make it a very versatile flying machine, which is far superior to a standard quadcopter.

Drones and remote controlled helicopters are big business, and it seems to become an increasingly larger part of the industrial future. Several ongoing research projects, involving the use of multi-rotor helicopters for inspecting power lines seems to corroborate this statement. The science done in this project is an important step in the evolution of the multi-rotor helicopter, which are now capable of performing 3d maneuvers, precision positioning and operate over vast areas in cold environments. This

thesis will be important for other students since it summarize important knowledge that is vital for anyone designing and creating its own helicopter. Hopefully this thesis will stimulate others to continue this project and develop a software, a control strategy and a navigation system for this helicopter.

Chapter 13

Further work

Although a lot of work has been done in this project, there is still much to be done. In the future there needs to be developed a software for the helicopter that is robust, easy to maintain and safe to use. A real-time operating system should be installed on the micro-controllers master subsystem, which handles scheduling and drivers. A recommended real-time operating system is the Texas Instruments own real-time operating system SYS/BIOS 6.x.

When the software part is done, there needs to be developed a fully functional control card that comprises the micro-controller, the inertial sensors, the GPS and the buffer card. The control card needs to be as small as possible, and the use of Surface Mounted Device (SMD) components is a must. For the helicopter to accommodate the long range objective, the suggested control strategy in this report should be further developed. The MPC controllers optimization routine is based upon an objective function which needs to be developed based on the helicopter's fuel/battery consumption. The MPC controller should further be included in the Simulink simulation already developed for this project. The helicopter should then be simulated to prove that the control strategy is working, and test results should be provided. The helicopter should then be tested with the new software and the new control strategy, to prove that this helicopter is working in real life. After the helicopter has been tested successfully, it can be experimented with the use of wings on the rotational rotors leg booms, which should provide the helicopter with additional lift.

References

[1] Aerostudents. Helicopters. [Online]. Available: http://www.google.no/url?sa=t&rct=j&q=&esrc=s&frm=1&source=web&cd=4&ved=0CEAQFjAD&url=http=AFQjCNGZ-8Tvv1LPzeLqNJfvgiuuiYRsWQ 46, 47, 49, 50, 53, 55

[2] Y. A. Cengel and J. M. Cimbala, *Fluid Mechanics Fundamentals and Applications*, 2nd ed. McGraw-Hill, 2010. 40, 41, 42

[3] O. Egeland and J. T. Gravdahl, *Modeling and Simulation for Automatic Control*, 2nd ed. Marine Cybernetics AS, 2003. 81, 82, 83

[4] T. I. Fossen, *Handbook of Marine Craft Hydrodynamics and Motion Control*. John Wiley and Sons Ltd, 2001. 30, 72, 114, 144, 146, 147

[5] Futaba. (2008) Fasst. [Online]. Available: http://www.futaba-rc.com/technology/fasst.html 108

[6] V. Gavrilets, B. Mettler, and E. Feron, "Dynamic model for a miniature aerobatic helicopter," 2000. 73

[7] ——, "Nonlinear model for a smallsized acrobatic helicopter," August 2001, paper AIAA 2001-4333. 73

[8] M. GmbH. Power line inspection. [Online]. Available: http://www.microdrones.com/index.php 19

[9] J. Haseltine. (2003) A U.S. V-22 Osprey tiltrotor aircraft flies a test mission. [Online]. Available: http://en.wikipedia.org/wiki/File:V-22_Osprey_tiltrotor_aircraft.jpg 23

REFERENCES

[10] T. Industries. Carbon fiber. [Online]. Available: http://www.torayca.com/en/index.html 60

[11] J. G. Leishman, *Principles of helicopter aerodynamics*, 2nd ed. Cambridge University Press, 2001. 39, 42, 44, 45, 53, 54, 55, 76, 77, 84, 93

[12] J. Maciejowski, *Predictive control with constraints*. Pearso Education Limited, 2002. 125, 126, 127

[13] S. Saelid, *TTK16-MPC-2011-part 1*. 129

[14] D. M. SCHAFROTH, "Aerodynamics, Modeling and Control of an Autonomous Micro Helicopter," Ph.D. dissertation, Swiss Federal Institute of Technology, Zurich, 2010. [Online]. Available: http://www.google.no/url?q=http://e-collection.library.ethz.ch/eserv/eth:1573/eth-1573-02.pdf&ei=9uegUNF8yYHgBJ60gHA&sa=X&oi=unauthorizedredirect&ct=targetlink&ust=1352724222019429&usg=AFQjCNEuZIXnlSMzPY4zGEoFi0UJ5ChsdQ 79

[15] J. Seddon and S. Newman, *Basic Helicopter Dynamics*, 3rd ed. John Wiley and Sons Ltd, 2011. 39, 41, 42, 43, 45, 46

[16] Shopswarf. Spur. [Online]. Available: http://www.shopswarf.orconhosting.net.nz/spur.html 110

[17] STMicroelectronics. (2003) 2n3904. [Online]. Available: http://www.st.com/internet/com/TECHNICAL_RESOURCES/TECHNICAL_LITERATURE/DATASHEET/CD00002987.pdf 106

[18] UNC, CFC, and USFK. (2008) Boeing ch-47 chinook. [Online]. Available: http://en.wikipedia.org/wiki/File:080301-F-2207D-394.jpg 24

[19] Wikipedia. Aluminium. [Online]. Available: http://en.wikipedia.org/wiki/Aluminium 60

[20] ——. Poly(methyl methacrylate). [Online]. Available: http://en.wikipedia.org/wiki/Poly(methyl_methacrylate) 60

Appendices

Appendix A

Rotation matrices

A.1 Rotation matrices around x, y and z-axis

The rotation around the x, y and z axis can be described by[4]:

$$\boldsymbol{R}_{x,\phi} = \begin{bmatrix} 1 & 0 & 0 \\ 0 & c\phi & -s\phi \\ 0 & s\phi & c\phi \end{bmatrix}, \boldsymbol{R}_{y,\theta} = \begin{bmatrix} c\theta & 0 & s\theta \\ 0 & 1 & 0 \\ -s\theta & 0 & c\theta \end{bmatrix}, \boldsymbol{R}_{z,\psi} = \begin{bmatrix} c\psi & -s\psi & 0 \\ s\psi & c\psi & 0 \\ 0 & 0 & 1 \end{bmatrix} \qquad \text{(A.1)}$$

The letter c and s are cosine and sinus, respectively, while ϕ, θ and ψ are the Euler angles.

A.2 Rotation matrix for 3d rotations

A rotation in 3d space can be described by combining the rotation matrices in A.1, which yields:

$$\boldsymbol{R}_b^n(\boldsymbol{\Theta}_{nb}) := \boldsymbol{R}_{z,\psi}\boldsymbol{R}_{y,\theta}\boldsymbol{R}_{x,\phi} = \begin{bmatrix} c\psi c\theta & -s\psi c\phi + c\psi s\theta s\phi & s\psi s\phi + c\psi c\phi s\theta \\ s\psi c\theta & c\psi c\phi + s\phi s\theta s\psi & -c\psi s\phi + s\theta s\psi c\phi \\ -s\theta & c\theta s\phi & c\theta c\phi \end{bmatrix} \qquad \text{(A.2)}$$

144

A.3 The inverse rotation matrix for 3d rotations

The inverse transformation matrix is given by:

$$\boldsymbol{R}_b^n(\boldsymbol{\Theta}_{nb})^{-1} := \boldsymbol{R}_n^b(\boldsymbol{\Theta}_{nb}) = \boldsymbol{R}_{x,\phi}^T \boldsymbol{R}_{y,\theta}^T \boldsymbol{R}_{z,\psi}^T \tag{A.3}$$

$$= \begin{bmatrix} c\theta c\psi & c\theta s\psi & -s\theta \\ -c\phi s\psi + s\phi s\theta c\psi & c\phi c\psi + s\phi s\theta s\psi & s\phi c\theta \\ s\theta s\psi + c\phi s\theta c\psi & -s\phi c\psi + c\phi s\theta s\psi & c\phi c\theta \end{bmatrix} \tag{A.4}$$

Appendix B

Transformation between body and NED-frame

B.1 Transformation of the velocity vector

The velocity vector i NED can be described by [4]:

$$\dot{\boldsymbol{p}}_{b/n}^{n} = \boldsymbol{R}_{b}^{n}((\boldsymbol{\Theta}_{nb})\boldsymbol{v}_{b/n}^{b} \tag{B.1}$$

Appendix C

Matrix definitions

C.1 The skew symmetric matrix

The skew symmetric matrix $\boldsymbol{S}$ is defined as[4]:

$$\boldsymbol{S}(\boldsymbol{\lambda}) = -\boldsymbol{S}^T(\boldsymbol{\lambda}) = \begin{bmatrix} 0 & -\lambda_3 & \lambda_2 \\ \lambda_3 & 0 & -\lambda_1 \\ -\lambda_2 & \lambda_1 & 0 \end{bmatrix} \tag{C.1}$$

Where

$$\boldsymbol{\lambda} = \begin{bmatrix} \lambda_1 \\ \lambda_2 \\ \lambda_3 \end{bmatrix}$$

C.2 The inertia matrix

The inertia matrix $\boldsymbol{I_g}$ is defined as[4]:

$$\boldsymbol{I_g} = \begin{bmatrix} I_{xx} & -I_{xy} & -I_{xz} \\ -I_{yx} & I_{yy} & -I_{yz} \\ -I_{zx} & -I_{zy} & I_{zz} \end{bmatrix} \tag{C.2}$$

Appendix D

Simulink/MATLAB diagrams
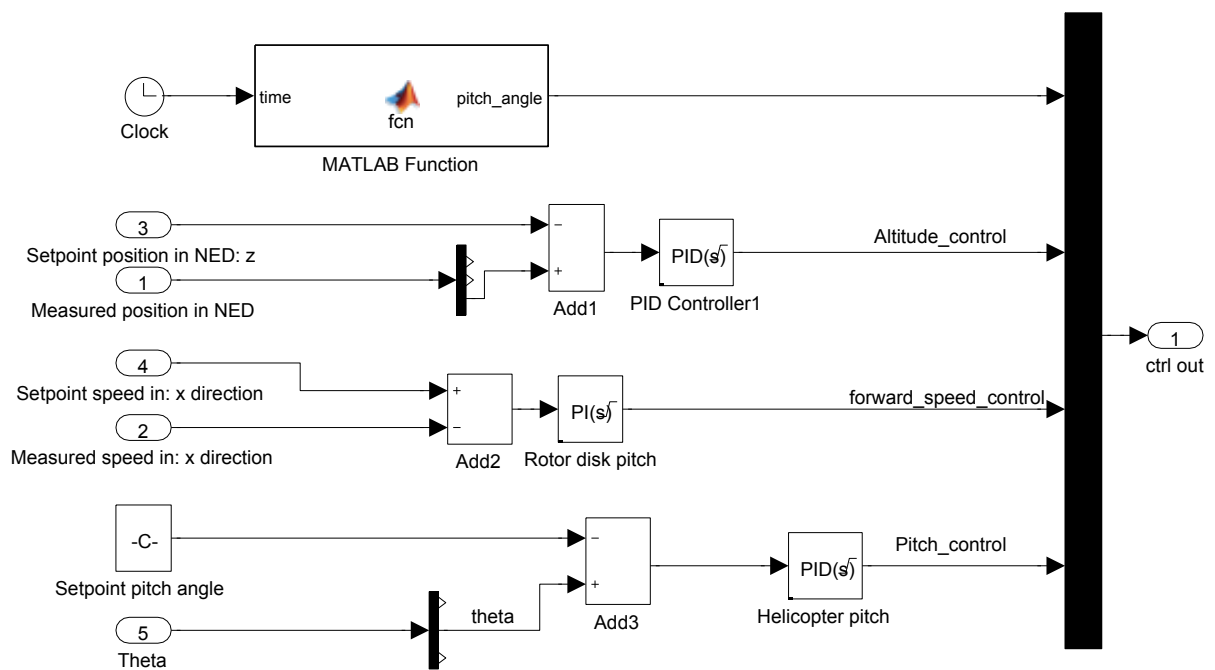
Figure D.1: Control subsystem

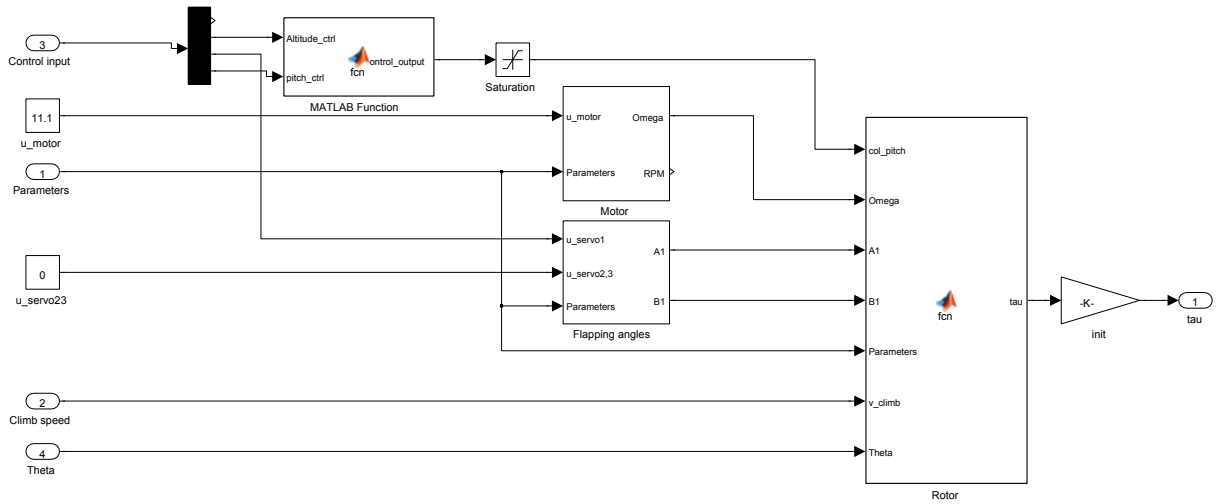The complete Simulink model is included as a separate zip file.
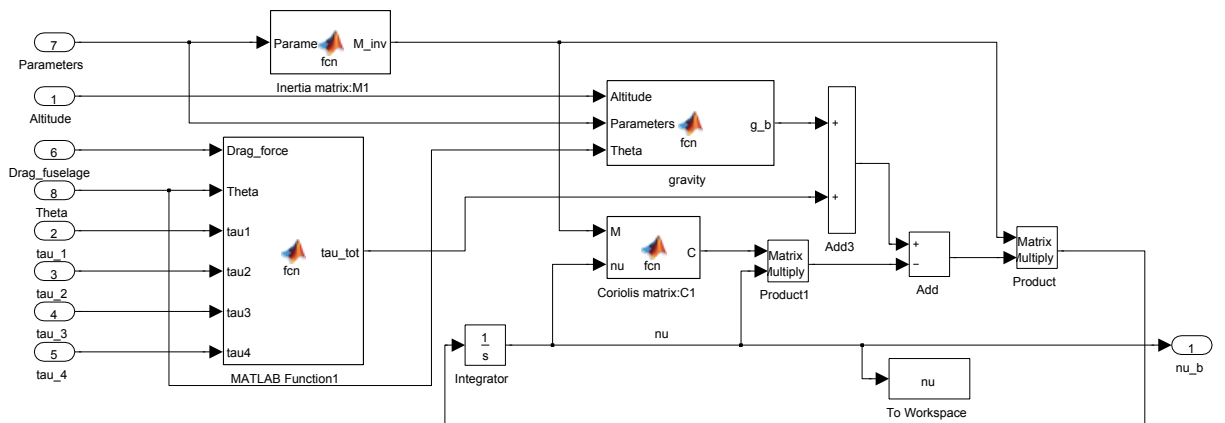
Figure D.2: Rotor subsystem

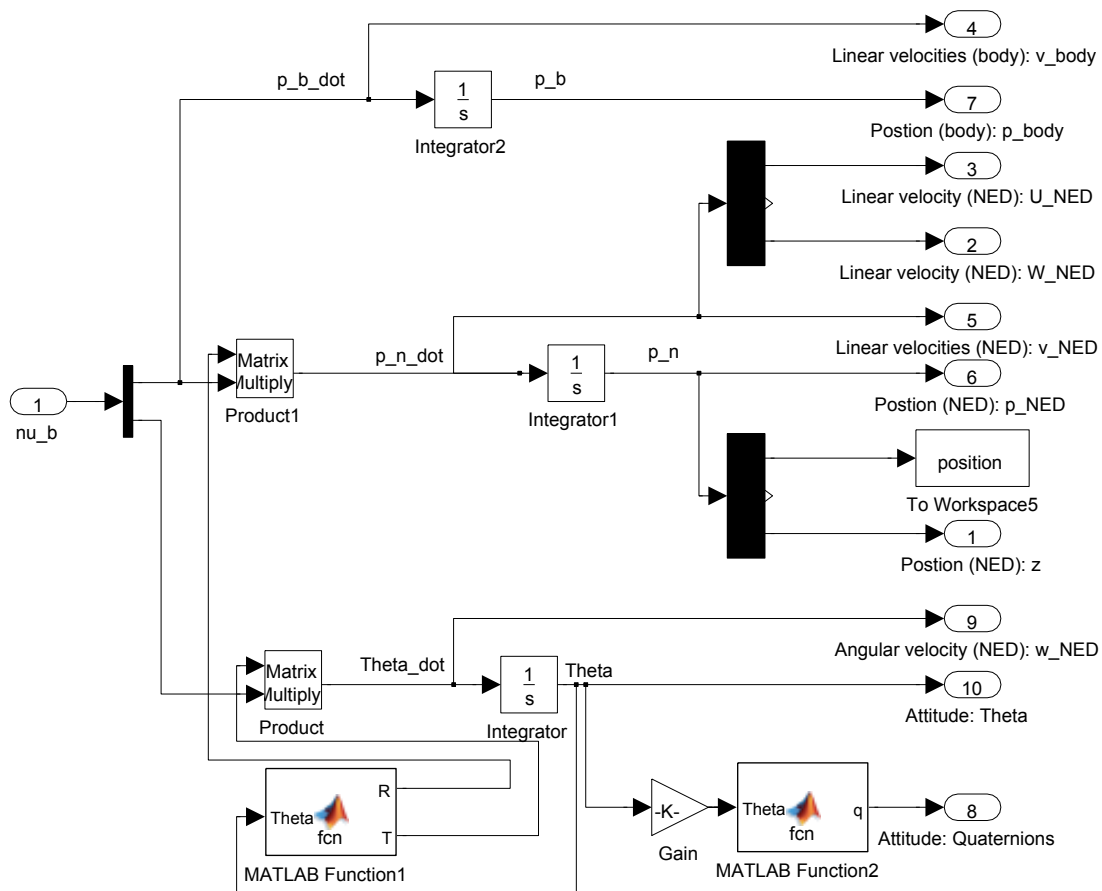**Figure D.3: Equation of motion subsystem**

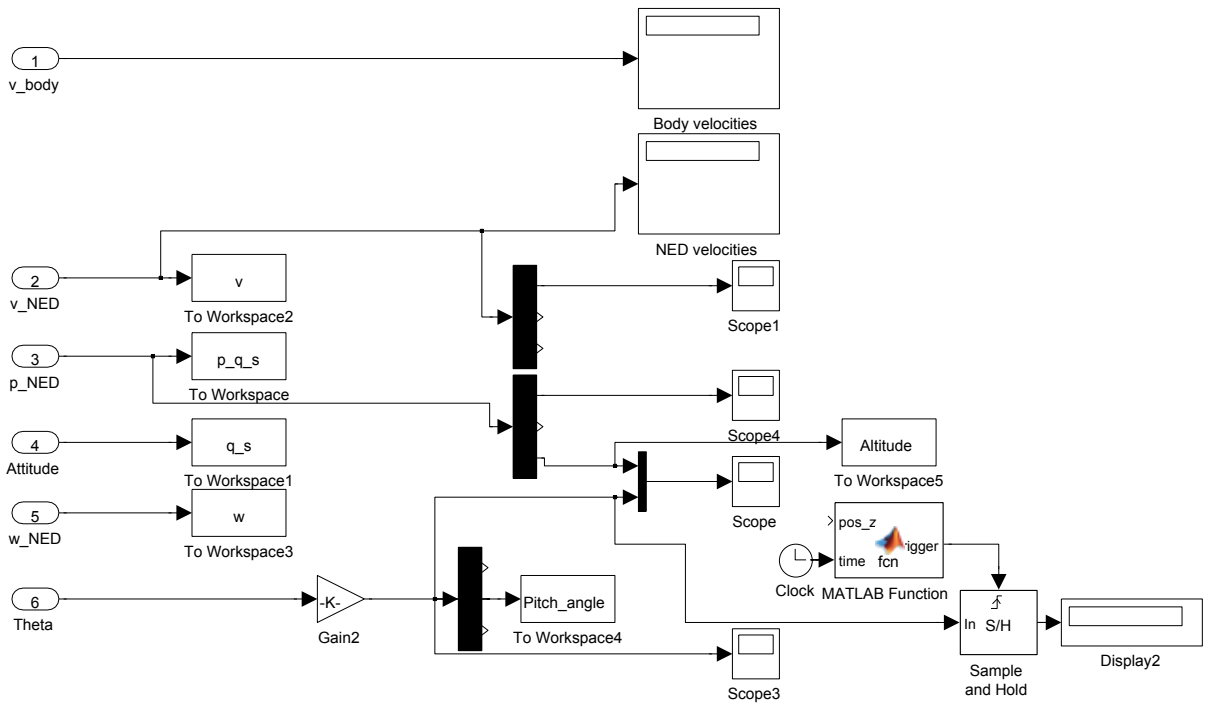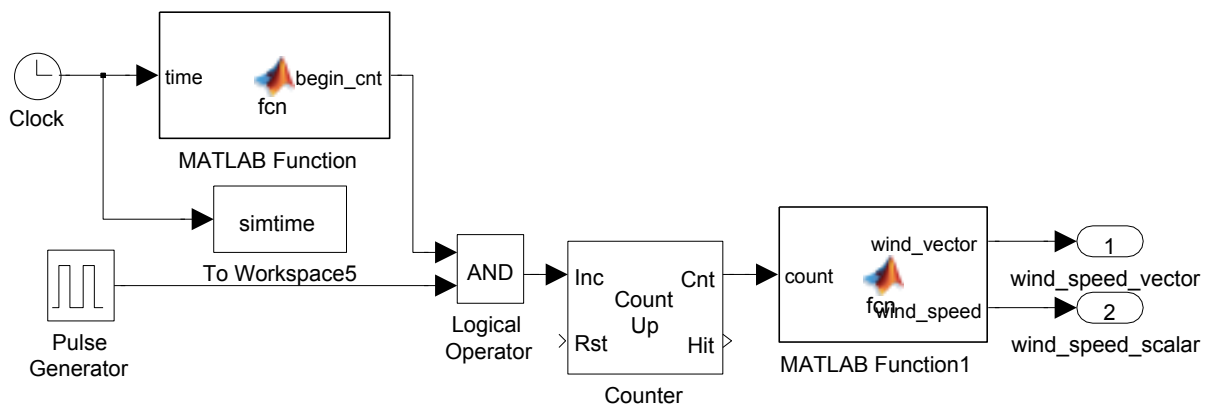**Figure D.4: Transformation from Body to NED subsystem**

Figure D.5: Measurement subsystem

Figure D.6: Wind simulator subsystem